RESTRICTED REPORT 274R

CSIRO
AUSTRALIA

Division of
EXPLORATION GEOSCIENCE

Institute of Minerals, Energy and Construction

MAGNETIC MINERALOGY OF FELSIC VOLCANICS OF THE CONWAY-BIMURRA AREA, NORTHEAST QUEENSLAND: RELATIONSHIPS TO AEROMAGNETIC ANOMALIES AND HYDROTHERMAL ALTERATION

M.A. LACKIE, D.H. FRENCH and D.A. CLARK

AMIRA P78/P96C: Rock Magnetism and
Magnetic Petrology Applied to
Geological Interpretation of
Magnetic Surveys

P.O. Box 136
North Ryde
NSW 2113

FEBRUARY 1992

This document is not to be given additional distribution or to be cited in other documents without the consent of the Chief of the Division.

AMIRA
Australian Mineral Industries Research Association Limited

CSIRO
AUSTRALIA

Division of Exploration Geoscience
Institute of Minerals, Energy and Construction
51 Delhi Road, North Ryde, NSW. Postal Address: PO Box 136, North Ryde, NSW 2113
Telephone: (02) 887 8666. Telex: AA25817. Fax: (02) 887 8909

Chief: Dr. B.J.J. Embleton

POLICY ON RESTRICTED REPORTS

Restricted Reports issued by this Division deal with projects where CSIRO has been granted privileged access to research material. Initially, circulation of Restricted Reports is strictly controlled, and we treat them as confidential documents at this stage. They should not be quoted publicly, but may be referred to as a "personal communication" from the author(s) if my approval is sought and given beforehand.

The results embodied in a Restricted Report may eventually form part of a more widely circulated CSIRO publication. Agreements with sponsors or companies generally specify that drafts will be first submitted for their approval, to ensure that proprietary information of a confidential nature is not inadvertently included.

After a certain period of time, the confidentiality of particular Restricted Reports will no longer be an important issue. It may then be appropriate for CSIRO to announce the titles of such reports, and to allow inspection and copying by other persons. This procedure would disseminate information about CSIRO research more widely to Industry. However, it will not be applicable to all Restricted Reports. Proprietary interests of various kinds may require an extended period of confidentiality. Premature release of Restricted Reports arising from continuing collaborative projects (especially AMIRA projects) may also be undesirable, and a separate policy exists in such cases.

You are invited to express an opinion about the security status of the enclosed Restricted Report. **Unless I hear to the contrary**, I will assume that in eighteen months time I have your permission to place this Restricted Report on open file, when it will be generally available to interested persons for reading, making notes, or photocopying, as desired.

Graham F. Taylor
Acting Chief

Floreat Park
Location: Underwood Avenue, Floreat Park
Postal Address: CSIRO Private Bag,
PO Wembley WA 6014
Telephone: (09) 387 0200
Fax: (09) 387 8642
Telex: AA92178

Townsville
Location: Davies Laboratory, University Road, Townsville
Postal Address: Private Mail Bag,
PO Aitkenvale QLD 4814
Telephone: (077) 71 9511
Fax: (077) 25 1009

Lindfield
Location: Bradfield Road, Lindfield
Postal Address: PO Box 218
Lindfield NSW 2070
Telephone: (02) 413 7733, 413 7211
Fax: (02) 413 7202
Telex: AA26296

RESTRICTED INVESTIGATION REPORT 274R Copy of 23 copies

Report to AMIRA Ltd

DISTRIBUTION LIST	Copy
AMIRA Ltd	1-18
CSIRO Division of Exploration Geoscience	
D.A. Clark	19
D.H. French	20
M.A. Lackie	21
G.F. Taylor	22,23

TABLE OF CONTENTS

	SUMMARY	i
1.0	INTRODUCTION	1
2.0	GEOLOGICAL SETTING AND AEROMAGNETIC SIGNATURES	1
3.0	PETROLOGICAL TECHNIQUES	3
4.0	ROCK MAGNETIC TECHNIQUES	3
5.0	PETROGRAPHY	12
6.0	MAGNETIC SUSCEPTIBILITY	18
7.0	REMANENCE AND PALAEOMAGNETISM	20
8.0	MAGNETIC MINERAL CHARACTERIZATION	22
9.0	MAGNETIC MINERAL PETROLOGY	25
10.0	CONCLUSIONS	28
11.0	ACKNOWLEDGEMENTS	30
12.0	REFERENCES	30
	APPENDIX I	

LIST OF TABLES

Table 1. List of samples examined petrographically.

Table 2. Basic Magnetic Properties.

Table 3. Remanence data. Site mean directions.

Table 4. SIRM and MDFs of SIRM and NRM.

Table 5. Fe-Ti Oxide Analyses of the Upper Carboniferous Units.

Table 6. Fe-Ti Oxide Analyses of the Stones Creek Formation.

LIST OF FIGURES

Fig. 1 Location of Bimurra and Conway prospects.

Fig. 2 Distribution of volcanics in northern Drummond Basin.

Fig. 3 Geology of Conway-Bimurra area.

Fig. 4 Aeromagnetic map of Conway-Bimurra area.

Fig. 5 Susceptibility, remanent intensity and Koenigsberger ratio of magnetic minerals.

Fig. 6 Presentation of stepwise demagnetization of remanence using orthogonal projections.

Fig. 7 Characteristic AF demagnetization curves of SD, PSD and MD grains of magnetite.

Fig. 8 Characteristic normalized k-T curves of paramagnetic, superparamagnetic, SD magnetite, MD magnetite and titanomagnetite grains.

Fig. 9 k-T curves for a monzonite containing magnetite and a basalt containing titanomagnetite with 60 mole% ulvospinel.

Fig. 10 k-T curve of an ilmenite separate from a beach sand.

Fig. 11 Diagnostic k-T curves of some iron ores.

Fig. 12 Susceptibility ellipsoid : magnetic fabric.

Fig. 13 Histograms of Susceptibility and NRM of DCv samples.

Fig. 14 Histograms of Susceptibility and NRM of CVi samples.

Fig. 15 Histogram of Susceptibility of samples from the Prospects.

Fig. 16 Orthogonal, intensity and stereographic plots of various thermally demagnetized specimens.

Fig. 17 Stereographic plots of site mean directions.

Fig. 18 Apparent polar wander path for Australia.

Fig. 19 k-T curves of the various rock types.

Fig. 20 AF demagnetization plots of the NRM and SIRM of various rock types. Lowrie plots of the same samples thermally demagnetized.

Fig. 21 Altered Ilmenite in Late Carboniferous Intrusive Rhyolite.

Fig. 22 Altered Titanomagnetite in the Locharwood Rhyolite.

Fig. 23 Altered Ilmenite in the Stones Creek Formation.

Fig. 24 Altered Titanomagnetite in the Stones Creek Formation.

SUMMARY

At Conway-Bimurra Late Devonian acid volcanics, which are prospective for epithermal gold, are difficult to distinguish from non-prospective Late Carboniferous acid volcanics. On a regional scale the aeromagnetics show a reasonable correlation with the mapped geology. Discrepancies in detail between aeromagnetics and the BMR geology map in several cases arise from misidentification of units during mapping. Other discrepancies simply reflect magnetic signatures arising from shallow, unexposed intrusives, illustrating the utility of magnetics for looking at the third dimension as well as a tool for surficial mapping. The Carboniferous units tend to be distinctly more magnetic and can therefore be distinguished using aeromagnetics.

There is a pervasive propylitic alteration in both the Carboniferous and Devonian volcanic suites, the intensity greater in the latter. Within the Devonian sequence, zones of more intense adularia-sericite hydrothermal alteration, typical of mineralised epithermal systems, occur locally. Within the Devonian volcanics these intense adularia-sericite alteration centres show up as very smooth, flat magnetic zones, reflecting magnetite destruction. Within these centres, titanomagnetite is replaced by sphene in the intense propylitic zone and by rutile in the phyllic zone. The susceptibilities of rocks from the intense alteration zones of the prospects are very low (weakly paramagnetic, < 10 μG/Oe [0.00013 SI], or diamagnetic), indicating that any ferromagnetic minerals pre-dating the alteration have almost been completely erased.

Outside the zones of intense alteration, the background susceptibilities of the Devonian volcanics are generally low, in the strong paramagnetic range ($\lesssim 100$ μG/Oe [0.00126 SI]). Relatively rare andesitic units within the Late Devonian sequence have higher susceptibilities (500-1000 μG/Oe [0.006-0.012 SI]). However, variations in paramagnetic iron contents and in the trace amounts of ferromagnetic minerals produce sufficient differences in magnetization to produce a texture in the aeromagnetic anomalies that is clearly distinguishable from the smooth flat response associated with the epithermal alteration systems.

A busy magnetic pattern associated with the Carboniferous volcanics reflects variations in susceptibility, which mainly reflects magnetite content, and Q value, which is dependent on grain size. Major shifts in magnetic base level reflect varying Q values, with reversed remanence overwhelming induced magnetization and producing magnetic lows when Q is greater than unity. Susceptibilities of Carboniferous volcanics range from ~2000 μG/Oe [0.025 SI] for dacitic flow units, to ~40 μG/Oe [0.0005 SI] for rhyolitic units. The susceptibility of the Devonian volcanics is probably lower because of a combination of initial bulk-rock chemistry (a preponderance of rhyolitic compositions) and the more intense pervasive propylitic alteration.

The oxide mineralogy is a function of the primary bulk-rock compositions and severity of alteration. Within each volcanic suite, susceptibility tends to decrease in the order andesite, dacite, rhyolite. The pervasive propylitic alteration reduces magnetization by partially replacing magnetic minerals, thereby reducing magnetic grain size and consequently increasing the stability of remanence as the susceptibility and remanence intensity decrease.

The Late Carboniferous units record a Permo-Carboniferous remanence component, directed south and steep down, which dominates the NRM of these units. Most Late Devonian units have NRMs that are dominated by a Permo-Carboniferous overprint, indistinguishable in direction from the primary remanence of the Late Carboniferous rocks. Some retain, in addition, a primary Late Devonian remanence, directed SW and shallow down. Recognition of this characteristic Late Devonian remanence in some units, that have been mapped as Carboniferous, shows that they are in fact of Devonian age. Ubiquitous Carboniferous overprinting of remanence in Devonian rocks suggests that the regional alteration is penecontemporaneous with the eruption of the Carboniferous volcanics.

There is a strong, noisy, positive aeromagnetic anomaly associated with andesitic units mapped by the BMR as DCv_A. Samples from this area have high susceptibilities, suggesting that the exposed units are responsible for the observed anomaly pattern. No trace of a Devonian remanence component underlying the Carboniferous magnetization is found during demagnetization of the samples. These characteristics are more consistent with a Carboniferous age, suggesting that this may be a Late Carboniferous unit.

This study area confirms the utility of aeromagnetics, both as a regional mapping tool in volcanic terrains and for detection of adularia-sericite alteration systems, which may be associated with epithermal gold deposits. Geological factors such as lithology and degree of alteration control the abundance, grain size and composition of ferromagnetic minerals in volcanic rocks, producing detectable variations in the associated aeromagnetic signatures. This study has also shown the potential for application of palaeomagnetism to detailed mapping in this and similar areas.

1.0 INTRODUCTION

The Conway-Bimurra prospects are located in northeast Queensland about 50km NNE of Mount Coolon and 40km SSE of the Burdekin Dam (Figs. 1 & 2). Gold mineralization was discovered in 1928 at the Bimurra prospect and mining occurred intermittently until 1935, but produced only a small quantity of gold (Wood et al 1990). At the two prospects hydrothermal alteration effects are observed over a significant area. Because of the significant hydrothermal alteration effects at the prospects and the proximity of Devonian and Carboniferous subaerial felsic volcanics, as well as the availability of detailed aeromagnetics, the Conway-Bimurra area was selected for a detailed rock magnetic study.

The aims of this study were:

(i) to measure the palaeomagnetic and rock magnetic properties of the Devonian and Carboniferous volcanics to determine differences and similarities between the two suites, and

(ii) to look at the rock magnetic and petrological properties of rocks within and nearby to the severe hydrothermal alteration zones to ascertain the effects of alteration upon those particular units.

One hundred and forty eight hand and core samples were collected from 65 sites within and around the prospects (Fig. 3), while a further 40 samples were collected from 15 sites within the felsic volcanics and related plutons to the north of the prospects (Fig. 2).

2.0 GEOLOGICAL SETTING AND AEROMAGNETIC SIGNATURES

The Conway-Bimurra prospects lie in the northern Drummond Basin (Figs. 1 & 2) about 50 km NNE of Mount Coolon in northeast Queensland. Until recently, the geology of the Conway-Bimurra area was thought to be primarily the Carboniferous Bulgonunna Volcanics (Malone 1969). In 1988, a joint mapping project between the BMR and the Queensland Department of Resource Industries was initiated (Oversby et al 1991), this following on from previous mapping by the Geological Survey of Queensland in the Mount Coolon and Byerwen 1:100,000 Sheet areas south of Conway (Hutton et al 1989). The result of this work was that the blanket "Bulgonunna Volcanics" observed on the Mount Coolon 1:250,000 geological map has been subdivided into units of Devonian and Carboniferous age (Fig. 2). The geology and stratigraphic nomenclature used in this report is derived from the preliminary maps of Oversby et al 1991, Hutton et al 1989, as well as various published iterations of the above mapping projects (Ewers et al 1991, Oversby et al 1990, Black et al 1990, Ewers et al 1989, Law et al 1989, Law 1988) and other published papers (Wood et al 1990, Hutton 1989, White et al 1989 and Irvine & Smith 1990).

The geology of the northern Drummond Basin (Fig. 2) consists of subaerial volcanigenic rocks ranging in age from Late Devonian to Late Carboniferous with Carboniferous/Permian granitoids intruding the volcanics. The currently accepted stratigraphy of the various volcanigenic rocks of the Northern Drummond Basin is one of a composite Late Carboniferous Group, the Ferndon Volcanic Group, and a Late Devonian Formation, the Stones Creek Formation. The Carboniferous Group is split into upper and lower units consisting of various Subgroups. The Ferndon Volcanic Group (upper) contains various Bulgonunna Volcanic Subgroups which lie unconformably above (Black et al 1990) the Ferndon Volcanic Group (lower) which contains various Smedley Volcanic Subgroups. Part of the Smedley Volcanic Subgroup (northwest) is the "Dam Ignimbrite" Member which outcrops at the Burdekin Dam and has been dated

at 297±3 Ma (Doug Mackenzie pers. comm. 1991, Black et al 1990).

In the vicinity of the Conway-Bimurra prospects (Fig. 3) the younger Carboniferous rocks dominate the eastern side of the sampled area while the older Devonian rocks predominate in the west. The Devonian Stones Creek Formation is represented mainly by the DCv (Bimurra Volcanics) member. The DCv member consists of rhyolitic to andesitic lavas and associated sediments. One distinct andesite unit (DCv_A) is mapped in the north of the area. The younger volcanic group consists of rocks of the Smedley Volcanic Subgroup (southeast). The rocks of this Subgroup are mainly rhyolitic to dacitic ignimbrites (the Cv_i unit). No units of the "true" Bulgonunna Volcanics (Ferndon Volcanic Group (upper) were sampled in the Conway-Bimurra area although sites elsewhere were sampled. The Late Devonian Mount Wyatt Formation occurs in the west of the area, the Formation consisting of epiclastic sandstone and fissile mudstone. The Middle Devonian Ukalunda Beds (fissile to cleaved epiclastic mudstone, ss, conglom, lime) also occur in the west of the area. The Carboniferous Roscow Granite outcrops to the NW of Conway, while various Carboniferous intrusive rhyolites occur to the SE of Conway. The Tertiary Suttor Formation (epiclastic sandstone, cong, mudstone and siltstone commonly lateritised) and some Tertiary basalts occur throughout the area.

The hydrothermal alteration covers an area of more than 10 km^2 at the Bimurra prospect and about 15 km^2 at Conway (Wood et al 1990, Irvine & Smith 1990). The Bluegum prospect shows hydrothermal alteration effects over an area of several km^2 while the alteration at the Battery Hill prospect is restricted to an area of less than 0.25 km^2 (Wood et al 1990). All the deposits conform to the adularia-sericite type of Heald et al (1987) and are characterised by a dominantly sericitic alteration-mineral assemblage (Wood et al 1990). Silica sinter deposits are present at the Conway and Bimurra prospects (White et al 1989, Wood et al 1990) indicating little eroded high level deposits. The gold mineralization at the prospects appears to be confined to silica-rich zones, either in veins or as breccia cement (Wood et al 1990). The age of the mineralization has been determined from potassium-argon dating of sericite, with ages of 314 ± 13Ma (Conway), 321 ± 3Ma (Bimurra) and 294 ± 10Ma (Bluegum) (G. Ewers, sited in Wood et al 1990) indicating Middle to Late Carboniferous hydrothermal events. The prospects occur in the pre-Carboniferous units.

A colour image of the BHP aeromagnetic survey data, with TMI contours, geology and site localities overlain, is shown in Fig. 4A. The most striking relationship between the aeromagnetic data and the mapped geology is the generally subdued magnetic pattern over the Devonian rocks compared to the active magnetic response over the Carboniferous volcanics. The magnetic contours are somewhat more useful for discriminating between Devonian and Carboniferous units than the colour image reproduced in Fig. 4a, because the typical "volcanics" texture associated with variable magnetization intensities, remanence polarities and unit thicknesses is apparent, irrespective of base level shifts due either to deeper rocks or to zones of differing predominant magnetization polarity within near surface rocks. It was shown by the sampling programme that base level shifts within the Carboniferous units are due to variable Q values, whereby Carboniferous remanence with reversed polarity opposes the induced magnetization to varying degrees. Units with low Q values are associated with higher magnetic base levels, whereas units with higher Q values correspond to relatively low base levels.

Close examination of the aeromagnetics reveals some discrepancies with the mapped geology. One example is the southern boundary of the extensive Cv_i units mapped in the NE of the study area. South of sites 3 and 57 the magnetic response abruptly becomes smoother, suggesting that the mapped lobe of Cv_i south of this boundary is in fact part of the Cubpo unit. This interpretation is also supported by the airborne radiometrics data (B. Dickson, pers. comm.).

Although the magnetic activity over the Devonian volcanics is subdued relative to that associated with Carboniferous units, there is still a characteristic, slightly noisy, texture, except in the zones of intense hydrothermal alteration, over which the magnetic response is very smooth and flat. An "alteration filter", designed specifically to highlight such responses, has been applied to the image shown in Fig. 4B (Irvine and Smith, 1990). A corridor of relatively smooth magnetic response, associated with regional alteration patterns is delineated by the image. The intense alteration systems at Conway and Bimurra correspond to particularly "flat" zones within this corridor. The aeromagnetic response of the alteration systems can be explained by total destruction of magnetic minerals within intensely altered rocks. This is consistent with other studies of the effects of similar hydrothermal alteration of originally magnetic rocks on magnetic mineral content, magnetization and associated magnetic anomalies (Ade-Hall et al, 1971; Bohlke et al, 1981; Criss and Champion, 1984, Criss et al, 1985; Rona, 1978; Wooldridge et al, 1990).

3.0 PETROLOGICAL TECHNIQUES

Polished thin sections were prepared for petrographic and electron microprobe analysis, which provide the advantage that both the opaque and translucent phases can be examined in the same sample and their relationships determined. The electron microprobe analyses were carried out on a CAMECA CAMEBAX automated scanning electron microprobe equipped with four wavelength-dispersive X-ray spectrometers, covering the elemental range boron to uranium and a KEVEX-7000 energy-dispersive X-ray spectrometer which is capable of analysing from sodium to uranium. The wavelength spectrometers were used for quantitative analysis, the energy-dispersive system being used for qualitative identification of the phases prior to quantitative analysis.

Two analytical programs were used for the determination of the oxide and sulphide phases. For analysis of sulphides an accelerating voltage of 20kV was used and 15kV for oxide analysis with a regulated beam current of 20nA being used in both cases. Each element was counted for 20 seconds or a precision of 0.5%, the count being terminated when either of these two conditions was fulfilled. All analyses were corrected for atomic number, X-ray absorption and fluorescence using an iterative ZAF procedure. Corrections for interfering elements due to X-ray line overlap were made offline.

4.0 ROCK MAGNETIC PRINCIPLES AND TECHNIQUES

4.1 Ferromagnetism, Paramagnetism and Diamagnetism

Diamagnetic minerals (e.g. calcite and quartz) have very weak, negative susceptibilities and can be regarded as nonmagnetic for geophysical purposes. Paramagnetic minerals (e.g. olivines, pyroxenes and pure ilmenite) have weak positive susceptibilities and do not carry remanence. They are, therefore, normally unimportant for magnetic interpretation. Magnetically ordered phases that possess spontaneous magnetisations can be ferromagnetic *sensu stricto* (e.g. iron) or

ferrimagnetic (e.g. magnetite). For simplicity, all these strongly magnetic minerals will be referred to hereafter as ferromagnetic. Ferromagnetic minerals lose their spontaneous magnetisation at a characteristic temperature, the Curie point, which is a function only of composition and which can therefore be used to detect particular ferromagnetic phases. Below its Curie temperature a ferromagnetic mineral has high susceptibility and can carry remanence. Above the Curie temperature the mineral becomes paramagnetic, with low susceptibility and no remanence. Paramagnetic minerals have greater susceptibility at low temperatures, reflecting a ~ 1/T dependence, and may become magnetically ordered, i.e. ferromagnetic or antiferromagnetic, below a transition temperature (the Curie point or the Néel point, respectively) which is composition dependent and can be used to determine the presence of particular paramagnetic minerals.

4.2 Domain Structure

The bulk magnetic properties of rocks reflect the modal proportions, compositions and microstructure of the magnetic mineral grains, which are usually present in only minor amounts. Microstructure includes, *inter alia*, grain size and shape, degree of crystallinity and textural relationships and strongly influences the magnetic domain state of the grains. The most important control on domain structure is the effective grain size, which is equivalent to the actual grain size in a homogeneous grain, but is related to lamella size in grains with exsolution lamellae and the size of the ferromagnetic zone in a zoned grain.

Sufficiently small grains are uniformly magnetised, i.e. they have single domain (SD) structure. Ultrafine SD grains (< 0.03 μm for equant magnetite) are sufficiently perturbed by thermal fluctuations that the orientation of the spontaneous magnetisation flips rapidly between two or more easy directions. Such grains cannot retain a stable remanence and their magnetisations tend to relax rapidly towards any applied field, leading to a very high susceptibility. This behaviour is called superparamagnetism, and the grains are termed superparamagnetic (SPM).

The relaxation time for superparamagnetism increases exponentially with grain volume. Thus slightly larger grains have very long relaxation times, even on a geological time scale, and can retain remanent magnetisation indefinitely. These stable SD grains, typically in the micron size range, are important carriers of remanent magnetisation in many rocks. Acicular grain shape, or elongated lamellar shape, favours SD behaviour and extends the maximum size for SD behaviour.

With increasing size it becomes energetically favourable for the grain to subdivide into a number of magnetic domains with differently oriented magnetisations. These multidomain (MD) grains have susceptibilities, controlled by self-demagnetisation, which in the case of strongly magnetic minerals, such as magnetite, are comparable to the susceptibilities of SD grains with similar composition. The remanence of MD grains is more easily demagnetised ("softer") than that carried by SD grains and is of lower specific intensity. The case of magnetite will be considered in some detail, but other magnetic minerals exhibit qualitatively similar behaviour. Magnetite grains larger than ~ 20 μm exhibit true MD behaviour. The coercivity, which is a measure of the ease of demagnetisation, and the remanent intensity decrease steadily with increasing grain size until they level out for grain sizes greater than ~ 100 μm. The measure of coercivity used in this study is the median destructive field (MDF) during alternating field demagnetisation (see below).

Grains smaller than ~20 μm have properties intermediate between those of SD and true MD grains and are called pseudosingle domain (PSD). Small PSD grains, a few microns in size, are relatively hard and carry relatively intense remanence. For this reason, small PSD grains are the most important remanece carriers in many rocks, in spite of the fact that they constitute a minor proportion of the magnetic mineral assemblage and even though relatively large MD grains may dominate the susceptibility of the rocks.

The behaviour of some important magnetic properties with increasing grain size (above the SPM threshold size) can be summarised as: remanence, coercivity and Koenigsberger ratio (remanent/induced magnetisation) decrease; susceptibility increases slightly. Typical values of susceptibility, remanent intensity and Koenigsberger ratio of various domain states for a number of magnetic minerals are summarised in Fig.5 (from Clark, 1983). The theoretical maximum sizes for superparamagnetic and single domain behaviour for equant grains of a number of magnetic minerals are summarised below:

Mineral	**SPM threshold size** (μm)	**Critical SD size** (μm)
Iron	< 0.008	0.023
Magnetite	0.03	0.06
Maghaemite	0.02	0.06
Titanomagnetite (60% usp; 40% mt)	0.08	0.40
Haematite	0.03	15.0
Monoclinic pyrrhotite	0.018	1.6

It has become apparent in recent years that magnetic grains frequently occupy metastable domain states of anomalously low domain multiplicity. The above values for the critical SD size assume equilibrium, i.e. that the grain is in the absolute energy minimum state. In fact, grains an order of magnitude larger than the theoretical size can remain in a metastable SD state, because formation of a domain wall requires an energy barrier to be overcome. Thus the effective upper limit for SD behaviour has been extended to ~ 1 μm for magnetite and by a similar factor for other minerals. The threshold sizes are also larger for elongated grains than for equant grains. The domain structure transition sizes for titanomagnetites and other spinel phases with lower spontaneous magnetisations are larger than for magnetite. Thus the single domain/two domain transition, the upper limit of the PSD size range etc. occur at larger grain sizes for spinels with decreasing magnetite contents. Taking metastable behaviour into account, the approximate size ranges and coercivities for SPM, (stable) SD, PSD and MD behaviour for magnetite are listed below:

Domain structure	**Size** (μm)	**Coercivity** (Oe)
SPM	< 0.05	0
(acicular) SD	0.05-1	> 600

PSD	~1-20	100-600
MD	> 20	< 100

4.3 Intrinsic_Magnetic_Properties_of_Minerals

The intrinsic magnetic properties spontaneous magnetisation at room temperature (J_s) and Curie temperature (T_C), which are dependent only on composition, are given below for a number of minerals, including some end-member spinel phases:

Mineral name	Chemical formula	Magnetic properties
Iron	Fe	T_C = 770°C, J_s = 1710 G
Awaruite	Ni_3Fe	T_C = 620°C, J_s = 950 G
Magnetite	Fe_3O_4	T_C = 580°C, J_s = 480 G
Ulvospinel	Fe_2TiO_4	T_C = -153°C, J_s = 0
Titanomagnetite (100x mole% usp)	$Fe_{3-x}Ti_xO_4$	$0 \leq x < 0.8$ ferro; $x \geq 0.8$ paramag.
Maghaemite	cFe_2O_3	$T_C \gg 300°C^*$, J_s = 440 G
Haematite	αFe_2O_3	T_C = 670°C, J_s = 2 G
Titanohaematite (100x mole% ilm)	$Fe_{2-x}Ti_xO_3$	$0 \leq x < 0.5$ antiferro; $0.5 \leq x \leq 0.8$ ferro; $0.8 < x < 1$ paramagnetic
Ilmenite	$FeTiO_3$	T_C = -205°C, J_s = 0
Monoclinic (4C) pyrrhotite	Fe_7S_8	T_C = 320°C, J_s = 90 G
Magnesioferrite	$MgFe_2O_4$	$T_C \lesssim 420°C$, $J_s \lesssim 220$ G
Chromite	$FeCr_2O_4$	T_C = -185°C, J_s = 0
Ferrichromite/ Cr-magnetite e.g.	$Fe_{3-x}Cr_xO_4$ Fe_2CrO_4	ferromagnetic for $0 \leq x \leq 1.2$, T_C = 200°C, J_s = 250 G
Hercynite	$FeAl_2O_4$	T_C = -265°C, J_s = 0
Magnesian ulvospinel	Mg_2TiO_4	diamagnetic
Picrochromite	$MgCr_2O_4$	T_C = -258°C, J_s = 0
Spinel	$MgAl_2O_4$	diamagnetic
Jacobsite/ Mn-magnetite e.g.	$Fe_{3-x}Mn_xO_4$ Fe_2MnO_4	ferromagnetic for $0 \leq x \leq 2.5$ T_C = 300°C, J_s = 398G
Trevorite	$NiFe_2O_4$	T_C = 595°C, J_s = 330 G
Coulsonite	FeV_2O_4	T_C = -164°C, J_s = 0

The Curie point of maghaemite cannot be observed directly because maghaemite inverts to haematite at temperatures above ~300°C, depending on impurities. The Curie temperature of magnetite-bearing spinel minerals varies systematically with magnetite content. To a first approximation, the Curie point of a particular spinel composition can be estimated by linear interpolation between T_C of the constituent end members. Diamagnetic minerals can be assigned a nominal T_C of absolute zero (-273°C) for this purpose. For the titanomagnetite series, a more accurate expression relating Curie temperature to mole fraction of ulvospinel (x) is:

$Fe_{3-x}Ti_xO_4$: T_C (°C) = 578 - 580x - 150x².

The effect on T_C of substitution of Cr, Al and V into magnetite is broadly similar to that of Ti substitution. Substitution of Ni increases the Curie point slightly, as does cation deficiency. Thus cation-deficient magnetites ("kenomagnetite"), representing compositions intermediate between stoichiometric magnetite and maghaemite, can have T_C above 600°C. Magnesioferrite is the only important spinel end member, other than magnetite, that is ferromagnetic at room temperature. The magnetic properties of magnesioferrite depend strongly on the cation distribution, which reflects thermal history. The Curie point of $MgFe_2O_4$ is given by:

$MgFe_2O_4$: T_C (°C) = 417 - 490f,

where f is the fraction of Mg^{2+} ions on tetrahedral sites. Because of the elevated T_C and high spontaneous magnetisation, magnesioferrite-rich spinels and Mg-magnetites are strongly magnetic and can be important contributors to the magnetic properties of rocks in which they occur.
The magnetic phase diagram of the titanohaematite series is complex and the magnetic properties of the compositions that are ferromagnetic at room temperature are influenced by thermal history. $FeTiO_3$-Fe_2O_3 solid solutions have been thoroughly studied. The Curie temperature decreases approximately linearly with increasing ilmenite content. Compositions with less than 20 mole% haematite are paramagnetic at room temperature.

Pure haematite has a diagnostic magnetic transition (the Morin transition) at -20°C. Below this temperature atomic magnetic moments are aligned with the crystallographic c-axis and haematite is antiferromagnetic. Above the transition the moments lie in the basal plane but are slightly canted out of antiparallelism, giving rise to weak ferromagnetism and an increased susceptibility. The Morin transition can also be exploited for diagnosis of well-crystallised haematite by the effect of low temperature demagnetisation on remanence (see below).

4.4 Palaeomagnetic_Cleaning_Techniques

The natural remanent magnetisation (NRM) of a rock may consist of components, carried by different subpopulations of magnetic minerals, acquired at different times. During initial cooling of an igneous rock, magnetic mineral grains make the transition from paramagnetism to ferromagnetism as they cool through their Curie points. A spontaneous magnetisation appears that is initially in equilibrium with the applied field, but becomes "frozen in" or blocked at a somewhat lower temperature, called the blocking temperature, when the relaxation time of the grain's magnetic moment increases prodigiously. Below the blocking temperature the magnetisation is a stable remanence that is known as thermoremanent magnetisation (TRM). If grain growth of magnetic

minerals or creation of new magnetic phases occurs below the Curie temperature, there is a huge increase in relaxation time as the grains become larger than the SPM threshold size. This produces a stable chemical remanent magnetisation (CRM). If CRM is acquired at elevated temperatures, the remanence has both thermal and chemical character and is known as thermochemical remanence.

Other components of remanence may be acquired at later times due to metamorphic overprinting, weathering etc. Each separate component of remanence is acquired parallel to the ambient field at the time of its acquisition. Rock samples may also acquire palaeomagnetic noise components due to exposure to magnetic fields, for instance during mining operations or during or after collection. All these components contribute to the measured NRM of a rock sample. Because different remanence components are carried by subpopulations of grains with different characteristics, they can usually be distinguished by their different responses to various demagnetisation techniques.

Alternating field (AF) demagnetisation is similar to degaussing of permanent magnetisation of ships or tape recorder heads. The sample is subjected to an alternating magnetic field that is gradually reduced to zero, thereby randomising the moments of all grains with coercivity less than the initial AF amplitude. This procedure is repeated at successively higher fields, demagnetising successively harder fractions of the magnetic mineral assemblage and isolating the most stable component of remanence. AF demagnetisation is particularly effective at removing isothermal remanent magnetisation (IRM) acquired by exposure to strong magnetic fields, such as those produced by mining equipment or lightning strikes etc.

Thermal demagnetisation involves heating the sample and recooling to room temperature, in zero magnetic field. This randomises the magnetic moments of all grains with blocking temperatures less than the heating temperature. This procedure is repeated at successively higher temperatures, thereby demagnetising successively higher blocking temperature fractions. Thermal demagnetisation is particularly effective at unravelling the thermal history of the rock, for instance by resolving primary TRM from a later metamorphic overprint.

Palaeomagnetic cleaning techniques have three main applications, which can be termed palaeomagnetic, petrophysical and rock magnetic respectively:

(i) Resolution of remanence components acquired at different times, allowing estimation of palaeofield directions and palaeopole positions at the time of formation, at the time of metamorphism etc.,

(ii) Removal of palaeomagnetic noise components, which are not representative of the bulk *in situ* properties, allowing characteristic NRMs of the rock to be determined,

(iii) Identification of magnetic minerals by their demagnetisation characteristics. Information on compositions, domain states and grain sizes of the magnetic minerals can be obtained.

The most useful method of depicting demagnetisation of multicomponent remanence is that of orthogonal projections. These are generally termed Zijderveld plots. The basic idea of these plots is illustrated in Fig.6. The end-points of the remanence vectors after successive demagnetisation steps describe a trajectory in 3D space. Over a treatment interval where a single remanence component is removed this trajectory defines a linear

segment. Where two or more remanence components are being removed simultaneously, due to their having overlapped stability spectra, the trajectory is curved. After removal of all less stable components, the trajectory of the most stable component is a straight line heading towards the origin, indicating decreasing intensity without change in direction. The stability spectrum corresponding to thermal demagnetisation is the blocking temperature spectrum and for AF demagnetisation it is the coercivity spectrum.

The differences in AF demagnetisation behaviour of acicular SD, small PSD and large MD magnetite is shown in Fig.7. The remanence that is being demagnetised is an artificially imparted saturation IRM (SIRM), produced by placing the samples in a very strong field. The plot shows the remanent intensity, normalised to the initial value before AF treatment, versus AF field. The corresponding coercivity spectra can be obtained from the demagnetisation curves by differentiation, as the coercivity spectrum is the magnitude of the slope of the demagnetisation curve. Thus the coercivity spectrum of the large MD grains peaks at low fields (less than 5 mT), the spectrum for the small PSD grains peaks at ~ 15 mT and that of the SD grains peaks above 40 mT. The Lowrie-Fuller test exploits the differences between AF demagnetisation behaviour of small and large grains. For SD and PSD grains weak field remanence, such as TRM, is more resistant to demagnetisation than strong field remanence, particularly SIRM. For true MD grains the relative stability of weak and strong field remanences is reversed.

Demagnetisation behaviour can be used to detect the presence of other magnetic minerals. For example, haematite is very hard (MDF > 1000 Oe) and does not thermally demagnetise until close to 670°C. Goethite has even greater coercivity than haematite, but breaks down to haematite at ~120°C, and is therefore very easily thermally demagnetised.

4.5 Thermomagnetic Analysis of Magnetic Mineralogy

The variation of magnetic properties of magnetic minerals with temperature depends on composition and, in some cases, on domain state and microstructure. This variation can therefore be used for analysis of magnetic minerals. The variation of susceptibility with temperature is particularly useful, because of the rapid change in susceptibility close to T_C, which enables well-defined Curie points to be determined, and because of the sensitivity of susceptibility to domain state and microstructure.

The characteristic susceptibility (k) versus temperature (T) behaviour of different magnetic minerals is shown in Fig.8. The k-T curve for paramagnetic minerals is hyperbolic, reflecting the 1/T dependence of paramagnetic susceptibility. The k-T curve of magnetite with MD structure, including PSD grains as well as true MD, grains is very diagnostic. There is a prominent peak at -155°C, which corresponds to the isotropic point of magnetite. Below this temperature the easy magnetisation directions are along the <100> cubic axes, whereas above it the easy directions lie along <111> body diagonals of the cubic unit cell. At the isotropic point the magnetisation rotates freely to align with an applied field, giving rise to an increase in susceptibility. The susceptibility of MD grains is limited by self-demagnetisation and the observed susceptibility remains almost constant until just below the Curie temperature, when it plummets to paramagnetic values. The isotropic point is very sensitive to composition and substitution of cations other than iron, or departures from stoichiometry, tend to lower the isotropic point. Titanomagnetites containing more than ~10 mole% ulvospinel have isotropic points below liquid nitrogen temperature. Thus

the presence of a well-defined peak at ~-155°C is diagnostic of the presence of nearly pure PSD and/or MD magnetite.

The titanomagnetite for which the k-T curve is shown has a Curie point of ~ 200°C and contains ~60 mole% ulvospinel. The k-T curve is irreversible on cooling from high temperature (not shown), due to exsolution of more magnetite-rich and magnetite-poor titanomagnetites than the original composition. Thus two Curie points, one above 500°C and the other shifted somewhat lower than the original T_C, would be seen in the cooling curve.

The k-T curve for SD magnetite does not exhibit a peak at the isotropic point because the properties of SD grains are controlled largely by shape anisotropy, rather than by magnetocrystalline anisotropy. The susceptibility is almost constant at low temperatures, but increases as the Curie temperature is approached. This increase in k reflects unblocking of fine grains below T_C.

The susceptibility of grains increases sharply at the unblocking temperature because the relaxation time suddenly decreases, allowing the magnetic moments of the grains to align freely with the applied field. Above the unblocking temperature the superparamagnetic susceptibility of grains of specified volume is proportional to J_s^2/T and is much higher than the room temperature susceptibility, until the Curie temperature is approached (at which point $J_s \rightarrow 0$, so $k \rightarrow 0$). Thus the presence of significant unblocking of remanence well below the Curie temperature indicates that this portion of the remanence is carried by very fine (submicron) single domain grains.

Even smaller grains unblock at much lower temperatures and exhibit superparamagnetism at room temperature. The k-T curve shown for SPM grains is idealised for an assemblage of identical grains. In rocks there is always a distribution of grain sizes and the superposition of unblocking peaks over a wide range of temperatures leads to a steady increase in susceptibility from below room temperature up to the maximum unblocking temperature of the ultrafine SPM + SD assemblage. This behaviour is commonly seen in soil samples, particularly lateritic soils.

As the Curie temperature of a magnetic mineral is approached, there is a rapid decrease in spontaneous magnetis-ation and an even more rapid decrease in magnetocrystalline anisotropy. As a consequence the remanence of even the most stable grains unblocks, but without an increase in k. In fact, the susceptibility plummets until it attains paramagnetic values at T_C.

Typical k-T curves of a monzonite containing only PSD/MD magnetite and a basalt containing only MD titaniferous magnetite are shown in Fig.9. The thermomagnetic curve of paramagnetic ilmenite separated from a beach sand deposit is depicted in Fig.10. The irreversibility of the curves for the basalt and the ilmenite extract indicates chemical change has occurred. This illustrates the sensitivity of k-T curves to changes, such as oxidation, exsolution and rehomogenisation, in magnetic minerals during heating.

Thermal demagnetisation of remanence provides another analytical technique. MD grains exhibit a spectrum of unblocking temperatures right up to T_C, whereas the unblocking temperature spectrum of SD grains cuts off below the Curie point. However, given that the grain size range of a particular mineral extends at least to the upper end of the SD range, the maximum unblocking temperature lies just below T_C. Thus Curie points can also be estimated from thermal demagnetisation data. Prominent

inflexions in the demagnetisation curve, corresponding to a sharp peak in the blocking temperature spectrum, indicate the approximate Curie temperature of a particular phase. Comparison of the blocking temperature spectra with k-T curves enable phases originally present in samples to be distinguished from phases created during heating. Low temperature demagnetisation also allows magnetic transitions characteristic of magnetite and haematite to be detected. Judicious application of a variety of rock magnetic techniques, including thermomagnetic analysis, allows the relative contributions to susceptibility and remanence of different compositions and grain size ranges to be estimated.

A variant of the traditional thermal demagnetisation of saturation remanence has recently been proposed by Lowrie (1990). This method involves saturating a specimen along one axis (the z-axis for this study), remagnetising in a field of lower strength along the y-axis, and finally applying a weaker field along the x-axis. The specimen then carries three orthogonal components, representing the highest coercivity fraction, an intermediate coercivity fraction and a low coercivity fraction respectively. Thermal demagnetisation of this remanence enables the unblocking temperature spectrum of each of these subsets of the magnetic grains to be determined simultaneously. This technique is particularly useful for detecting the presence of minerals of differing magnetic hardness (e.g. goethite, which is harder than haematite, but demagnetises below 200°C; haematite, which is harder than magnetite and demagnetises predominantly between 600°C and 670°C; magnetite, which demagnetises predominantly between 500°C and 580°C; and pyrrhotite, which may have comparable coercivity to magnetite (depending on grain size), but which demagnetises predominantly between 280°C and 320°C).

Thermomagnetic curves for a number of iron ore samples with different mineralogies are presented in Fig.11. The detection of MD magnetite, SD magnetite, haematite and maghaemite by thermomagnetic analysis is well illustrated by this collection of k-T curves.

4.6 Anisotropy of Magnetic Susceptibility (AMS)

When a material containing magnetic minerals (e.g. magnetite) is placed in an applied field, a magnetization is induced in it. If the applied field is weak, i.e. $\leq$10 Oersteds (Oe) (~0.0008 A/m), the component of the induced magnetization parallel to the field (M) is proportional to the field (H), with the coefficient of proportionality equal to the magnetic susceptibility k, i.e. k = M/H. In general, the value of the susceptibility depends on the direction in which it is measured, i.e. it is anisotropic. In anisotropic rocks the relationship between magnetization and applied field components is essentially linear and the low-field susceptibility can be expressed as a tensor k_{ij}, defined by

$$M_i = \Sigma k_{ij} H_j \quad (i,j = x, y, z)$$

The susceptibility tensor is symmetric ($k_{ij} = k_{ji}$, for all i,j) and can therefore be diagonalized. This means that it is possible to find three mutually orthogonal directions along which the applied field induces a magnetization parallel to itself. One of these directions corresponds to the maximum observable susceptibility k_1, another with the minimum susceptibility, k_3. The third direction is referred to as the intermediate susceptibility k_2. These are the principal susceptibilities.

The AMS may be represented by an ellipsoid (Fig. 12), known as the magnetic fabric ellipsoid, which is aligned with the principal susceptibilities. The maximum susceptibility axis defines the magnetic lineation. The magnetic foliation is the plane of relatively high susceptibility containing the maximum and intermediate susceptibility axes. The minimum susceptibility axis, which is orthogonal to the maximum and intermediate axes, is therefore the magnetic foliation pole. The AMS defines a magnetic fabric analogous to conventional petrofabric.

Various parameters are used to quantify the degree of anisotropy (A), the intensity of linear-parallel orientation (L), the intensity of planar-parallel orientation (F), the shape of the AMS ellipsoid. The parameters normally used are:

The anisotropy magnitude $A = k_1/k_3$

The magnetic lineation magnitude $L = k_1/k_2$

The magnetic foliation magnitude $F = k_2/k_3$

The shape factor which is defined as

$$T = 2(n2 - n3) / (n1 - n3) - 1 \quad \text{(Jelinek 1981)}$$

where n1,n2,n3 are the natural logarithms of the principal susceptibilities.

5.0 PETROGRAPHY

5.1 Introduction

A subset of thirty-eight samples were selected from the original collection of one hundred and eighty-eight samples for detailed petrographic examination and electron microprobe analysis. This subset was supplemented by a further eighteen samples collected as part of the Radiometrics project (AMIRA project P263). The lithologies covered by these samples are listed in Table 1.

5.2 Late Carboniferous

5.2.1 Roscow Granite (Cug)

The Roscow Granite crops out on the western margin of the study area and is comprised of two phases; a granodiorite enclosing a granite core. The granite is an alkali-feldspar microgranite comprised of strongly kaolinised alkali feldspar and quartz and displaying a hypidiomorphic-granular texture. The feldspar occurs as heavily kaolinised subhedral to anhedral equant to tabular grains. Although the severity of the alteration precludes optical recognition of the feldspar in most instances, the presence of plagioclase is indicated by the occurrence of rare relict albite twinning. The mafic minerals tend to occur in millimetre- sized aggregates consisting of anhedral scraps of altered biotite (partially replaced by chlorite) in association with less common altered hornblende and scattered subhedral to anhedral magnetite and ilmenite. Aplitic veining was also observed in one sample, the aplite consisting of a fine grained saccharoidal intergrowth of quartz and alkali feldspar.

The granodiorite phase is mineralogically variable and appears to grade from a quartz diorite on the margins of the intrusion to a monzongranite against the alkali-feldspar granite with decreasing

plagioclase and mafic mineral content and a concomitant increase in quartz and potash feldspar. Plagioclase occurs typically as coarse (5mm) subhedral-anhedral zoned grains giving the rock a weakly porphyritic appearence. Incipient sericitisation and kaolinisation is widespread. Anhedral flecks of biotite are common, becoming finer-grained and less abundant in the leucocratic facies. Zoned stout subhedral-anhedral amphibole is present in the mafic rocks and becomes scarce to absent in the granitic phases. The mafic minerals tend to occur in clumps in association with subhedral to anhedral magnetite and scarce ilmenite. Quartz and potash feldspar occur initially as sparsely distributed anhedral grains in the marginal quartz diorite, the potash feldspar tending to occur as subhedral to anhedral heavily kaolinised grains which become more abundant in the granitic phases. Coarse graphic intergrowths of quartz and potash feldspar are also more common in the granitic facies.

5.2.2 Sunbeam Granodiorite

The sole sample examined of this unit was a coarse, hypidiomorphic-granular quartz monzodiorite. Plagiclase occurs as coarse (1-5mm) euhedral to anhedral zoned tabular grains exhibiting incipient kaolinisation and sericitisation. Biotite is present as coarse anhedral flecks which tend to clump together in association with magnetite and less commonly amphibole. Coarse grained anhedral quartz is common and sparse potash feldspar is present as finer anhedral kaolinised grains.

5.2.3 Undifferentiated Intrusive Rhyolite (Cubpo)

All of the samples taken from this unit are of a quartz-feldspar porphyry, the origin of which is uncertain. Subhedral to anhedral embayed quartz phenocrysts (0.5-3.0mm) occur in association with altered, kaolinised, euhedral to subhedral feldspar phenocrysts (0.5-3.0mm). Microphenocrystic ?amphibole and less abundant ?biotite may have been present but are now pseudomorphed by chlorite and epidote. Epidote and chlorite also occur in anhedral patches and the former as finely granular material in the groundmass. Relict 100-300um subhedral ilmenite grains are sparsely distributed although primary magnetite is commonly replaced by sphene. The groundmass consists of potash feldspar, albite and quartz occurring in a finely granular intergrowth although one example of a felted intergrowth was observed. Occasionally a spherulitic groundmass texture is well developed with the spherules appearing to show preferential nucleation on feldspar phenocrysts and quartz phenocrysts being rimmed by chalcedonic silica. Calcite is rarely present in the groundmass occurring as anhedral "lakes".

5.2.4 Intrusive Rhyolite (rhl)

Of the two samples from this unit the one collected at the Battery Hill prospect (sample 112302, site 34) has also been ascribed to the Ukalunda Beds but its petrological affinities would suggest that is from the Stones Creek Formation. The other sample is a quartz-feldspar porphyry containing sparse euhedral to subhedral, rounded 1mm quartz phenocrysts, some of which are embayed. Altered euhedral to subhedral coarse (3-5mm) feldspar phenocrysts are also present, some of which are dusted with fine ?goethite. Subhedral bleached biotite grains occur as smaller (0.5mm) microphenocrysts, commonly associated with feldspar phenocrysts. The groundmass consists of fine (0.12mm) equant grains of quartz and alkali feldspar. Goethite veins are also present and finely granular ?hematite forms partial rims on

some altered biotite microphenocrysts.

The other sample (sample 109544) is of a brecciated quartz feldspar porphyry cemented by chalcedonic silica. Under the microscope the clasts can be seen to contain 0.5 to 1.0mm long broken and embayed quartz grains and subhedral 0.5 -1.0mm altered feldspar crystals both set in an altered vitroclastic groundmass pseudomorphed by quartz and alkali feldspar and heavily dusted with finely granular iron oxide (?hematite). This lithology is characteristic of the Stones Creek Formation and the allocation of this sample to either the Ukalunda beds or an intrusive rhyolite unit is incorrect.

5.2.5 Ferndon Volcanic Group

5.2.5.1 Bulgonunna Volcanic Subgroup

5.2.5.1.1 Locharwood Rhyolite (Cubib).

The Locharwood Rhyolite characteristically contains subhedral to euhedral coarse (0.5-1mm) embayed quartz crystals and altered subhedral to euhedral feldspar laths, most of which appear to have been plagioclase, set in a fine grained devitrified groundmass of intergrown quartz and potash feldspar. Lithic fragments are common and in some instances are of stretched and flattened pumice fragments (fiamme) which give the appearance of flow banding. In some instances a well defined eutaxitic texture is displayed. Alteration is common, patchy calcite and siderite selectively replacing lamellae in the lithic fragments which are also commonly dusted with fine-grained hematite. The textures displayed are typical of ignimbrites (welded ash-flows) and the unit can best be described as a crystal-lithic rhyolitic ignimbrite.

5.2.5.2 Smedley Volcanic Subgroup

5.2.5.2.1 Dacitic Ignimbrite (Cvi).

This unit is characterised by the presence of abundant euhedral to subhedral plagioclase and minor potash feldspar crystals varying in size from 0.1 to 3.mm and a variable content of subhedral embayed quartz phenocrysts which are absent from some samples. Relict prismatic amphibole microphenocrysts (0.1- 1.0mm) are present, in some instances showing incipient marginal chlorite alteration. Chlorite is also present in some samples pseudomorphing a microphenocrystic mafic phase, possibly clinopyroxene. Microphenocrysts of subhedral to anhedral (0.1-0.3mm) magnetite and ilmenite are sparsely distributed. Very finely granular iron oxides also occur as a dusting along cleavage and fracture planes in some altered feldspar grains and rarely in association with chloritic alteration. Lithic fragments are common and in many instances are deformed. The groundmass frequently displays a eutaxitic texture which mimics flow banding and is pseudomorphed by a fine, equigranular quartz/alkali feldspar intergrowth. In some samples a eutaxitic texture is not evident but the outline of glass shards may be recognised. The principle variation observed is in total phenocryst content, quartz/feldspar phenocryst ratio and grain size of phenocrysts and lithic fragments. Alteration is generally minor but in some samples feldspar is sericitised in association with minor kaolinisation and all mafic minerals are replaced by chlorite which becomes brownish due to oxidation and replacement by ?smectite.

One sample (sample 112287, site 6) from the southern portion of the outcrop is distinctive both texturally and in the severity of the degree of alteration. Coarse (0.5-3.0mm) subhedral plagioclase is less abundant and is strongly sericitised and also partially replaced by carbonate. Rare microphenocrystic mafics are pseudomorphed by chlorite which occasionally occurs in association with calcite. Secondary hematite and goethite are also associated with some mafic mineral alteration, the latter possibly being a result of weathering. subhedral microphenocrysts (0.1-0.3mm) of altered magnetite and ilmenite are scattered through the sample. The groundmass consists of finely granular intergrown quartz and alkali feldspar dusted with fine altered magnetite. Minor patches of calcite are also present in the groundmass. There is no evidence of a pyroclastic origin of this sample which appears to be of a severely altered porphyritic dacite flow.

5.3 Late Devonian -Early Carboniferous

5.3.1 Stones Creek Formation

5.3.1.1 Undivided Volcanics (DCV)

The sample collection is dominated by rhyolitic lavas and ash-flow tuffs with subordinate andesitic lavas and pyroclastics. All samples have been altered to varying degrees, although in most cases the primary textures and mineralogy may be discerned.

The rhyolitic lavas contain subhedral to anhedral, embayed phenocrystic (0.5-3.0mm) quartz and turbid, altered, euhedral to subhedral feldspar phenocrysts (0.5-3.0mm). A subhedral, phenocrystic (0.5-1.0mm) mafic phase is pseudomorphed by chlorite and epidote, both of which also occur in the matrix, chlorite often rimming epidote. Subhedral, altered magnetite and ilmenite microphenocrysts (0.1-0.4mm) are scattered through a groundmass of finely intergrown quartz and potash feldspar. In one severely altered and brecciated sample (sample 112305, site 45) feldspar phenocrysts are almost wholly replaced by illite which is also replacing sparse microphenocrystic biotite and the groundmass is extremely turbid, being almost opaque. The clasts are cemented by a network of chalcedonic silica.

The rhyolitic ash-flow tuffs are characterised by the presence of subhedral, embayed quartz phenocrysts (0.5-2.0mm) and euhedral to subhedral feldspar(plagioclase and potash feldspar) phenocrysts (01.0-2.0mm). The faint outlines of lithic fragments may also be determined in a groundmass composed of a coarse equigranular intergrowth of quartz and potash feldspar. Scattered altered, subhedral magnetite grains are present and areas of the groundmass are rendered almost opaque by the occurrence of abundant finely granular hematite. Calcite is present in some samples, occurring in the groundmass and as lenticular "lakes". In more severely altered samples feldspar may be replaced by calcite and illite and the groundmass is dominantly quartz/illite with the occurrence of lenticular chalcedonic silica patches. Rarely a spherulitic texture is exhibited with the spherules apparently nucleating preferentially on feldspar. Chlorite is rare, being present in only one sample. Most samples appear to be ignimbritic although in one case possible undeformed shards could be faintly discerned, indicative of an unwelded ash-flow tuff.

Only one example (sample 109542) of a porphyritic andesite was identified, being comprised of turbid euhedral to subhedral

plagioclase phenocrysts (0.3-3.0mm), which tend to form glomeroporphyritic aggregates, frequently in association with altered subhedral phenocrystic (0.2-1.0mm) mafics (?clinopyroxene). Chlorite replaces the mafic phases and is also partially replacing feldspar. The groundmass is a fine intermixture of quartz and alkali feldspar.

An intensively altered sample (sample 112289, site 9) may be of an altered andesitic pyroclastic although the primary textures and mineralogy have been largely obliterated, rare microphenocrystic (0.5mm) quartz being the only remaining primary phase. The shadowy outlines of euhedral to subhedral phenocrystic (0.5-1.5mm) feldspar are preserved and ghosts of altered lithic fragments may be discerned. The groundmass consists of a strongly inequigranular intergrowth of quartz and potash feldspar with the occurrence of coarse, ameboid patches of chalcedonic silica. Chlorite is patchily distributed throughout the matrix along with rare subhedral, altered magnetite grains (0.2mm) and finely divided ?hematite forms irregular trails in the matrix. A similar sample (sample 112304, site 40) appears to be more acidic, phenocrystic (0.5-1.0mm), subhedral, embayed quartz being slightly more abundant. Feldspar has been replaced by calcite and faint outlines of lithic fragments may be observed. As in the previous samples chalcedonic silica is present in ameboid patches and also forms irregular veinlets.

One example (sample 112292, site 13) was noted of a strongly altered pyroclastic in which no primary textures may be observed microscopically, although its fragmental nature is evident in the hand specimen. Microscopically the sample consists of clasts replaced by a fine quartz-illite intergrowth sparsely distributed in an opaque matrix of hematite formed by the aggregation of fine particles.

5.3.1.2 Andesitic Volcanics (DCv_A)

Euhedral to subhedral plagioclase phenocrysts (0.5-3.0mm) are common and in some samples are badly fractured and kaolinised with chlorite occurring as a patchy alteration product or selectively replacing cores. Rarely relict amphibole phenocrysts (0.5-1.0mm) are present but commonly mafic phases are pseudomorphed by chlorite and epidote. Subhedral microphenocrystic (0.1 0.3mm) magnetite and ilmenite are ubiquitous. The groundmass is texturally and compositionally variable. One variant is a coarse (0.1-0.2mm) intergrowth of equant quartz and potash feldspar and another is comprised of fine felted plagioclase dusted with fine (10um) subhedral to euhedral magnetite in which spherulitic and concentrically zoned chlorite fills cavities.

One unusual sample (sample 109550) contained abundant subhedral to euhedral feldspar phenocrysts (0.2 -1.5mm) which are extensively kaolinised and sericitised. Many phenocrysts are also fractured. Epidote is common, forming 0.2-1.0mm anhedral granular aggregates and pseudomorphing rare microphenocrystic mafics. Rare calcite and chlorite form small anhedral patches in the groundmass. The groundmass is variable, in some places consisting of an intergrowth of equant quartz and potash feldspar as described above and in others of abundant fine plagioclase with intergrown ?chlorite. The strongly inequigranular nature of the sample and the occurrence of broken feldspar suggests that the sample may be of a flow breccia.

5.3.1.3 Undivided epiclastics (DCVs)

Of the three samples examined from this unit two are of tuffaceous origin while the third is of an andesitic volcanic which would appear

to have been miscorrelated. The two tuffaceous samples are texturally similar, both containing 0.5-1.0mm anhedral, subangular to subrounded quartz grains with rounded and embayed grains being present in sample 112058 (site 79). Turbid brown, coarse (0.5 3.0mm) illitic patches are common, possibly pseudomorphs of feldspar. The matrix is a fine intermixture of quartz and illite dusted with goethite in sample 112058 (site 79) which also contains patches of coarser chalcedonic silica, occasionally forming small veinlets. Sample 112057 (site 79) contains faint ovoid structures 1.0-4.0mm across distinguished by differing proportions or grain size of quartz and illite pseudomorphs and frequently rimmed by clear illite which are possible chalazoidites.

Sample 112059 (site 79) contains ghostly outlines of turbid, almost opaque, strongly altered subhedral feldspar phenocrysts varying from 1.0-3.0mm in grain size. Primary subhedral microphenocrystic (0.5mm) mafics are pseudomorphed by chlorite and epidote which also occur as anhedral patches associated with altered feldspar phenocrysts and distributed throughout the groundmass. The groundmass consists of quartz, albite and calcite which pseudomorph stumpy matrix feldspar and still preserves evidence of an original spherulitic texture. The sample is of an altered andesitic flow and would appear to have been miscorrelated.

5.4 Late Devonian

5.4.1 Mount Wyatt Formation

Of the five samples examined from this unit only one could be confidently ascribed to it the others clearly being of a volcanic origin. The one definite sample is of a tuffaceous siltstone containing sparse subrounded to subangular quartz grains set in a fine matrix of albite, potash feldspar and ?cristobalite. Fine (10 μm) ?goethite grains are dusted through the matrix.

The other samples are of altered ash-flow tuffs and should probably be correctly ascribed to the Stones Creek Formation. One is of uncertain origin, consisting of finely intergrown quartz, illite and potash feldspar. Veinlets of goethite and manganese oxides are common and elongate rutile grains are dispersed through the sample. No primary volcanic texture can be discerned and the sample may be of an altered obsidian.

One of the ash-flow tuffs contains both rounded and embayed quartz phenocrysts (0.2-1.0mm) in conjunction with angular, broken grains. Similarly subhedral to anhedral feldspar phenocrysts (0.2-0.6mm) have a similar mode of occurrence. Both potash and plagioclase feldspar are present and are heavily altered, being kaolinised and sericitised also with patchy calcite alteration of plagioclase. Rare bleached biotite microphenocrysts are also present. The groundmass consists of intergrown quartz, potash feldspar and illite which are also pseudomorphing lithic fragments and deformed lenticular pumice. Well preserved undeformed shards are pseudomorphed in the groundmass. Secondary goethite /hematite is present in the groundmass and replacing primary magnetite. In another similar sample the phenocryst content is dominated by heavily altered feldspar, quartz being practically absent. Lithic fragments are also less common and the faint outlines of shards may occasionally be discerned in the groundmass. Alteration of the oxide minerals is also less intense, being confined to development of a fine dusting of ?goethite in the adjacent groundmass. The remaining sample is of an altered ignimbrite

containing scattered rounded and embayed quartz phenocrysts (0.5-2.0mm) and the ghostly outlines of intensively altered turbid feldspar (possibly including both potash feldspar and plagioclase) phenocrysts (0.5-2.0mm). Pumiceous lithic fragments are abundant and are replaced by a coarse intergrowth of quartz and potash feldspar. The faint outlines of deformed shards may occasionally be discerned in the matrix.

5.5 Middle Devonian

5.5.1 Ukalunda Beds

Two samples were collected from this unit, one from the western margin of the study area and the other from the north at the Battery Hill prospect (Fig.2). Both samples are of ash-flow tuffs and thus have been misidentified as Ukalunda Beds, most probably belonging instead to the Stones Creek Formation. The sample (sample 112293, site 40) from the western margin is of a rhyolitic ash-flow tuff containing 0.5-2.0mm long subhedral to anhedral, rounded and embayed quartz grains set in a turbid vitroclastic groundmass pseudomorphed by a quartz/alkali feldspar intergrowth. Epidote is common and appears to be pseudomorphing feldspar. Ghostly relics of deformed pumiceous fragments and sparse 0.1-0.2mm subhedral magnetite grains are present.

The other sample (sample 112303, site 38) from the Battery Hill prospect is of an andesitic ignimbrite which contains abundant 0.5-2.5mm subhedral altered plagioclase set in a turbid, flow banded matrix consisting of a quartz/alkali feldspar intergrowth dusted with fine iron oxide (?hematite) and occasional patches of siderite. Sparse chlorite is present pseudomorphing microphenocrystic ?amphibole and rare subhedral magnetite crystals are also present. Flattened and deformed pumiceous lithic fragments are common.

6.0 MAGNETIC SUSCEPTIBILITY: ITS VARIATION WITH GEOLOGY AND THE DEGREE OF ALTERATION

Stones Creek Formation (DCv)

The susceptibility of the DCv volcanic units is generally low (0 - 100 μG/Oe [0 - 0.00126 SI]) except for samples from six of the sites (89, 8, 9, 37, 38 and 10 which have susceptibilities greater than 100 μG/Oe [0.000126 SI] but less than 1500 μG/Oe [0.0189 SI] (Table 2, Fig. 13). The three sites (9,37,38) which record the highest susceptibilities are all andesites, whereas all the sites where a low (<100 μG/Oe [0.00126 SI]) susceptibility is observed are all rhyolitic (see Tables 1 & 2). The susceptibility of the DCv_A unit (andesitic) is high, with susceptibilities greater than 1600 μG/Oe [0.02 SI] (see Fig. 14). The susceptibility of this andesitic unit is higher than the susceptibility of the other andesitic flows sampled from the Stones Creek Formation (DCv). Close to the Bluegum prospect a mapped fresh rhyodacite (site 62) has a moderate susceptibility (462 μG/Oe [0.0058 SI]) and is most likely part of the DCv or possibly the DCv_A unit. The measured susceptibilities of the DCv volcanics agree with the low magnetic response which is observed over them (Fig. 4A), as does the high response observed over the high susceptibility DCv_A andesitic unit (i.e. the topmost magnetic high in Fig. 4A).

Within the Stones Creek Formation it is apparent that andesitic flows (volcanic and pyroclastic) have higher susceptibilities than rhyolitic flows. The DCv_A andesitic unit has the highest susceptibilities, but the degree of alteration (see sections 5.3.1.2 & 9.5.1) is not as great as

with the andesites from the DCv volcanics. This may have arisen because of variable degree of alteration of the Devonian units, although the illitic/potassic alteration appears widespread (see sections 5 & 9) or because the DCv_A unit is Carboniferous in age and thus has not suffered the same degree of alteration. The susceptibilities of the CVi dacitic ignimbrites and the DCv_A andesites are similar, (Fig. 14) this supporting a Carboniferous age for the unit.

Smedley Volcanics (CV_i)

Samples from the CV_i unit have susceptibilities greater than 800 μG/Oe [0.01 SI] with the exception of site 58 (Table 2, Fig. 14). The samples with the lowest susceptibility (sites 58 & 6) are from altered volcanic flows (see section 5) with intense alteration having occurred to samples from site 58. The aeromagnetic anomaly associated with the CV_i ignimbrites is quite distinct (Fig. 4A) with zones of very high response as well as zones of very low response. Samples from both the high (e.g. site 5, Table 2) and the low regions (e.g. site 1, Table 2) have high susceptibilities indicating that non-magnetic rocks are not the explanation for the magnetic lows. The ignimbrites sampled beneath the magnetic lows (i.e. sites 1,3,4,57) have Koenigsberger (Q) ratios greater than unity (Table 2) and this coupled with a steep down remanence (Table 3, Fig. 17) results in a total magnetization which is down and opposite in sense to the induced component. Thus the strong magnetic lows observed within the anomaly associated with the CV_i volcanics result from reversely magnetized ignimbrites whose Q ratios are greater than unity. The embayment of CV_i into the Cub_{rh} rhyolite to the south of sites 57 and 3 (see Figs. 3 & 15) has a magnetic signature similar to the Cub_{rh} rhyolite rather than the strong magnetic anomaly which is observed over the remainder of the CV_i unit. This coupled with a similar response observed in the radiometrics (Dickson and Scott 1991) suggests that the embayment is not part of the CV_i unit.

Samples from two sites (54, 55) from the intrusive rhyolite (Cubpo) south of the sampled CVi flows have low (<50 μG/Oe [0.0006 SI]) susceptibilities. This agrees with the low magnetic response which is observed over the Cubpo rhyolite (Fig. 4A). As with the Devonian volcanics, the susceptibility of the dacitic units (CVi) is greater than that of the rhyolitic units sampled.

At the Burdekin Falls Dam, some samples (20,21,25, Fig. 2) were taken from the "the Dam Ignimbrite" which is part of the northwest Smedley Volcanic Subgroup. Moderate (500 μG/Oe [0.0063 SI]) to high susceptibilities (2300 μG/Oe [0.0289 SI]) were measured, these values similar to the CVi ignimbrites sampled around the Conway-Bimurra area. Also, some samples (64-69, Fig. 2) were taken from the Bulgonunna Volcanic Subgroup which is also part of Ferndon Volcanic Group and unconformably overlies the Smedley Volcanic Subgroup. The susceptibility of the Bulgonunna rhyolites ranged from 100 μG/Oe [0.00126 SI] to ~2000 μG/Oe [0.0251 SI]. This variation is dissimilar to what is observed in the Conway-Bimurra area where the Carboniferous volcanics generally have a consistently high (>1000 μG/Oe [0.0126 SI] susceptibility.

Other Palaeozoic units

The susceptibility of samples (sites 48,49,51, Fig. 3) of the sedimentary Mount Wyatt Formation (Dum) is low, usually less than 100 μG/Oe [0.00126 SI]. Two sites (50 & 52) which were sampled in the "mapped" Mount Wyatt Formation are volcanic and most likely are part of the DCv unit. One sample from site 52 has a susceptibility of ~1500 μG/Oe [0.0188 SI]. As well, a basalt sampled by Bruce Dixon (~200m South

of site 50, see Figs. 3 & 15) also has a high susceptibility (~2000 μG/Oe [0.025 SI]. The low susceptibilities of the Mount Wyatt sediments sampled cannot explain the aeromagnetic anomaly which is observed (Fig. 15) over part of the Formation. The basalt sampled by Bruce Dixon and the single sample from site 52 have susceptibilities strong enough to explain the anomaly if they outcrop over a large enough area. The age of the basalt is not known. A further possibility is that a Late Carboniferous intrusive lies beneath the Formation. The mapped Mount Wyatt Formation in the north of the area (Fig. 4A) has a weak magnetic signature except in the southwest where a magnetic high is observed. This magnetic high may be related to an uncovered part of the Roscow Granite which outcrops to the immediate west and has a strong magnetic high associated with it.

The Roscow Granite is split into a granite member and a granodiorite member (Fig. 3). The susceptibilities of the granodiorite member are greater than 3000 μG/Oe [0.038 SI] while the granite member has susceptibilities of about 2000 μG/Oe [0.025 SI]. This division is not so obvious with the aeromagnetics although the magnetic highs tend to be over the granodiorite member.

Prospects

Figure 14 shows a histogram of the susceptibility of rocks from within the zones of intense adularia-sericite hydrothermal alteration at the prospects. It is apparent that the susceptibility of the samples is very low with eight samples having diamagnetic susceptibilities and only two samples having susceptibilities greater than 20 μG/Oe [0.00025 SI]. The rock types ranged from silicified rhyodacites and sediments to clay altered volcanics. For comparison, sites 37, 38, (both andesitic flows) were sampled close (<100 m) to the Battery Hill prospect and have susceptibilities greater than 500 μG/Oe [0.0063 SI] (see Table 2). In the paper by Irvine and Smith (1990) an "alteration" filter (Fig. 4B, their Fig. 3C) has been applied to the magnetics data set (Fig. 4A, their Fig. 3A) resulting in a "flat" magnetic response over the Bimurra and Conway alteration systems. They relate this to magnetite destruction in the areas of hydrothermal alteration. The susceptibility of samples from the prospects clearly supports this conclusion, with very low susceptibility observed in all samples taken. However, samples just outside the most intense alteration still retain reasonably high/variable susceptibility and would contribute far less to a magnetic "flat" zone.

7.0 REMANENCE AND PALAEOMAGNETISM

The natural remanent magnetization (NRM) of the Carboniferous CVi pyroclastic flows ranges from moderate to high (300 μG [mA/m] to 5000 μG [mA/m]) (Table 2, Fig. 13) with the Koenigsberger ratio (Q) of samples from five of the sites being greater than unity (Table 2). Four of the sites sampled (1,3,4,57) are from beneath two magnetic lows (central east of area, Fig. 4A). The high Q ratios coupled with the positive inclination of the NRM's results in a magnetization with a positive inclination and this explains these strong magnetic lows. The aeromagnetic texture within the lows is similar to that within the magnetic highs (best seen with contour maps rather than colour images, see Fig. 4A), but the dominant magnetization direction results in a lower magnetic base level rather than that in the remainder.

The NRM of the DCv flows is low, usually less than 200 μG [mA/m] and generally less than 10 μG [mA/m] (Fig. 12, Table 2). However, the NRM of the andesites (sites 9, 37, 38) is higher with a range of 200 - 1000 μG

[mA/m] (Fig. 12). The Q ratio is generally less than unity with the exception of the four pyroclastic flows sampled at sites 13, 14, 84 and 90 (see Table 2). The Q ratio of the two northern andesites (sites 37 & 38) is also greater than unity. The sites with higher NRM's are also the sites with the higher susceptibilities.

The NRM's of the Roscow Granite (sites 15-18) and other Carboniferous granites (sites 19 & 64) are high but usually have Q ratios less than 0.5. Two samples from the granodiorite member of the Roscow Granite did have Q ratios of ~3.0. Similarly the NRM's of the andesites of the DCv_A are high (~1000 μG [mA/m]) but have Q ratios close to unity. The andesite flow sampled at site 31 is dissimilar and has a NRM of ~4000 μG [mA/m] and a Q of ~5.0. As with the susceptibility, the NRM of the DCv_A unit is dissimilar to the other volcanics of the Stones Creek Formation.

The NRM of samples from the Mount Wyatt Formation are low (<10 μG [mA/m] as are those sites sampled within the prospects. Most of the samples from the prospects are diamagnetic and any remanence measured is associated with recent haematite/goethite weathering. Two samples, one from the Conway Prospect (site 40) and one from the Bluegum prospect (site 61) retained a more ancient magnetization.

Thermal Demagnetization

At least two specimens from each sample were subjected to detailed thermal demagnetization. Samples were progressively heated with steps of 200°C, 300°C, 350°C, 400°C, 450°C, 500°C, 525°C, 550°C, 575°C and if required 600°C, 630°C, and 670°C. The prevalent magnetization direction observed in most rock units sampled is steep and down (Fig. 16 & 17, Table 3). Figure 16 shows orthogonal plots from representative specimens from all the major units found in the area.

The two examples from the CVi pyroclastics (A,B, Fig. 16) show very steep down directions with the sample from site 3 (Fig. 16B) having a small viscous component in accordance with the strong magnetic low resulting from the remanence dominated pyroclastic flow. Examples (C-H, Fig. 16) from the DCv flows also display this steep down direction, the magnetization generally held in magnetite except for some samples which also hold the magnetization in haematite (D, G, Fig. 16). Some samples show the steep direction as an overprint with a higher temperature component which is shallow and to the west (see Fig. 16I). In most cases where the steep down direction is observed as an overprint the higher temperature "primary" direction could not be resolved. The pyroclastic flow sampled at site 53 clearly shows the steep overprint as well as a well defined shallow up northeast direction (Fig. 16J). Samples from site 84 (see Fig. 16K) do not show the overprint but only show a small viscous component and a "primary" shallow up southwest component. Two samples from within the hydrothermal alteration zones of the prospects (see L, M, Fig. 16) also show the steep down direction, with the magnetization held by magnetite. The sample (Fig. 16N) from the DCv_A andesite also shows the steep down direction but is overprinted by a north moderate up direction (dipole field). Similarly the two Roscow Granite members (see O & P, Fig. 16) also show the steep down direction and have a dipole field overprint. The sample from the Carboniferous rhyolitic phorphry (Fig. 16Q) only displays the steep down direction. Two samples from ~ 30 m south of the area (sites 95 & 96, see Appendix I for grid reference) which are mapped as Carboniferous volcanics (Hutton et al 1989) do not show a steep down direction (R, S, Fig. 16) but rather a southwest shallow down direction. This shallow direction indicates an older age for the volcanics. This concurs with the more altered appearance of the flows (see section 9.3) indicating a volcanic

which is part of the Devonian sequence. Two samples (T, U, Fig. 16) from the Dam Ignimbrite (also part of the Smedley volcanic subgroup) near the Burdekin Dam clearly show the steep down direction. One sample (Fig. 16V) from the Bulgonunna volcanics also shows a steep down direction, although the inclination is not as steep as those observed near Conway-Bimurra.

The dominant direction observed in both the Carboniferous and Devonian units is steep and down. Figure 17A shows the stereographic plots of the site mean directions for the Carboniferous volcanics and intrusives, while figure 17B shows the mean directions from the Devonian volcanics. The direction observed in the Devonian units is clearly an overprint with some samples still retaining an older direction (see Fig. 16I, J, K). The Late Devonian direction for Australia is shallow and to the southwest (Li et al 1988), this being observed in the pyroclastic flow at site 84 (Fig. 16K) and site 53 (opposite direction, Fig. 16J). The mean direction obtained from the Carboniferous units is Dec = 204.8°, Inc = 78.6° (N = 12, α_{95} = 9.6°, K = 21) (see Table 3) while that obtained from the Devonian lithologies is Dec = 193.7°, Inc = 79.4° (N = 20, α_{95} = 8.1°, k = 17) (see Table 3). The two mean directions are indistinguishable (Figs. 17A, B emphasise this) and thus the entire data set has been combined (Fig. 17C), resulting in a mean direction of Dec = 198.1°, Inc = 79.2° (N = 32, α_{95} = 6.0°, k = 19). This direction results in a south palaeomagnetic pole of 40.6°S, 139.0°E (dp = 10.9°, dm = 11.4°).

The steep down direction observed in the volcanics and intrusives of the Conway-Bimurra area is very similar to the Permo-Carboniferous magnetization observed at Mount Leyshon (Lackie et al 1991). The resultant palaeomagnetic pole plots on the Australian Apparent Polar Wander Path (APWP) very close to pole from the Mount Leyshon complex (DCV & MTL, Fig. 18). This indicates that the magnetization of the Conway-Bimurra area is penicontemporaneous with the Smedley Creek Volcanics.

8.0 MAGNETIC MINERAL CHARACTERIZATION

Magnetic mineral characterization was carried out on selected samples of the Devonian and Carboniferous volcanics, other Palaeozoic units and samples from the prospect's zones of strong alteration. For samples with moderate to high susceptibilities (> 100 μG/Oe [0.00126 SI]) low-field susceptibility versus temperature (k-T) curves were performed. Lowrie tests (Lowrie 1990) were performed on selected low susceptibility (< 100 μG/Oe [0.00126 SI]) samples as well as representative samples with higher susceptibilities. More detailed descriptions of the techniques are shown above in section 4.0 of this report. For this study specimens were saturated (~10,000 Oe) along the Z-axis, given an intermediate remanence (200 - 1000 Oe) along the x-axis and given a weak (<200 Oe) remanence along the y-axis of the specimen. Where possible, samples for which k-T curves and/or Lowrie tests were run were also studied petrologically. Figures 19 and 20 show all the k-T and all the Lowrie test results respectively.

Thermomagnetic Curves

Most of the CVi volcanic units sampled have high susceptibilities (Fig. 14) and thus are amenable to running k-T curves. Seven K-T curves from samples of the CVi flows are displayed over the first two pages (A - G) of figure 19. The curves reveal the presence of magnetites with variable titanium content. In all the samples the presence of end-member magnetite is evidenced by Curie Points of 580°C for the curves (see B in

Fig. 19C). Some samples show curves which continue to temperatures greater than 600°C (e.g. observe A in Fig. 19B) indicating the presence of cation-deficient magnetite. The unblocking of the magnetite usually begins at ~500°C indicating that a small percentage of titanium (2-5wt%) is present. The samples from the ignimbrites sampled at sites 2-5 all show inflexions of the heating curves at approximately -50°C which drop rapidly before levelling off at about 0°C (see C in Fig. 19D). Apon cooling the inflexion is reversible. This characteristic indicates the presence of a high titanium titanomagnetite (TM) such as TM80 (TM corresponds to $Fe_{3-x}Ti_xO_4$ which is denoted by TM(100x), Clark & Schmidt 1982) which would contain ~25wt% TiO_2. The heating curve of sample dcv02b3 (Fig. 19C) does not drop as rapidly as the other three and levels off at about 80°C indicating a larger spread of titanium percentages. Also, an irreversible "hump" is observed centred at about 300°C (e.g. see D in Fig. 19E) in all the samples except dcv02b3 this being caused by the presence of titanomaghaematite.

Five samples were able to be run from the Devonian volcanics (H-L, Fig. 19), three from pyroclastic flows (sites 8, 9, 84) and two from volcanic flows (sites 10,38). In four of the samples the main magnetic mineral present is end-member magnetite. Cation-deficient magnetite is observed in two of the pyroclastic flows (H & L, Fig. 19), while maghaemite (see E in Fig. 19H) is observed in four samples. In the fifth sample (site 8, a volcanic flow), titanomagnetite is observed as well as end-member magnetite. The isotopic point of end-member magnetite is not observed and a large "hump" is observed from ~150°C to ~500°C (see F in Fig. 19K) indicating the presence of titanomagnetite. The "hump" changes character after heating indicating a slight change in the magnetic mineral composition. Unlike the Carboniferous pyroclastic samples, no high titanium (TM80) titanomagnetites are observed. The volcanic flow of site 8 being the only sample with a titanomagnetite present (~TM20).

Three samples were run from the Roscow Granite, one from the granite member (Fig 19M) and two from the granodiorite member (N & O, Fig 19). All three curves show multi-domain end-member magnetite as indicated by the steep drop of the curve to the Curie Point of 580°C (see G in Fig. 19N) as well as the distinct isotropic point at ~-150°C (see H in Fig. 19N). The small irreversibility of the Hopkinson Peak observed in figure 19M indicates that a tiny amount (<1wt%) of titanium is present. The small irreversible "hump" on the heating curves (see I in Fig. 19N) indicates maghaemite.

One andesite sample (site 11) and rhyodacite sample (site 62) were run from the DCv_A unit (P & Q, Fig. 19). Both show end-member magnetite and maghaemite. The andesite sample shows a typical end-member magnetite Hopkinson Peak on the heating run, which becomes very spread on the cooling run (see J in Fig 19P) indicating that titanium has most likely entered the magnetite structure during heating.

One sample (site 20) was run from the Dam Ignimbrite, which is part of the northern Smedley Volcanic Subgroup. The curve (R, Fig. 19) shows the presence of end-member magnetite, maghaemite (irreversible "hump" on heating curve) and some cation-deficient magnetite (see K in Fig. 19R). Unlike the Carboniferous CVi ignimbrites from the Conway-Bimurra area, no substantial amount of titanium is present in the magnetite.

SIRM demagnetization, Lowrie Test

Lowrie tests were conducted on 17 specimens from the collection, the results being displayed in figure 20 and table 4. Initially the specimens were simply AF demagnetized, then were given a saturation

magnetization remeasured and then AF demagnetized. Following this the Lowrie test was carried out on the specimen.

Two samples from the CVi pyroclastics were studied. Both have high saturation remanence (Jr) values in the order of 100,000 μG [mA/m] which would correspond with the approximately one percent magnetite which can be inferred from the susceptibility of the samples (Table 2). Both have Median Destructive Fields (MDF) for the NRM greater than the corresponding MDF of the SIRM indicating that single domain (SD)/ pseudo-single domain (PSD) size (< 20 μm) grains dominate the remanence of the samples. The Lowrie test for both samples shows magnetite (see A, Figs. 20A & 20B) as well as cation-deficient magnetite (see B, Figs. 20A, B).

Eight samples from the DCv flows were studied (C-J, Fig. 20), three being volcanic flows (sites 81,82,47) and five pyroclastic flows (sites 84,85,9,14,63). The only sample to have a high Jr value (>100,000 μG [mA/m]) was the andesite from site 9, the remainder being significantly lower (see table 4). Magnetite was observed in all samples, while haematite also was observed in samples from sites 9 (Fig. 20C), 63 (Fig. 20F), 47 (Fig. 20E), 84 (Fig. 20I) and 85 (Fig. 20H).

One sample was selected from the DCv_A andesite (site 11, Fig. 20K) and one from the site 62 rhyodacite (possible DCv_A) (Fig. 20L). Both show the presence of magnetite.

Two samples from the intense andularia-sericite alteration zones of the Bimurra and Bluegum prospects show that some (although ppm) magnetite can survive in these zones (Fig. 20M & 20N). The SIRM of the samples (table 4) shows the scarcity of the magnetite (compare against sample 02A). The sample from site 62 still retains the Permo-Carboniferous overprint (Table 3) in the magnetite (Fig. 16L). Although the majority of samples from the prospects were diamagnetic, some have weak susceptibilities and are capable of retaining a remanence (as samples from site 62 show) and thus are capable of recording a remanence associated with the alteration event.

The sample from the Mount Wyatt Formation (Fig. 20O) shows the presence of goethite (see C in Fig. 20O) and magnetite (see D in Fig. 20O). Optically, only goethite is observed (see section 9.6). The MDF(NRM) is 3000 Oe (Table 4, Fig 20O) indicating that goethite is the dominant remanence carrier. The Lowrie plot shows that the high and intermediate (Z & X) coercivity goethite grains hold more than 60% of the remanence. Intermediate coercivity magnetite holds most of the remainder.

The magnetic mineralogy of the Roscow Granite (see section 9.1) is essentially coarse grained magnetite with minor haematite present in the granodiorite member. This is reflected in the low MDF(NRM) which is only 45 Oe (Table 4, Fig. 20P) indicating coarse multidomain magnetite. Similarly the Lowrie plot shows the soft magnetite unblocking by 300°C (E in Fig. 20P) and the remainder at 575°C. A small haematite presence is also observed (see expanded plot in Fig. 20P). The lowest coercivity (Y) grains are the dominant remanence carriers.

The Lowrie test on the sample from the northern Smedley Volcanic Subgroup Dam Ignimbrite (Fig. 20Q) shows the presence of maghaemite, cation-deficient magnetite and magnetite. This is in good agreement with the K-T curve (Fig. 19R) for the ignimbrite. The MDF(NRM) is greater than the MDF(SIRM) (Fig. 20Q, Table 4) indicating that single domain or PSD size magnetite is the main remanence carrier. This is reflected in the high (~2.0) Q ratio of the flow.

9.0 MAGNETIC MINERALOGY

9.1 Roscow Granite

The primary oxide phases in the mafic facies are titaniferous magnetite and minor ilmenite. The magnetite occurs as subhedral to anhedral grains, varying in size from 20-200μm, with most grains falling within the range of 70-200μm.The most common exsolution texture is a fine micron-scale cross-hatch exsolution in which the nature of the exsolved phase could not be ascertained. Many grains are unexsolved and others contain broad ilmenite lamellae pseudomorphed by pseudobrookite. Chemically most grains are of a mildly titaniferous magnetite with TiO_2 contents ranging from 0.5-8.0 wt% and most falling within the range of 3.0-5.0 wt% (Table 5). Minor vanadium and manganese are also present. Incipient maghemitisation is rare and grains of hematite are present, occurring as an alteration product of the mafic silicates. Ilmenite was present as discrete anhedral grains and as exsolution lamellae in magnetite but has been replaced by pseudobrookite containing minor manganese (2.0-3.0 wt% MnO).

Magnetite has a similar mode of occurrence in the alkali granite, although most grains fall within a narrower size range of 100-150μm and exsolved grains are rare. The composition is essentially end-member magnetite, containing only minor amounts (0.5 wt%) of titanium, vanadium, chromium and manganese. Ilmenite displays a similar habit and frequently exhibits marginal replacement by sphene. Chemically it is a manganoan ilmenite containing 19.0-20.0 wt% MnO (Table 5).

9.2 Intrusive Rhyolite

In spite of the apparent superficial uniformity of this unit differences exist in the iron-titanium oxide assemblage which must reflect subtle, primary bulk-compositional variation. In sample 109519 ilmenite appears to have been the sole primary oxide phase, occurring as euhedral to subhedral microphenocrysts (200-300μm) in which relict ilmenite is preserved in a matrix of sphene and rutile (Fig. 21). Chemically it is a manganoan ilmenite, the sole analysis obtained of an unaltered ilmenite showing the presence of 8.0 wt% MnO. Following the initial replacement by sphene and rutile the remanent ilmenite has been altered to pseudorutile which is managanese poor (1.0-6.0 wt% MnO).

In sample 109526 titaniferous magnetite was the dominant primary oxide phase with ilmenite being subordinate. The spinel occurs either as euhedral to subhedral microphenocrysts varying from 50-200μm in length or as subhedral to anhedral matrix grains with an average size of 10μm. The microphenocrysts may contains sparse fine ilmenite exsolution lamellae or coarse, irregular patches suggestive of replacement, rather than exsolution. Other grains display a complex relationship between spinel and ilmenite in which a core of spinel is being replaced by ilmenite, both of which in turn are partially enclosed by a rim of titanomagnetite which contains sparse fine ilmenite exsolution lamellae. Primary compositions are absent, all spinel being replaced by titanomaghemite containing 1.0-8.0 wt% TiO_2 (Table 5). Some groundmass grains have been replaced by goethite as a result of weathering.

Ilmenite commonly occurs in association with spinel as described above, although corroded microphenocrysts are present. Only one primary composition was noted, being of an end-member ilmenite. All other compositions are of pseudorutile, apart from one of a pseudobrookite. Rutile is also present as an alteration product of ilmenite.

9.3 Locharwood Rhyolite

A mildly titaniferous magnetite appears to have been the sole primary iron-titanium phase in this unit, originally occurring as subhedral microphenocrysts varying in diameter from 100-200μm. Titanium contents show a limited range of 6.0-7.0 wt% TiO_2 in association with minor (1.0-2.0 wt%) contents of aluminium, calcium and zinc (Table 5). All of the grains examined are severely altered, the primary titanomagnetite occurring as relics varying from 10- <1.0μm, some of which have been altered to titanomaghemite. The pseudomorphed grains typically have a calcitic core, rimmed by zoned siderite, working its way into the interior of the grain along cleavage and fracture planes (Fig. 22). Anhedral rutile is often present in the carbonate matrix. Rare magnetite relics have been replaced by goethite which may be a secondary feature related to weathering.

9.4 Dacitic Ignimbrite (Cvi)

The primary oxide assemblage in this unit was dominated by titaniferous magnetite in association with minor ilmenite. The spinel occurs as euhedral to subhedral microphenocrysts falling in the range 100-200μm and as fine (5μm) subhedral grains in the matrix. All grains have suffered maghemitization and display a narrow compositional range of 4.0-5.0 wt% TiO_2 and minor vanadium. manganese, silicon and aluminium contents (Table 5). In sample 112287 (site 6) which has suffered more severe illite/carbonate alteration the titanomaghemite has a greater compositional spread and contains from 8.0 to 22.0 wt% TiO_2, most analyses falling in the range 8.0-13.0 wt% TiO_2. Exsolution of ilmenite is also common in this sample. Both features reflect a primary compositional difference rather than being a consequence of the severity of alteration. Fine groundmass spinels in the ignimbrite may be replaced by goethite which also partially replaces phenocrystic spinel in the porphyritic dacite.

Within the ignimbrite ilmenite is typically present as euhedral to anhedral microphenocrysts with a size range of 100-700μm, although most grains lie within the range 100-200μm. Chemically it is a ferrian ilmenite containing 15.0 to 19.0 wt% Fe_2O_3 and minor (1.0-2.0 wt%) aluminium and manganese (Table 5). Patchy alteration to pseudorutile is present in some grains and very rarely replacement by pseudobrookite has occurred. The altered porphyritic dacite lacks coarse microphenocrystic ilmenite, the size range being from 60μm to 250μm. Primary ilmenite compositions are absent, being replaced initially by pseudobrookite followed by pseudorutile. Sporadic rutile is also present in the porphyritic dacite, apparently replacing titanomaghemite.

9.5 Stones Creek Formation

9.5.1 Andesite

Magnetite and less abundant ilmenite are both present, apart from sample 112301 (site 30) in which magnetite is the sole oxide phase. Magnetite in samples 112301 (site 30) and 109550 occurs as subhedral grains occupying two distinct size ranges, one from 40 to 250μm and

the other from 5 to 10μm whereas the dominant mode of occurrence in sample 112291 (site 11) is as subhedral microphenocrysts varying from 70 to 400μm which commonly contain ilmenite exsolution lamellae, tending to be concentrated on the grain margins. The coarser grains in sample 112301 (site 30) are frequently zoned and the finer grains are associated with the matrix and chlorite/epidote alteration of primary mafic minerals. Compositionally the magnetites are titanomagnetites (titanium contents varying from 1.0 to 145.0 wt% TiO_2) but those in sample 112301 (site 30) are distinctive in containing significant chromium (0.4-3.0 wt% Cr_2O_3) and sporadic high zinc (to 1.7 wt% ZnO) (Table 6). Minor (to 0.5 wt% V_2O_3) is present in those from sample 112291 (site 11). Marginal alteration to titanomaghemite is present in both samples 112291 (site 11) and 112301 (site 30) and more extensive replacement has occurred in sample 109550. Rare groundmass grains in sample 112301 (site 30) have been replaced by goethite, a result of weathering.

Ilmenite is present as subhedral grains, varying in size from 100-200μm and also as exsolution lamellae in titanomagnetite grains in sample 112291 (site 11). Fine exsolution lamellae of titaniferous magnetite occur in the subhedral ilmenite grains. Compositions are distinctive in both samples, those from sample 109550 containing moderate (7.0-9.0 wt% MnO) manganese, compared to the higher contents (22.0-26.0 wt% MnO) in sample 112291 (site 11) (Table 6). Apart from one analysis containing 17.0 wt% Fe_2O_3 ferric iron is absent in sample 109550 whereas ferric iron contents vary from 4.0 to 16.0 wt% Fe_2O_3 in analyses from 112291 (site 11). Alteration to an assemblage of rutile and sphene is pervasive in both samples (Fig. 23).

9.5.2 Epiclastics

Rutile is the dominant oxide phase in the tuffs, although limonite and goethite are common in sample 112058 (site 79). The typical occurrence is as euhedral to subhedral grains which vary in size from 50 to 300μm, although within any one unit the size range is much narrower, reflecting the efficiency of the sorting process. The grains often show a complex internal structure, due to a varying iron content and differing degrees of hydration. In sample 112058 (site 79) rutile is present as relics in a goethite matrix, which in turn is being replaced by limonite. In both instances rutile is clearly pseudomorphing primary iron-titanium oxides, which have also been replaced by secondary iron oxides. The origin of these secondary oxides is unclear as they may be the result of either the intense alteration (illite-sericite) or of weathering.

9.5.3 Undivided Volcanics

A variety of iron-titanium phases are present, reflecting the nature of the protolith, degree of alteration and the effects of weathering.

Primary oxides are absent in the altered rhyolites, all of which have suffered illitic or potassic alteration. Rutile is the most common phase, occurring as fine anhedral grains in illitised biotite and as possible pseudomorphs of primary ilmenite and titanomagnetite. Goethite is also common as a fine mesh-like vein and cavity filling and in sample 112306 (site 47), pseudomorphing euhedral titanomagnetite grains. Manganoan pseudorutile is present in sample 112306 (site 47) as subhedral to anhedral, spongy pseudomorphs of ilmenite.

The oxide parageneses observed in the altered andesite are essentially the same as described above for the andesitic unit (DCva), maganoan ilmenite being replaced by rutile and sphene and titanomagnetite by marginal titanomaghemite (Table 6). In one sample (sample 109542) pseudobrookite is present as a rare alteration product of ilmenite.

As in the epiclastic unit (DCvs) rutile is the most common oxide phase in the tuffs. In sample 112060 (site 80) which has undergone chlorite/calcite alteration primary titanomagnetite has been pseudomorphed by calcite containing fine, euhedral rutile. Marginal chlorite alteration has occurred in some grains and 1-10μm titanomagnetite relics have been almost completely replaced by titanomaghemite. Goethite/limonite pseudomorphs after pyrite (due to weathering) are also present in this sample. Titanomaghemite is still present in samples which have undergone illitic alteration, occurring as pseudomorphs of titanomagnetite and as granular aggregates, clearly of secondary origin.

The rhyolitic ash-flow-tuffs show the greatest variability. Where illitic alteration has occurred, primary titanomagnetite has been pseudomorphed by goethite and limonite which still preserve the primary exsolution textures and, in one instance, a primary titanomagnetite has been replaced by kaolinite, but fine ilmenite exsolution is still evident. Rutile occurs as an alteration product of ilmenite and also as fine grains formed during the illitisation of biotite. Relict primary ilmenite has been replaced by pseudorutile. Where milder potassic alteration has occurred primary microphenocrystic titanomagnetite has been replaced by titanomaghemite and undergone peripheral replacement by rutile (Fig. 24). Finer groundmass maghemite has been replaced by goethite. Ilmenite shows patchy rutile alteration and relict ilmenite has been replaced initially by pseudobrookite followed by pseudorutile. Biotite is frequently replaced by fine rutile and weakly titaniferous maghemite.

9.6 Mount Wyatt Formation.

Goethite is the sole oxide phase recorded in the one sample which can be confidently ascribed to this unit. It occurs as fine grains which aggregate to form a mesh-like structure and in rarer colloform grains, possibly pseudomorphing pyrite. The fine grains typically contain 3.0 wt% Al_2O3 and 9.0wt% SiO_2 whereas those pseudomorphing ?pyrite lack significant aluminium and contain approximately 5.0 wt% SiO_2.

10.0 CONCLUSIONS

(i) At Conway-Bimurra, Late Devonian acid volcanics, which are prospective for epithermal gold, are difficult to distinguish from non-prospective Late Carboniferous acid volcanics. On a regional scale the aeromagnetics show a reasonable correlation with the mapped geology. The Carboniferous units are distinctly more magnetic and can therefore be distinguished using aeromagnetics.

(ii) There is a pervasive propylitic alteration in both the Carboniferous and Devonian volcanic suites, the intensity greater in the latter. Within the Devonian sequence, zones of more intense adularia-sericite hydrothermal alteration, typical of mineralised epithermal systems, occur locally.

(iii) Within the Devonian volcanics intense adularia-sericite alteration centres show up as very smooth, flat magnetic zones, reflecting magnetite destruction. Within these centres, titanomagnetite is replaced by sphene in the intense propylitic zone and by rutile in the phyllic zone. The susceptibilities of rocks from the intense alteration zones of the prospects are very low (weakly paramagnetic, <10 μG/Oe [0.00013 SI], or diamagnetic), indicating that any magnetic minerals pre-dating the alteration have almost been completely erased.

(iv) Outside the zones of intense alteration, the background susceptibilities of the silicic Devonian volcanics are generally in the strong paramagnetic range ($\lesssim$ 100 μG/Oe However, variations in paramagnetic iron contents and in the trace amounts of ferromagnetic minerals produce sufficient differences in magnetization to produce a texture in the aeromagnetic anomalies that is clearly distinguishable from the smooth flat response associated with the epithermal alteration systems.

(v) A busy magnetic pattern associated with the Carboniferous volcanics reflects variations in susceptibility, which mainly reflects magnetite content, and Q value, which is dependent on grain size. Major shifts in magnetic base level reflect varying Q values, with reversed remanence overwhelming induced magnetization and producing magnetic lows when Q is greater than unity. Susceptibilities of Carboniferous volcanics range from ~2000 μG/Oe [0.025 SI] for andesitic flow units, to ~40 μG/Oe [0.0005 SI] for rhyolitic units. The susceptibility of the Devonian volcanics is probably lower because of a combination of initial bulk-rock chemistry (a preponderance of rhyolitic compositions) and the more intense pervasive propylitic alteration.

(vi) The oxide mineralogy is a function of the primary bulk-rock compositions and severity of alteration. Within each volcanic suite, susceptibility tends to decrease in the order andesite, dacite, rhyolite. The pervasive propylitic alteration reduces magnetization by partially replacing magnetic minerals, thereby reducing magnetic grain size and consequently increasing the stability of remanence as the susceptibility and remanence intensity decrease.

(vii) The Late Carboniferous units record a Permo-Carboniferous remanence direction, directed south and steep down, which dominates the NRM of these units. Most Late Devonian units have NRMs that are dominated by a Permo-Carboniferous overprint, indistinguishable in direction from the primary remanence of the Late Carboniferous rocks, which dominates the NRM of these units.

(viii) Some Late Devonian units retain, in addition to the Late Carboniferous overprint, an underlying primary Late Devonian remanence, directed SW and shallow down. Recognition of this characteristic Late Devonian remanence in some units, that have been mapped as Carboniferous, shows that they are in fact of Devonian age. Ubiquitous Carboniferous overprinting of remanence in Devonian rocks suggests that the regional alteration is penecontemporaneous with the eruption of the Carboniferous volcanics.

(ix) There is a strong, noisy, positive aeromagnetic anomaly associated with andesitic units mapped by the BMR as DCv_A. Samples from this area have high susceptibilities, suggesting that the exposed units are responsible for the observed anomaly pattern. No trace of a Devonian remanence component underlying the Carboniferous magnetization is found during demagnetization of the samples. The samples are less altered than typical DCv rocks and the susceptibilities are higher than those of Devonian andesites that are interbedded with the Ukalunda Beds. These

characteristics are more consistent with a Carboniferous age, suggesting that this may be a Late Carboniferous unit.

11.0 ACKNOWLEDGMENTS

BHP Exploration is thanked for their assistance with the various field trips to the area. Lily Haas is thanked for supplying detailed geological maps of the prospects, and Dick Irvine is thanked for supplying the colour image of the aeromagnetics. We thank Doug Price and Tom Whiting for their interest in the project and for useful discussions of the aeromagnetics.

BMR personnel, including Doug McKenzie, Jocelyn McPhie and Doone Wyborn, assisted with suggestions for sampling localities and with geological maps.

12.0 REFERENCES

Ade-Hall, J.M., Palmer, H.C. and Hubbard, T.P., 1971. The magnetic and opaque petrological response to regional hydrothermal alteration. Geophys. J.R. astron. Soc., 24, 137-174.

Black L., Mackenzie D., Oversby B. & McPhie J. 1990. Setting of epithermal gold mineralization in the northern Drummond Basin further refined. BMR Research Newsletter 12, 14-15.

Bohlke, J.K., Honnorez, J., Honnorez-Guerstein, B.-M., Muelenbachs, K. and Petersen, N., 1981. Heterogeneous alteration of the upper oceanic crust: correlation of rock chemistry, magnetic properties, and O isotope ratios with alteration patterns in basalts from site 396B, DSDP. J. Geophys. Res., 86, 7935-7950.

Clark D.A. 1983. Comments on magnetic petrophysics. Bull. Aust. Soc. Expl. Geophys. 14, 49-62.

Clark D.A. & Schmidt P.W. 1982. Theoretical analysis of thermomagnetic properties, low-temperature hysteresis and domain structure of titanomagnetites. Phys. Earth Planet. Int. 30, 300-316.

Criss, R.E. and Champion, D.E., 1984. Magnetic properties of granitic rocks from the southern half of the Idaho Batholith: influences of hydrothermal alteration and implications for aeromagnetic interpretation. J. Geophys. Res., 89, 7061-7076.

Criss, R.E., Champion, D.E. and McIntyre, D.H., 1985. Oxygen isotope, aeromagnetic, and gravity anomalies associated with hydrothermally altered zones in the Yankee Fork Mining District, Custer County, Idaho. Econ. Geol., 80, 1277-1296.

Embleton B.J.J. & McDonnell K.L. 1980. Magnetostratigraphy in the Sydney Basin, southeastern Australia. J. Geomag. Geoelect. 32, SIII 1- SIII 10.

Ewers G., Mackenzie D., McPhie J., Oversby B., Wyborn D., & Law S. 1989. New mapping extends Drummond Basin gold potential. BMR Research Newsletter 10, 1-4.

Ewers G., Mackenzie D., Oversby B., & Wyborn D. 1991. Regional oxygen-isotope patterns: Implications for epithermal gold exploration. BMR Research Newsletter 14, 1-2.

Fisher R. 1953. Dispersion on a sphere. Proc. Roy. Soc. A217, 295-305.

Hartley J.S., Peters S.G. & Beams S.D. 1989. Current developments in Charters Towers geology and gold mineralization. Abst. NQ Gold '89 Conference, Townsville, 7-14.

Heald P., Foley N.K. & Hayba D.O. 1987. Comparative anatomy of volcanic-hosted epithermal deposits: Acid-sulfate and adularia-sericite types. Bull. Soc. Econom. Geol. 82, 1-26

Hurley N.F. & Van Der Voo R. 1987. Paleomagnetism of Upper Devonian reefal limestones, Canning Basin, Western Australia. Geol. Soc. Am. Bull. 98, 138-146.

Hutton L.J. 1989. A stratigraphy and tectonic model for the Drummond Basin and its relationship to gold mineralization. NQ Gold '89 Conference Proceedings, 31-40.

Hutton L.J., Law S.R. & Grimes K.G. 1989. Mount Coolon 1:100,000 Geological Map. Queensland Department of Mines.

Irvine R.J. & Smith M.J. 1990. Geophysical exploration for epithermal gold deposits. J. Geochem. Expl. 36, 375-412.

Irving E. 1966. Palaeomagnetism of some Carboniferous rocks from New South Wales and its relation to geological events. J.G.R. 71, 6025-6051.

Jelînek V. 1981. Characterization of the magnetic fabric of rocks. Tectonophysics 79, T63-T67.

Lackie M.A. 1989. The rock magnetism and palaeomagnetism of granitic and ignimbritic rocks in the Lachlan and New England Fold Belts, N.S.W.. PhD thesis (unpub), Macquarie University, Australia, pp 154.

Lackie M.A., Clark D.A. & French D.H. 1991. Rock Magnetism and Palaeomagnetism of the Mount Leyshon gold mine in northeast Queensland. CSIRO Restricted Report 217R.

Law S.R. 1988. The Bulgonunna Volcanics - A Carboniferous ignimbritic cauldron complex in central Queensland. Geol. Soc. Aust. Abs. 21, 238.

Law S., Mackenzie D., McPhie J., Oversby B., Wellman P. & Wyborn D. 1989. Geological setting of gold mineralisation in the Northern Drummond Basin: significance of the Bulgonunna Volcanics. NQ Gold '89 Conference Proceedings, 47-50.

Li Z.X., Schmidt P.W. & Embleton B.J.J. 1988. Palaeomagnetism of the Harvey Group, central New South Wales and its tectonic implications. Tectonics 7, 351-367.

Lowrie W. 1990. Identification of ferromagnetic minerals in a rock by coercivity and unblocking temperature properties. Geophys. Res. Let. 17, 159-162.

Oversby B.S., Ewers G.R., Mackenzie D.E., McPhie J., Wyborn D., Law S. & Black L.P. 1990. Volcanic setting of epithermal gold mineralization in the northern Drummond Basin, Queensland. Geol. Soc. Aust. Abs. 25, 36.

Oversby B.S., Mackenzie D.E., McPhie J., Law S. & Wyborn D. 1991. Catalogue of field compilation sheets of Late Palaeozoic ignimbrites and associated rocks in the Burdekin Falls- "Conway" area (Glendon and adjacent parts of Strathalbyn, Harvest Home, and Collinsville 1:100,000 sheet areas), Northeastern Queensland. BMR Record ?/91 (Preliminary Copy).

Rona, P.A., 1978. Magnetic signatures of hydrothermal alteration and volcanogenic mineral deposits in oceanic crust. J. Volca. Geotherm. Res., 3, 219-225.

Schmidt P.W. 1976a. A new palaeomagnetic investigation of Mesozoic igneous rocks in Australia. Tectonophysics 33, 1-13.

Schmidt P.W. 1976b. The non-uniqueness of the Australian Mesozoic palaeomagnetic pole position. Geophys. J. Roy. Astr. Soc. 47, 285-300.

Schmidt P.W., Embleton B.J.J. & Palmer H.C. 1987. Pre- and post- folding magnetization from the Early Devonian Snowy River Volcanics and Buchan Caves Limestone, Victoria. Geophys. J. Roy. Astr. Soc. 91, 155-170.

Thrupp G.A., Kent D.V., Schmidt P.W. & Powell C. McA. 1991. Palaeomagnetism of red beds of the Late Devonian Worange Point Formation, SE Australia. Geophys. J. Int. 104, 179-201.

White N.C., Wood D.G. & Lee M.C. 1989. Epithermal sinters of Paleozoic age in north Queensland, Australia. Geology 17, 718-722.

Wood D.G, Porter R.G. & White N.C. 1990. Geological features of some Paleozoic epithermal gold occurrences in northeast Queensland, Australia. J. Geochem. Expl. 36, 413-443.

Wooldridge, A.L., Haggerty, S.E., Rona, P.A. and Harrison, C.G.A., 1990. Magnetic properties and opaque mineralogy of rocks from selected seafloor hydrothermal sites at oceanic ridges. J. Geophys. Res., 95, 12,351-12,374.

Table 1. List of Samples Examined Petrographically.

Sample Number	Site Number	Mapped Unit	Assigned Unit	Lithology
109401	-	Cugr	Cugr	Monzogranite
109402	-	Cugr	Cugr	Monzogranite
109475	-	DCv	DCv	Rhyolitic ash-flow tuff
109488	-	Dum	DCv	?Rhyodacitic ash-flow tuff
109490	-	Dum	?DCv	?Altered obsidian
109499	-	Dum	Dum	Tuffaceous siltstone
109507	-	Cvi	Cvi	Dacitic ignimbrite
109513	-	Cubpo	Cubpo	Quartz-feldspar porphyry
109519	-	Cubpo	Cubpo	Quartz-feldspar porphyry
109526	-	Cubpo	Cubpo	Quartz-feldspar porphyry
109530	-	Cubpo	Cubpo	Quartz-feldspar porphyry
109536	-	Cvi	Cvi	Dacitic ignimbrite
109542	-	DCv	DCv	Porphyritic andesite
109544	-	rhl	rhl	Quartz-feldspar porphyry
109546	-	Dum	DCv	Rhyolitic ignimbrite
109550	-	DCva	DCva	?Andesitic flow breccia
112057	CT79	DCvs	DCvs	Rhyol accretionary lapilli tuff
112058	CT79	DCvs	DCvs	Rhyolitic crystal tuff
112059	CT79	DCvs	DCv	Porphyritic andesite
112060	CT80	DCv	DCv	Rhyolitic crystal tuff
112061	CT84	DCv	DCv	Rhyolitic ash-flow tuff
112062	CT86	DCv	DCv	Rhyolitic ash-flow tuff
112063	CT87	DCv	DCv	Rhyolitic ash-flow tuff
112064	CT90	DCv	DCv	Rhyolitic ash-flow tuff
112065	CT94	Cubib	Cubib	Rhyolitic ignimbrite
112066	CT95	Cubib	Cubib	Rhyolitic ignimbrite
112067	CT96	Cubib	Cubib	Rhyolitic ignimbrite
112280	DCV01	Cvi	Cvi	Dacitic ash-flow tuff
112281	DCV01	Cvi	Cvi	Dacitic ash-flow tuff
112282	DCV62	Dum	DCv	?Rhyodacitic crystal-lithic tuff
112283	DCV02	Cvi	Cvi	Dacitic ignimbrite
112284	DCV03	Cvi	Cvi	Dacitic ignimbrite
112285	DCV04	Cvi	Cvi	Dacitic ignimbrite
112286	DCV05	Cvi	Cvi	Dacitic ignimbrite
112287	DCV06	Cvi	Cvi	?Porphyritic dacite
112288	DCV08	DCv	DCv	Altered ?rhyolite
112289	DCV09	DCv	DCv	Altered ?andesitic pyroclastic
112290	DCV10	DCv	DCv	Porphyritic rhyolite
112291	DCV11	DCva	DCva	Porphyritic andesite
112292	DCV13	DCv	DCv	Altered ?pyroclastic
112293	DCV14	Dk	DCv	Rhyolitic ash-flow tuff
112294	DCV15	Cugr	Cugr	Quartz diorite
112295	DCV17	Cugra	Cugra	Alkali microgranite
112296	DCV19	Cugms	Cugms	Quartz monzodiorite
112297	DCV20	Cvd	Cvd	Dacitic ignimbrite
112298	DCV21	Cvd	Cvd	Dacitic ignimbrite
112299	DCV22	DCv	DCv	Altered ?porphyritic andesite
112300	DCV23	ODr	ODr	Quartz diorite
112301	DCV30	DCva	DCva	Porphyritic andesite
112302	DCV34	rhl	DCv	Brecciated qtz-feldspar porphyry
112303	DCV38	Dk	DCv	Andesitic ignimbrite
112304	DCV40	DCv	DCv	Altered ?rhyolitic pyroclastic
112305	DCV45	DCv	DCv	Brecciated porphyritic rhyolite
112306	DCV47	DCv	DCv	Porphyritic rhyolite

Table 2. Basic magnetic properties of samples from the Conway/Bimurra area.

Site (lithology)	k (μG/oe)	A (%)	NRM(μG)	Vector Mean (Dec,Inc,J_{NRM})	Q
79(altered)1-12 (DCv_s??, VF & rhyolitic tuff)		2	2.2	(4.5,-13,2)	~0.4
80 (DCv, VF)	40	3	2.8	(64,-15,2.7)	0.1
81 (DCv, VF)	20	2	1.5	(312,-8,1.3)	0.15
82 (DCv?, VF)	40	2	0.5	(279,5,0.4)	0.03
83 (DCv, VF)	40	2	5.6	(127,65,5.1)	0.3
84 (DCv, PF)	90	3	100	(235,-24,96)	2.2
85 (DCv, PF)	50	4	19	(9,36,19)	0.8
86 (DCv, PF)	0	-	2	-	
87 (DCv, PF)	15	3	3.3	(201,60,3.2)	0.4
88 (DCv, PF)	15	2	5.4	(128,-17,4.3)	0.7
89 (DCv, PF)	400	3	45	(65,-29,43)	0.2
90 (DCv, Altered PF)	15	2	30	(0,-69,28)	4.0
91 (DCv, PF?)	32	2	4.5	(28,59,4.3)	0.25
94 (Cubib, PF)	150	4	108	(196,50,103)	1.4
95 (Cubib, PF)	100	3	169	(254,22,167)	3.4
96 (Cubib, PF, rhyolitic)	100	2	132	(238,22,131)	2.6
01 (CV_i, PF)	2326	3	2666	(77,70.6,1890)	2.3
02 (CV_i, PF)	2433	5	646	(219,61,626)	0.5

03	2338	3	5404	(272,7,4257)	4.6
(CV_i, PF)					
04	2260	3	1714	(283,46,1285)	1.5
(CV_i, PF)					
05	1278	3	299	(314,-21,257)	0.5
(CV_i, PF)					
06	845	3	488	(43,-26,476)	1.2
(CV_i, VF, altered)					
07	565	4	154	(357,-36,147)	0.5
(Cgm)					
08AC	134	4	15	(335,6,13)	0.2
B	981	4	200	(39,-33,200)	0.4
(DCv, PF?)	B appears weathered				
09	920	7	202	(138,-52,156)	0.4
(DCv, PF)					
10	497	4	193	(26,-22,184)	0.8
(DCv, VF)					
11	2643	4	1184	(43,6,1181)	0.9
(DCv_A, andesite)					
12	2721	3	1184	(13,-40,1178)	0.9
(DCv_A, andesite)					
13	40	6	123	(302,78,121)	6.2
(DCv, PF)					
14	24	1	20	(210,74,19)	1.7
(DCv?, altered PF)					
15	3460	3	923	(161,-14,776)	0.5
(Cug_r)					
16	3918	2	736	(7,-49,733)	0.4
(Cug_r)					
17	1922	5	190	(333,-46,155)	0.2
(Cug_{ra})					
18A	3015	5	692	(142,-14,688)	0.5
BC			5015	(14,-25,3411)	3.3
(Cug_r)					
19	1002	9	104	(12,-35,92)	0.2
(Cug)					
20	2316	5	2433	(160,76,2407)	2.1
(Dam Ig)					
21	1586	3	783	(214,54,451)	1.0
(Dam Ig?)					
22	544	3	176	(5,-32,165)	0.65
(DCv?, VF)					

25A	48	2	66	(244,51,65)	2.8
BC	466	4	137	(272,54,130)	0.6
(DCv??, VF)					
26	7	3	0.8	(126,66,0.8)	0.2
(CPg??, altered volcs)					
27	12	3	1.6	(28,47,1.6)	0.3
(CPg??, altered volcs)					
28	20	3	1.0	(167,74,0.9)	0.1
(Star Hope Fm)					
29A	4613	3	763	(186,-52,756)	0.3
BC	6	2	0.8	(242,52,0.8)	0.3
(DCv???)					
30	2099	3	862	(247,-55,705)	0.8
(DCv_A, andesite flow)					
31	1718	3	4020	(254,27,4015)	4.7
(DCv_A, PF)					
32	13	2	1.3	(276,43,1.2)	0.2
(DCv, VF)					
Battery Hill Prospect					
{					
33	-	-	6	-	
(Dk?/DCv, Silified rhyodacite)					
34ABC	-	-	7	-	
D			33		
(Dk?/DCv, Silif rhyodac)					
35	-	-	15	-	
(Dk/DCv?, Silic lake seds)					
36	-	-	30	-	
(Dk?/DCv, silic Qtz vein breccia)					
37	1133	3	596	(336,-61,574)	1.0
(Dk??/DCv?, andesitic lava)					
38AC	582	3	958	(206,-66,646)	3.3
B			5720	(107,84,5708)	19.3LS??
(DCv?, PF, andesitic ignimbrite)					
}					
39A	21	3	6	(226,57,6)	0.6
B	377	3	86	(46,-33,78)	0.5
(Dk?/DCv, silif volc)					
Conway prospect					
{					
40	32	2	10	(12,-27,9)	0.6
(DCv, andesites?/epiclastics- altered)					
41	-	-	0.3	-	
(DCv, andesite-clay alteration)					
}					

Bimurra Prospect

{

42	-	-	-	-	
(DCv, rhy ashflow tuffaceous-siliceous)					
43	-(33 with recent weath)		0.6, 10(weath)	-	
(DCv, hydrothermal breccia)					
44	-	-	0.5	-	
(DCv, altered volc)					
45	7	3	4	(7,-54,3.8)	1.1
(DCv, rhyolitic-clay alteration)					
46	7	2	0.9	(18,-43,0.9)	0.3
(DCv, rhy ashflow tuff)					
}					
47	20	2	6.2	(112,68,6)	0.6
(DCv, altered volc)					
48	10	2	9.1	(347,-44,9)	1.8
(Dum)					
49	7	2	0.3	(344,-55,0.5)	0.09
(Dum)					
50	3	2	0.4	(352,-55,0.4)	0.3
(DCv?)					
51	6	3	1.5	(11,-45,1.5)	0.5
(Dum)					
52A (dyke?)	66	3	61	(178,80,61)	1.9
B	1506	5	515	(355,1,515)	0.7
(DCv?, VF)					
53	48	3	12	(61,-15,12)	0.5
(DCv, PF)					
54ABC	14	2	10	(289,-17,7)	1.4
D	5				4.0
(Cub_{po})					
55A	30	3	91	(148,22,83)	6.1
BC	7		5.7	(102,76,5.6)	1.6
(Cub_{po}/Cub_{ia})					
56	718	5	95	(358,-60,94)	0.3
(CPg?, altered volc)					
57	1680	2	4165	(300,42,4137)	5.0
(CVi, PF)					
58	11	2	2.2	(335,-12,2.2)	0.4
(Cvi, altered)					

Bluegum Prospect

{					
59A	-	-	5		-
B	9		60	(358,-62,56)	13.3
(Dum?/DCv??, silified Qtz breccia)					
60	2	4	11	(161,-10,10)	11.0
(Dum?/DCv, silified breccia)					
61	22	3	1.6	(280,32,1.6)	0.1
(Dum?/DCv, oxidized ignimbrite)					
62	453	4	?? (Samples lightning struck)		
(rhyodacite, DCv_A)					
63	13	2	0.9	(255,50,0.7)	0.1
(DCv, altered rhyolitic ignimbrite)					
}					
64	2836	8	378	(23,-57,368)	0.3
(Cug)					
65A	2539	6	710	(3,66,705)	0.6
B	1326	14	147	(244,-73,146)	0.2
(Cubib?, brecciated volc)					
66	1382	5	525	(132,-36,525)	0.8
(Cubib, PF)					
67A	222	4	661	(174,59,657)	6.0
BC	82	3			16.0
(Cubib, PF)					
68	312	5	51	(321,-79,51)	0.3
(Cubib, altered volc)					
69	129	3	41	(107,63,41)	0.6
(Cubib, breccia)					

NRM = NRM intensity in microgauss (cgs) = milliAmp/m (SI) = 0.1 gamma
Q = Koenigsberger ratio for an ambient field of 50,000 nT
Susceptibility: k (SI) = 4π * k (μG/Oe) / 10E+6
A (degree of Anisotropy of susceptibility)
= ((max susc / min susc) - 1.0) * 100

NRM intensity is a scalar mean of all measured specimens, excluding any thought to be lightning struck.

Means given for susceptibility and NRM are for unimodal distributions. Means have a coefficient of variation < 40% and usually < 25%. If a bimodal distribution is evident and it is sample related then the sample means are displayed.

Lithology and age of unit are located in reference list for geological map (Fig. 3). VF, volcanic flow. PF, pyroclastic flow. Particular descriptions for sites from the various prospects are from BHPs detailed geological mapping. Sites 19-29 and 64-69 are from Late Devonian and Carboniferous units (see Fig. 2) elsewhere in the northern Drummond Basin.

Table 3. Palaeomagnetism of Conway-Bimurra area.

Overprint magnetization for Devonian Lithologies

Site	N/No	Mean Direction [Dec(°), Inc(°)]
08	2/2	93.8, 86.9
11	1/2	65.6, 61.9
12	1/2	287.0, 80.0
13	2/2	280.8, 81.8
14	1/2	221.5, 58.5
39	3/3	235.2, 72.0
40	2/3	246.7, 71.8
47	2/2	119.1, 62.2
49	1/1	231.7, 53.4
52	2/2	284.1, 83.5
61	1/1	211.1, 68.8
79	2/3	162.0, 65.5
80	2/2	194.2, 67.9
81	3/3	279.2, 82.3
82	2/2	203.5, 75.4
83	2/2	196.3, 72.7
85	1/1	58.1, 69.5
87	2/2	176.9, 56.3
89	1/1	163.7, 58.2
91	1/1	39.9, 85.8

Mean 193.7, 79.4 (N=20, α_{95}=8.1, k(precis) = 17)

Late Carboniferous Flows and Intrusives

01	2/2	188.0, 61.6
02	3/3	202.5, 79.7
03	1/3	149.9, 78.7
04	4/4	288.0, 68.6
05	1/3	158.6, 67.5
07	2/2	285.1, 61.0
15	2/3	186.2, 68.1
17	3/3	239.0, 61.4
18	3/3	199.6, 77.1
55	3/3	124.4, 65.0
56	2/2	216.8, 84.9
57	1/1	253.2, 89.3

Mean 204.8, 78.6 (N=12, α_{95}=9.6, k=21)

Mean (overprint and Carboniferous lithologies)
198.1, 79.2 (N=32, α_{95}=6.0°, k=19)

Geographic Location 147.4°E, 21.0°S

Palaeomagnetic pole 40.6°S, 139.0°E (dp=10.9°, dm=11.4°)

Other results

DCv (non overprint directions...primary?)

84	2/2	229.2,	-7.8
53	2/2	61.5,	-13.6

Mapped as Locharwood Rhyolite (Cubib). Directions would suggest an older age for the samples.

95	2/2	247.9,	18.5
96	2/2	237.3,	13.8

Samples near Burdekin Dam

20	3/3	164.3,	72.3
21	3/3	192.0,	69.0
26	1/1	171.6,	60.9
27	2/2	160.8,	77.2
29	2/2	204.3,	64.0
66	2/3	169.0,	51.2
67	3/3	178.9,	56.9

Note...No, number of samples measured. N, number of samples used to calculate site mean. Dec, declination. Inc, inclination. α_{95}, radius of confidence cone (Fisher 1953). dp, dm, the semiaxes of the elliptical error around the pole at a probability of 95%, dp in colatitude direction and dm perpendicular to it.

Table 4. SIRM and MDFs of SIRM and NRM of selected samples.

Spec	J_r (μG)	MDF_{NRM} (Oe)	MDF_{SIRM} (Oe)	Magnetic mineral
02a2c	164773	550	175	Mgt, KM
03b2d	118980	275	130	Mgt, KM
09c1	167091	75	250	Mgt, Hem
11a3b	333681	40	85	Mgt
14a1a	3504	305	210	Mgt, KM, MgH
16a1b	130683	45	55	Mgt, Hem
20b3c	106315	340	105	Mgt, KM, MgH
45a2b	946	680	300	Mgt, KM
47b3	8410	500	1375	Hem, Mgt
48a2b	923	2000	430	Gt, Mgt
61a1	352	125	875	Mgt, MgH, Gt, KM
62b2b	84977	-	140	Mgt
63a1a	172	605	480	Mgt, Hem, MgH, Gt
81b2	422	170	250	Mgt, TM, KM
82a2	1111	220	175	Mgt, MgH
84a5	20102	200	330	Hem, Mgt, MgH, KM
85b2	18665	70	410	Hem, Mgt, MgH, KM

Note. J_r, SIRM. MDF_{NRM}, Median destructive field of the NRM. MDF_{SIRM}, MDF of the SIRM. Mgt, magnetite. KM, cation-deficient magnetite. Hem, Haematite. MgH, maghaemite. Gt, goethite.

Table 5. Representative Electron Microprobe Analyses of Fe-Ti Oxides in the Carboniferous Units.

	Roscow Granite			Intrusive Rhyolite		Locharwood Rhyolite
	112294	112295		109526		112067
Oxide	Ti-	Magnetite	Mn-	Ti-	Ilmenite	Ti-
wt%	Magnetite		Ilmenite	Maghemite		Magnetite
SiO_2	0.11	0.13	0.06	0.11	0.06	0.11
TiO_2	3.04	0.45	51.93	3.96	52.59	6.82
Al_2O_3	0.77	0.09	0.01	0.05	0.17	1.64
Cr_2O_3	0.02	0.13	0.03	<0.01	0.02	0.03
V_2O_3	0.78	0.29	<0.01	0.03	0.05	0.25
FeO	87.67	91.90	27.17	85.99	43.60	80.60
MnO	0.20	0.13	19.86	0.04	0.92	0.09
MgO	<0.01	0.01	0.03	<0.01	0.26	<0.01
CaO	<0.01	0.01	0.13	0.07	0.18	1.26
CoO	0.05	0.03	<0.01	<0.01	<0.01	0.06
NiO	0.04	<0.01	0.02	<0.01	0.03	0.05
ZnO	0.16	0.03	0.13	0.04	0.02	1.96
Total	92.84	93.20	99.37	90.29	97.89	92.88
FeO	33.36	31.43	26.29	3.53	43.60	33.72
Fe_2O_3	60.35	67.21	0.98	91.64	<0.01	52.10
Total	98.89	99.94	99.47	99.47	97.89	98.10

Table 5. (continued)

Dacitic Ignimbrite

Oxide wt%	112287 Ti-Maghemite	109507 Ti-Maghemite	109507 Ferrian Ilmenite
SiO_2	0.13	0.10	0.04
TiO_2	12.11	5.06	43.46
Al_2O_3	1.53	1.10	0.11
Cr_2O_3	<0.01	<0.01	<0.01
V_2O_3	0.34	0.34	0.09
FeO	77.10	82.48	51.44
MnO	0.35	0.72	1.23
MgO	<0.01	1.27	1.95
CaO	<0.01	0.04	0.03
CoO	0.01	0.02	0.02
NiO	0.01	<0.01	0.04
ZnO	0.25	0.18	<0.01
Total	91.84	91.30	98.41
FeO	10.45	1.45	34.30
Fe_2O_3	74.08	90.05	19.05
Total	99.26	100.33	100.32

Table 6. Representative Electron Microprobe Analyses of Fe-Ti Oxides in the Stones Creek Formation.

	Andesitic Unit				Undivided Volcanics	
	112301	109550		112291	109542	
Oxide wt%	Ti-Magnetite	Ti-Magnetite	Mn-Ilmenite	Mn-Ilmenite	Mn-Ilmenite	Ti-Magnetite
SiO_2	0.43	0.21	0.08	0.17	0.13	0.28
TiO_2	5.77	5.93	52.46	49.84	52.94	5.45
Al_2O_3	0.13	0.28	0.04	0.03	0.03	0.06
Cr_2O_3	2.31	0.02	0.01	<0.01	<0.01	0.01
V_2O_3	0.29	0.35	0.15	0.17	0.06	0.16
FeO	84.02	86.48	37.83	25.75	30.99	87.98
MnO	0.10	0.02	8.90	22.07	15.01	0.04
MgO	<0.01	<0.01	0.06	0.03	0.05	0.02
CaO	0.22	0.09	0.24	0.64	0.79	0.53
CoO	<0.01	0.01	<0.01	<0.01	<0.01	<0.01
NiO	<0.01	0.06	<0.01	<0.01	0.01	0.03
ZnO	<0.01	0.14	<0.01	<0.01	0.09	<0.01
Total	93.28	93.58	99.78	98.71	100.10	94.55
FeO	36.22	36.30	37.83	21.78	30.99	35.86
Fe_2O_3	53.12	55.76	<0.01	4.42	<0.01	57.92
Total	98.60	99.17	99.78	99.15	100.10	100.35

Figure 1. Location of Bimurra and Conway prospects in northeast Queensland. Taken from Irvine and Smith (1990).

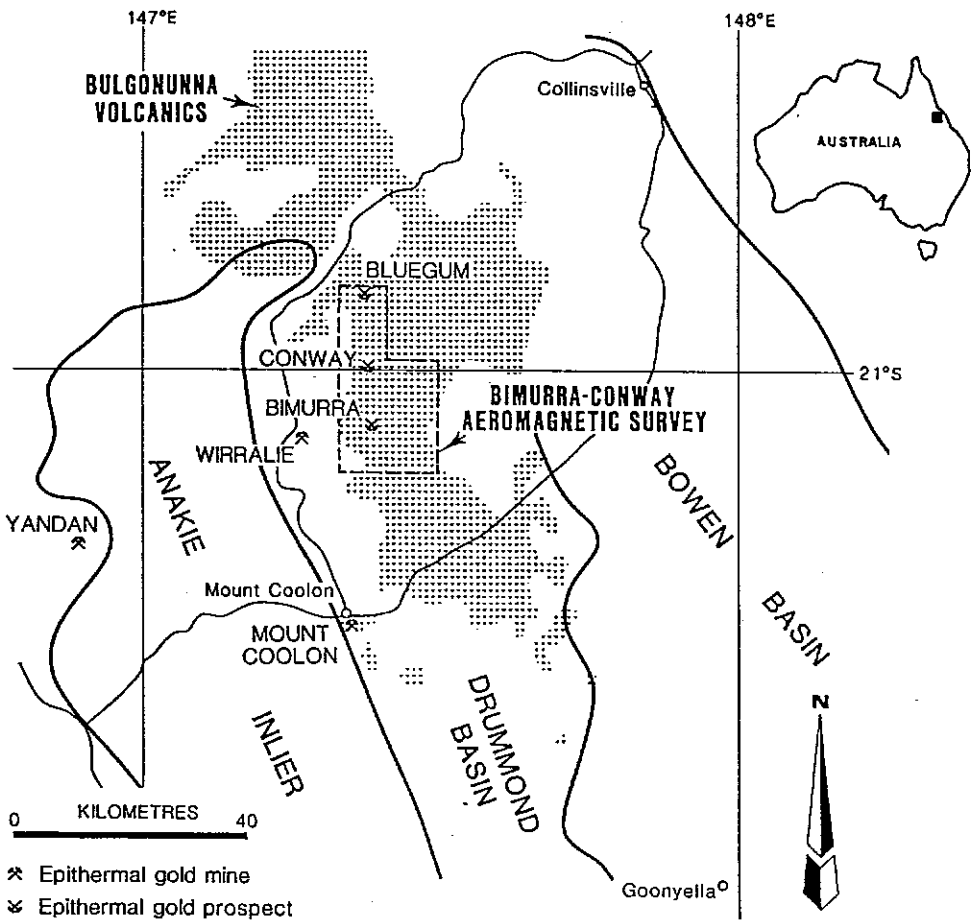
147°E
148°E
BULGONUNNA VOLCANICS
Collinsville
AUSTRALIA
BLUEGUM
CONWAY
21°S
BIMURRA
BIMURRA-CONWAY AEROMAGNETIC SURVEY
WIRRALIE
ANAKIE
BOWEN
YANDAN
Mount Coolon
MOUNT COOLON
BASIN
INLIER
DRUMMOND BASIN
N
0 KILOMETRES 40
Epithermal gold mine
Epithermal gold prospect
Goonyella

Figure 2. Distribution of Devonian and Late Carboniferous Volcanics and associated rocks of the northern Drummond Basin. Adapted from Ewers et al (1991). Sites sampled north of the Conway-Bimurra area are indicated by their site numbers.

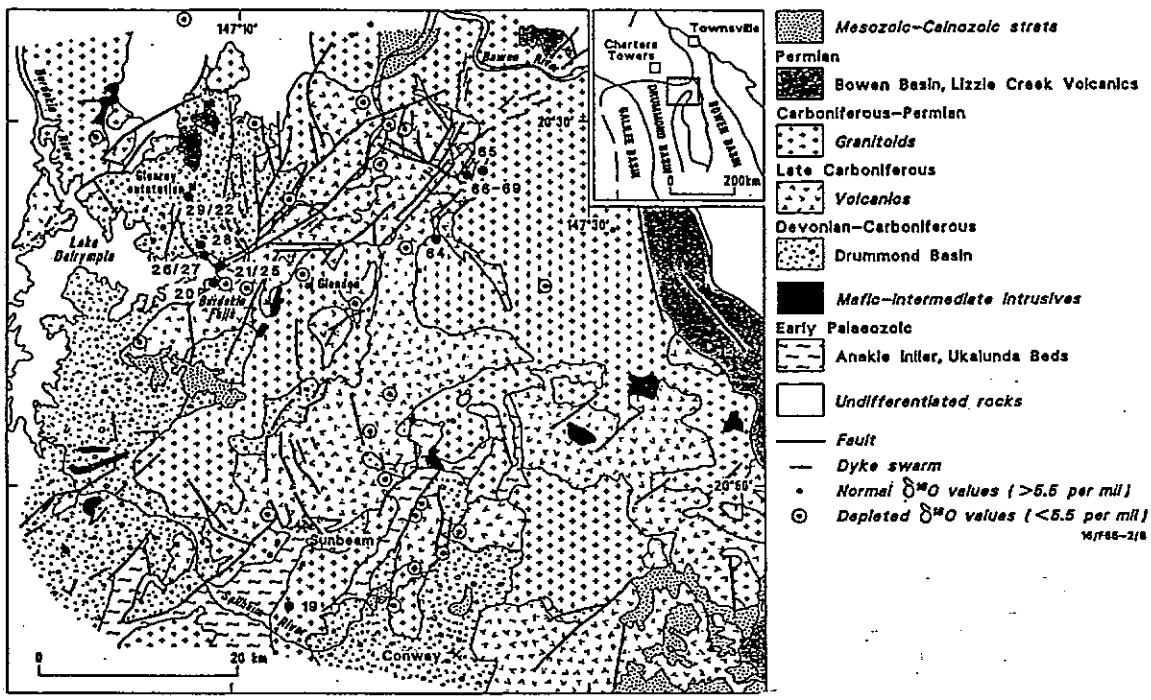
147°10'
147°30'
20°30'
20°50'
Townsville
Charters Towers
GALILEE BASIN
DRUMMOND BASIN
BOWEN BASIN
0
200km
Lake Dalrymple
Glenroy extension
Bardekin River
Bowen River
Glendon
Sunbeam
Conway
Sunbeam River
29/22
28
26/27
21/25
20
19
64
65
66-69
0
20 km
Mesozoic–Cainozoic strata
Permian
Bowen Basin, Lizzie Creek Volcanics
Carboniferous–Permian
Granitoids
Late Carboniferous
Volcanics
Devonian–Carboniferous
Drummond Basin
Mafic–intermediate intrusives
Early Palaeozoic
Anakie Inlier, Ukalunda Beds
Undifferentiated rocks
Fault
Dyke swarm
Normal δ18O values (>5.5 per mil)
Depleted δ18O values (<5.5 per mil)
16/F65-2/8

Figure 3. Geology of the Conway-Bimurra area. Sample localities are indicated by site number. Three digit sample numbers refer to sample localities of Dickson et al (1991). Prospects are indicated by bold first letter of prospect name. Map is a compilation of the BMR preliminary geological map of the Burdekin Falls - "Conway" area (Oversby et al 1991) and the Mount Coolon 1:100,000 Geological Map compiled by the Queensland Department of Mines (Hutton et al 1989). Note, there are some boundary differences between the two maps and "?" next to a unit name infers that the geology may not be as mapped.

(Figure is overleaf)

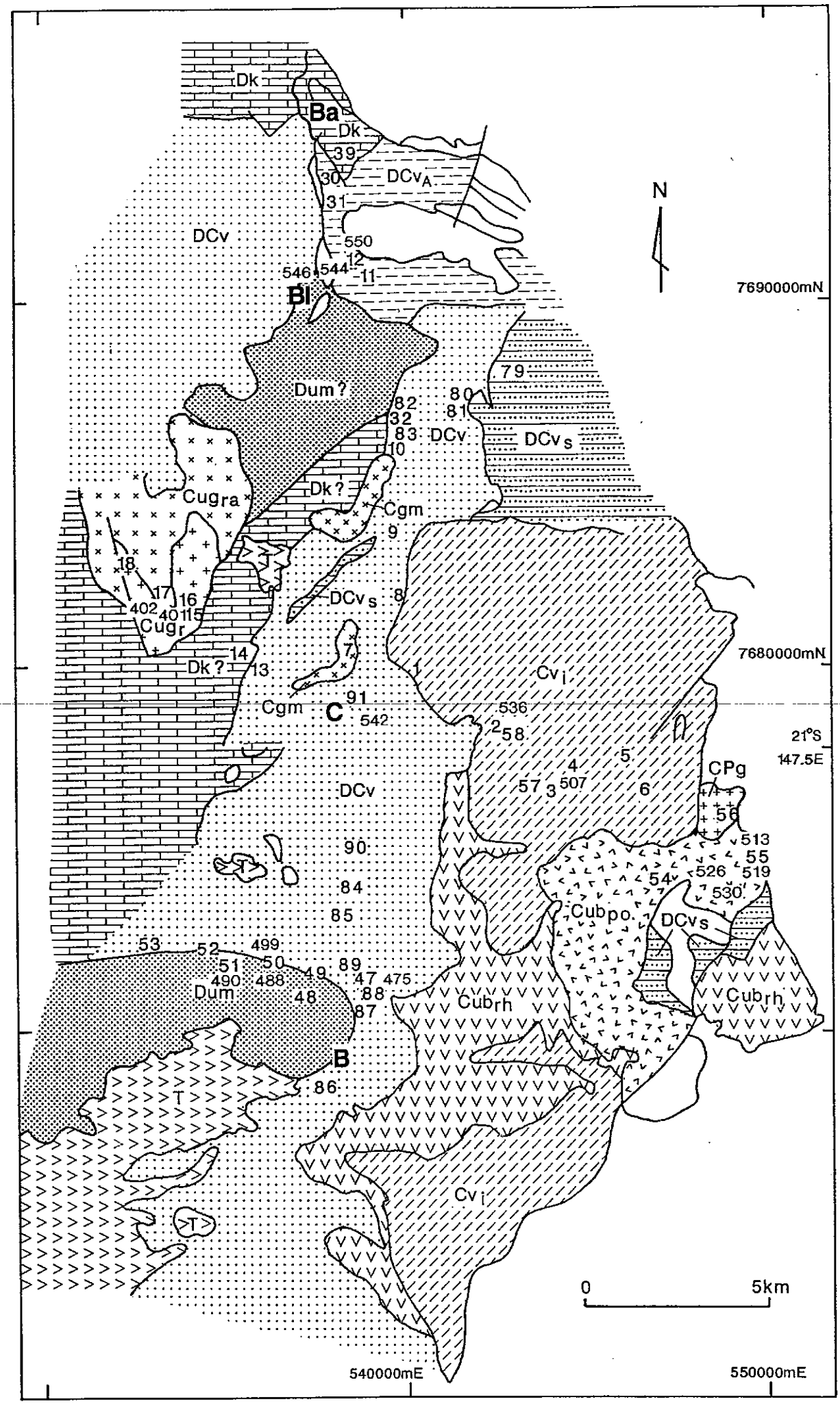
Dk
Ba
Dk
39
30
DCv$_A$
31
DCv
550
12
546
544
11
Bl
N
7690000mN
Dum?
79
80
82
81
32
83
DCv
DCv$_s$
10
Dk?
Cugra
Cgm
9
18
17
16
402
40
115
Cugr
DCv$_s$
8
7
14
Dk?
13
1
Cv$_i$
Cgm
C
91
542
536
2
58
7680000mN
21°S
147.5E
4
5
CPg
57
3
507
6
56
513
55
526
519
54
530
90
Cubpo.
DCv$_s$
84
85
53
52
499
51
50
49
89
47
475
490
488
Dum
48
88
87
Cubrh
Cubrh
B
86
Cv$_i$
0
5km
540000mE
550000mE

Reference for geological map and magnetic property table

Tertiary

T: Suttor Formation or basalt

Upper Carboniferous

Ferndon Volcanic Group (upper)
contains various Bulgonunna Volcanic Subgroups

Cub_{ia} Bobby Dazzler Dacite

Cubib Locharwood Rhyolite

Ferndon Volcanic Group (lower)
contains various Smedley Volcanic Subgroups

CV_i dacitic ignimbrite with Hb
equivalent to Cli

Dam Ig? Dam Ignimbrite member at Burdekin Dam

Cgm undivided diorites/basalts to gabbros

CPg fine-grained Bi granite

Cug_r Roscow Granite, granodiorite member

Cug_{ra} Roscow Granite, granite member

Cub_{po} undifferentiated intrusive rhyolite

Cub_{rh} intrusive rhyolite

Upper Devonian to Lower Carboniferous

Stones Creek Formation

DCv undivided rhyolitic to andesitic lavas to lithic sandstone to siltstone
equivalent to DCb (Bimurra Volcanics)

DCv_A mainly andesitic rocks

DCv_s undivided, mainly epiclastic

Upper Devonian

Dum Mount Wyatt Formation
epiclastic sandstone, mudstone
equivalent to DCm

Middle Devonian

Dk Ukalunda Beds
fissile to cleaved epiclastic mudstone, ss, conglom, lime

PROSPECTS

B....Bimurra

C....Conway

Bl...Bluegum

Ba...Battery Hill

nb. Formation names and descriptions taken from the BMR preliminary geological maps of the Burdekin-Conway Palaeozoic volcanics and associated rocks, as well as from the Mount Coolon 1:100000 geological map produced by the Queensland department of mines.

Figure 4. A. Colour total magnetic intensity image of the Conway-Bimurra area.

Overlays are:

(1) an outline of the geology and sample sites
(2) the magnetic contours of the same data set.

B. Image of the data set after an "alteration" filter was applied. Flat zones indicate areas of constant susceptibility, while "busy" zones indicate variable susceptibility. Colour image supplied by Dick Irvine (BHP). Images from Irvine & Smith (1990).

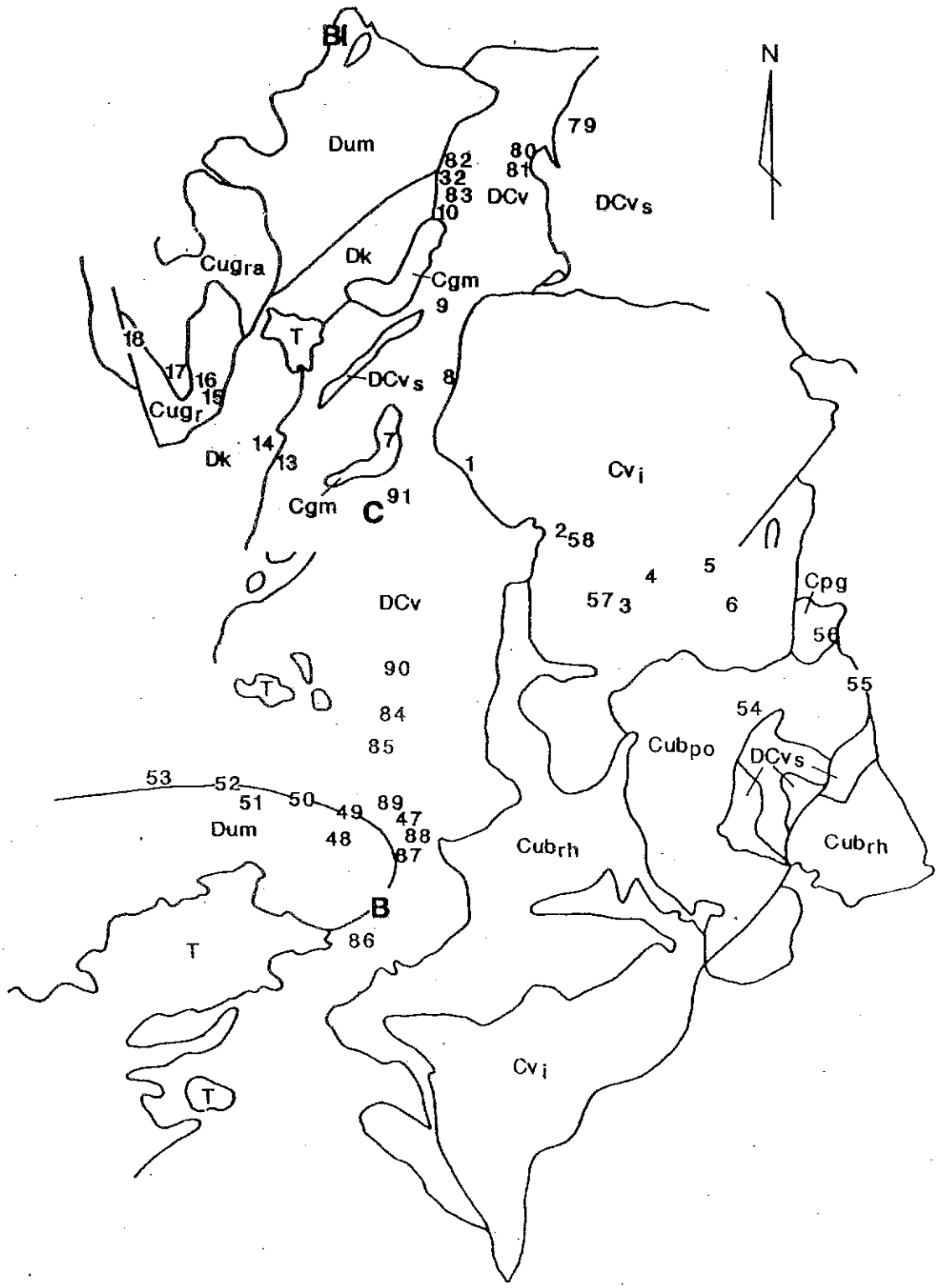
Bl
N
Dum
79
80
81
82
32
83
10
DCv
DCvs
Cugra
Dk
Cgm
9
T
18
17
16
15
Cugr
DCvs
8
Dk
14
13
7
Cgm
C
91
1
Cvi
2
58
4
5
57
3
6
Cpg
7
56
55
DCv
90
84
85
T
54
Cubpo
DCvs
53
52
51
50
49
89
47
88
87
48
Dum
Cubrh
Cubrh
B
86
T
Cvi
T

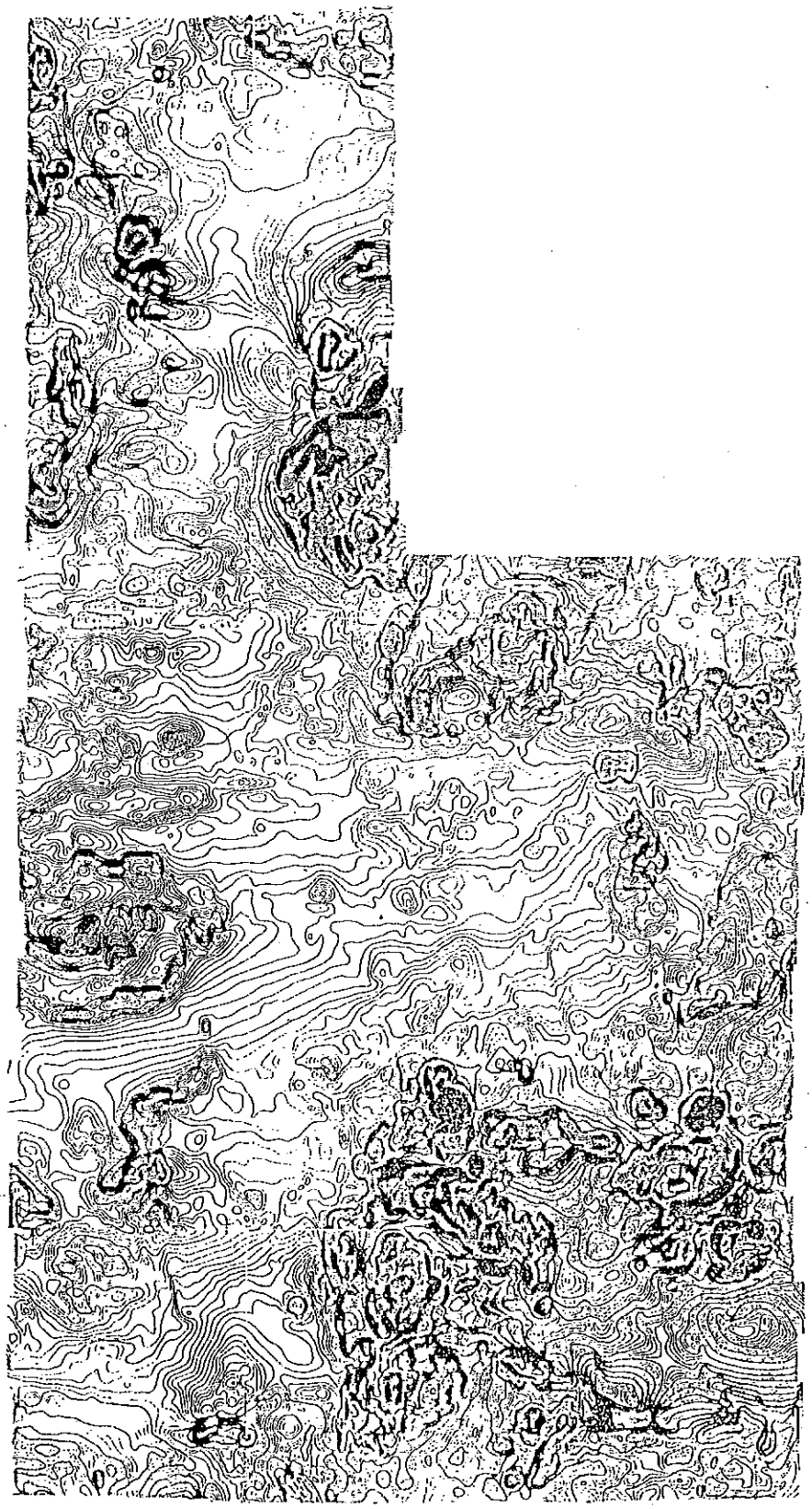

BHP-UTAH MINERALS INTL.
BIMURRA - CONWAY QLD

TOTAL MAGNETIC INTENSITY
PLHEQ STRETCH
SF55 1:1000000 PROJ=AMG ZONE=55

SM. 682

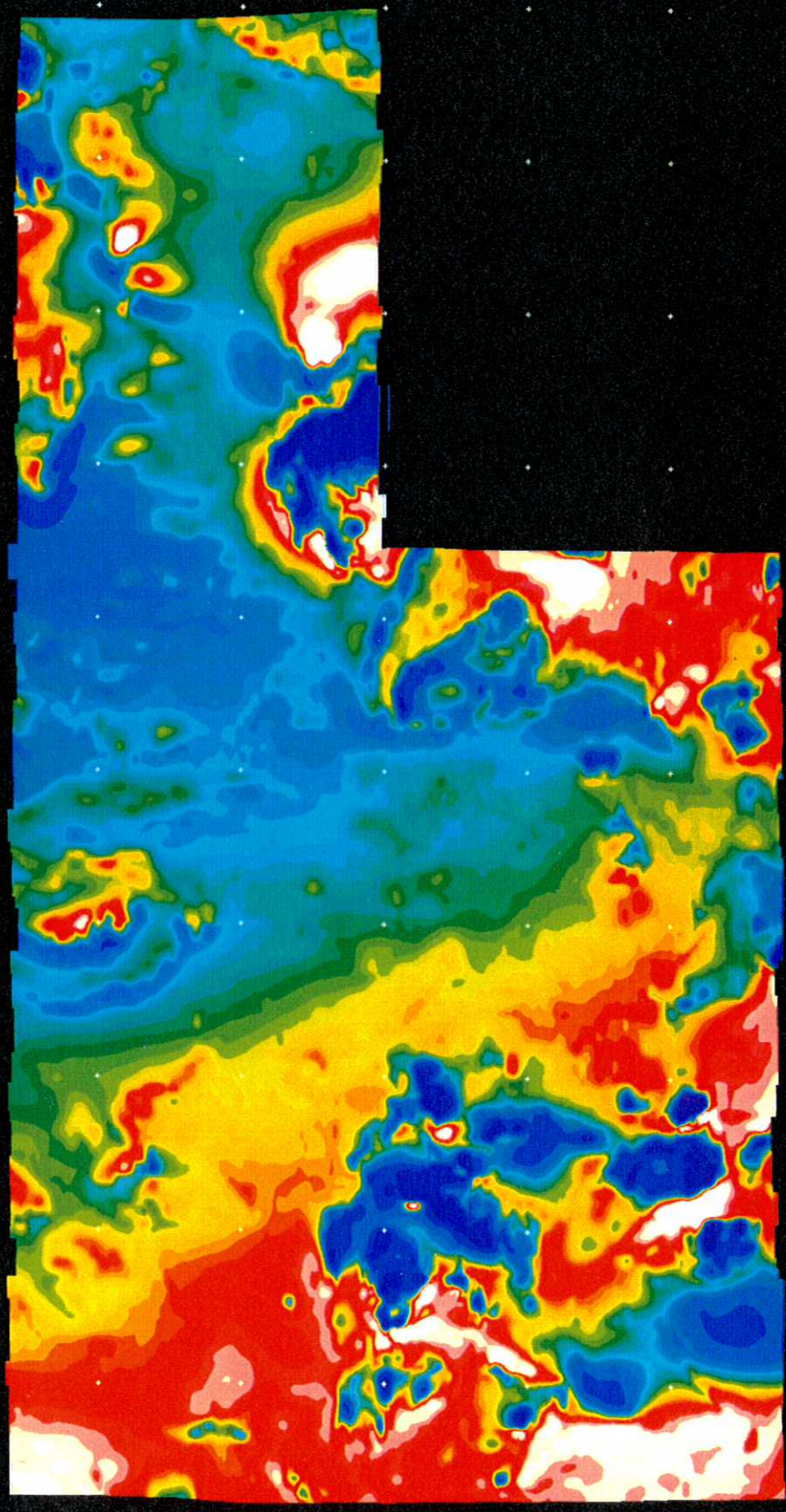

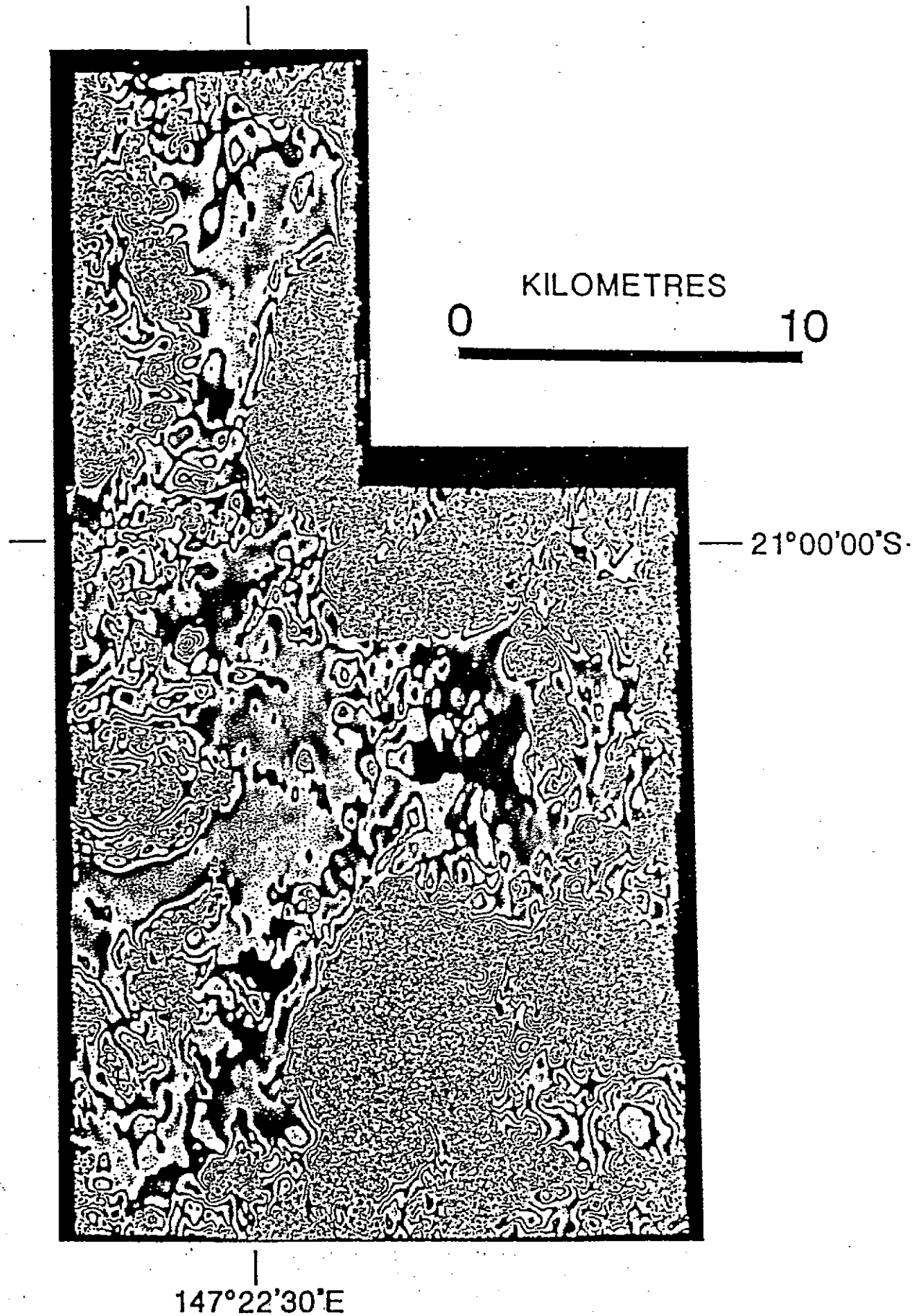
KILOMETRES
0
10
21°00'00"S
147°22'30"E

Figure 5. Susceptibility, remanent intensity and Koenigsberger ratio of magnetic minerals as a function of domain state and remanence type. The properties apply to dispersed grains, but k and J are normalised to unit volume.

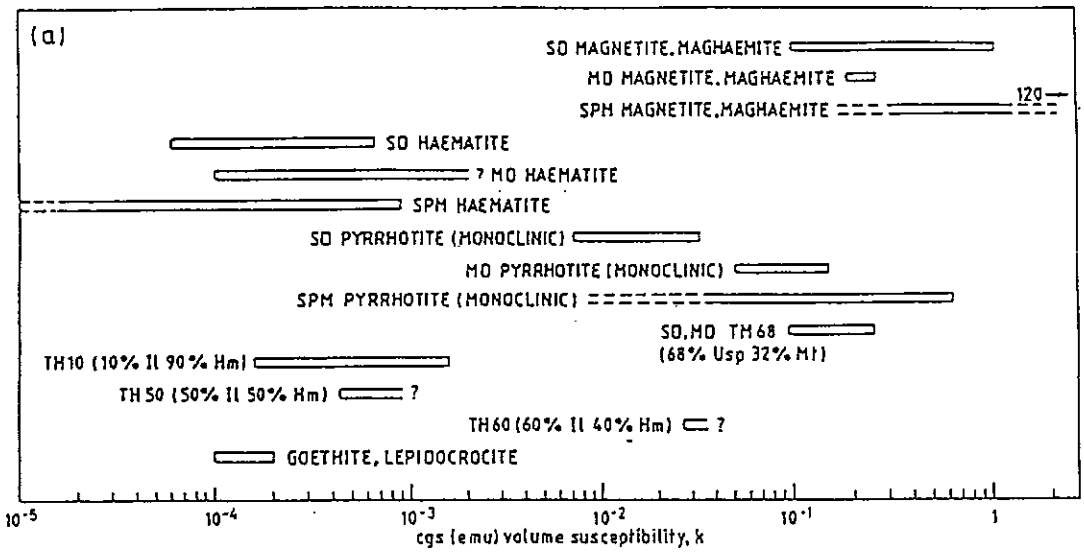
(a)
SD MAGNETITE, MAGHAEMITE
MD MAGNETITE, MAGHAEMITE
SPM MAGNETITE, MAGHAEMITE
120
SD HAEMATITE
? MD HAEMATITE
SPM HAEMATITE
SD PYRRHOTITE (MONOCLINIC)
MD PYRRHOTITE (MONOCLINIC)
SPM PYRRHOTITE (MONOCLINIC)
SD, MD TM 68
(68% Usp 32% Mt)
TH 10 (10% Il 90% Hm)
TH 50 (50% Il 50% Hm) ?
TH 60 (60% Il 40% Hm) ?
GOETHITE, LEPIDOCROCITE
10^{-5} 10^{-4} 10^{-3} 10^{-2} 10^{-1} 1
cgs (emu) volume susceptibility, k

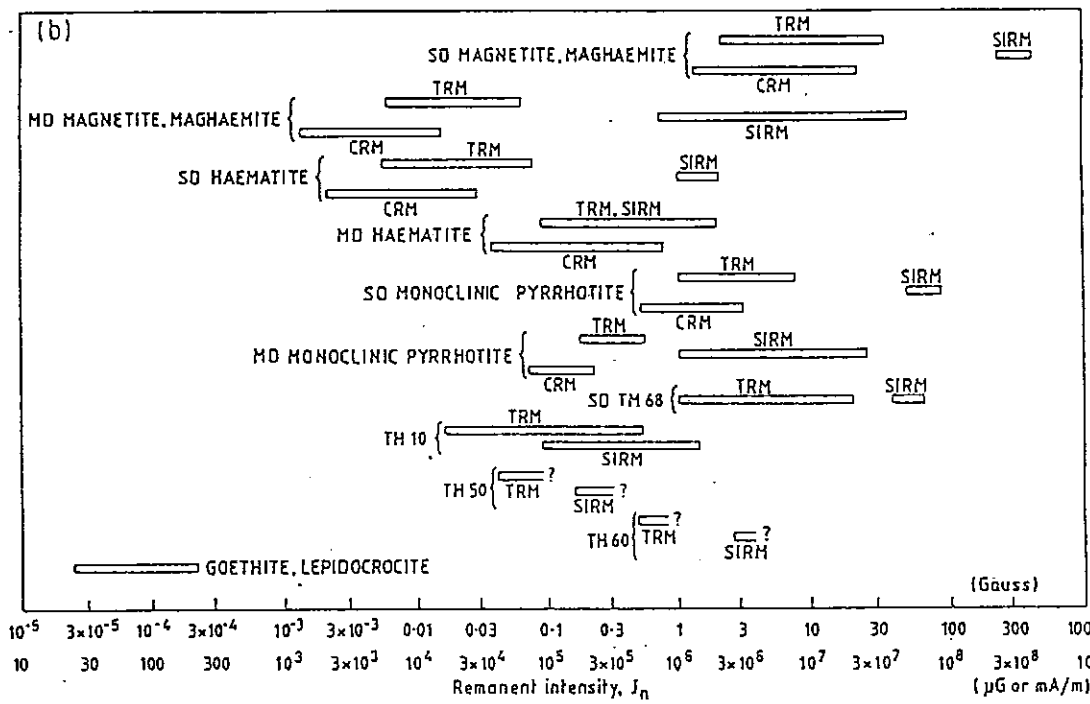
(b)
SD MAGNETITE, MAGHAEMITE
MD MAGNETITE, MAGHAEMITE
SD HAEMATITE
MD HAEMATITE
SD MONOCLINIC PYRRHOTITE
MD MONOCLINIC PYRRHOTITE
SD TM 68
TH 10
TH 50
TH 60
TRM
CRM
SIRM
TRM, SIRM
GOETHITE, LEPIDOCROCITE
(Gauss)
10^{-5} 3×10^{-5} 10^{-4} 3×10^{-4} 10^{-3} 3×10^{-3} 0·01 0·03 0·1 0·3 1 3 10 30 100 300 1000
10 30 100 300 10^{3} 3×10^{3} 10^{4} 3×10^{4} 10^{5} 3×10^{5} 10^{6} 3×10^{6} 10^{7} 3×10^{7} 10^{8} 3×10^{8} 10^{9}
Remanent intensity, J_n
(μG or mA/m)

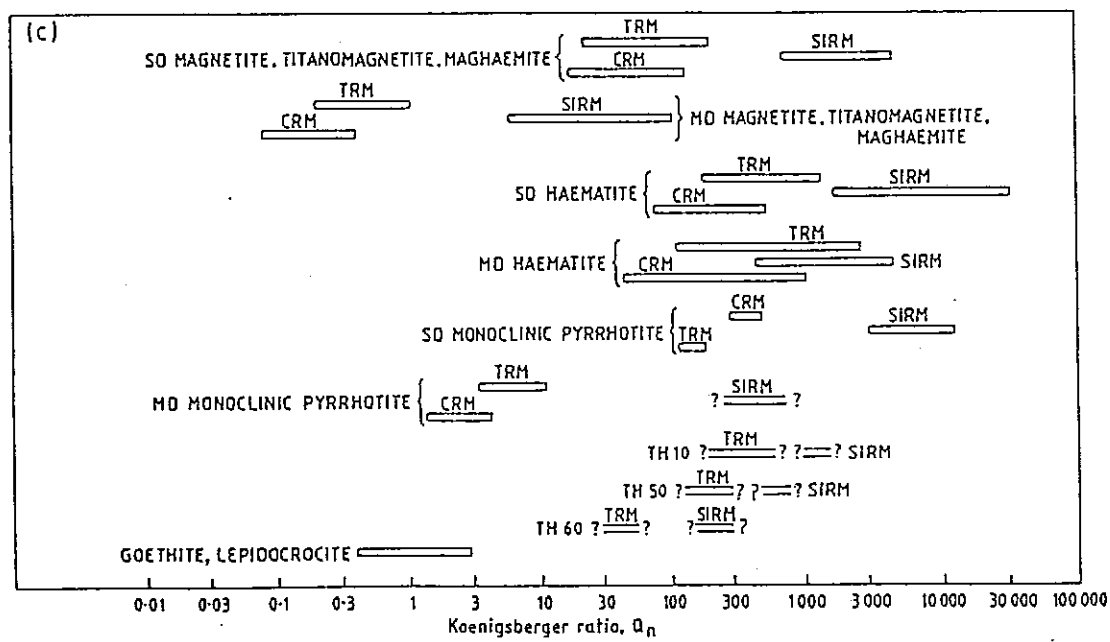
(c)
SD MAGNETITE, TITANOMAGNETITE, MAGHAEMITE
MD MAGNETITE, TITANOMAGNETITE, MAGHAEMITE
SD HAEMATITE
MD HAEMATITE
SD MONOCLINIC PYRRHOTITE
MD MONOCLINIC PYRRHOTITE
TH 10
TH 50
TH 60
TRM
CRM
SIRM
GOETHITE, LEPIDOCROCITE
0·01 0·03 0·1 0·3 1 3 10 30 100 300 1000 3 000 10 000 30 000 100 000
Koenigsberger ratio, Q_n

Figure 6. Principle of Zijderveld plots of demagnetization data. The remanence vector is remeasured after successive demagnetization steps.

(a) Successive remanence vectors, showing initial removal of a low stability component (linear segment), followed by simultaneous removal of two components with overlapped stability spectra (curved trajectory) and, finally, removal of the most stable component (linear segment, heading towards the origin).

(b) By simply plotting the vector end-points the diagram is clarified. However the directions of the low and high stability components are not very clear from this single diagram.

(c) The NRM as the resultant of soft and hard remanence components. When the directions of the components have been determined by fitting straight lines to the soft and hard segments, the intensities of each component can be calculated.

(d) By projecting the vector end-points onto orthogonal planes, the horizontal plane and either the N-S or the E-W vertical plane, the directions of the remanence components can be visualised. Corresponding segments that are linear in both projections indicate linear trajectories in 3-space, i.e. single remanence components. When a segment is curved in at least one projection, more than one component is being removed by the demagnetisation. If the linear segments representing the most stable resolved component are bypassing the origin, this indicates the presence of a harder unresolved component.

ORTHOGONAL PROJECTIONS (ZIJDERVELD PLOTS)

(a) Successive remanence vectors

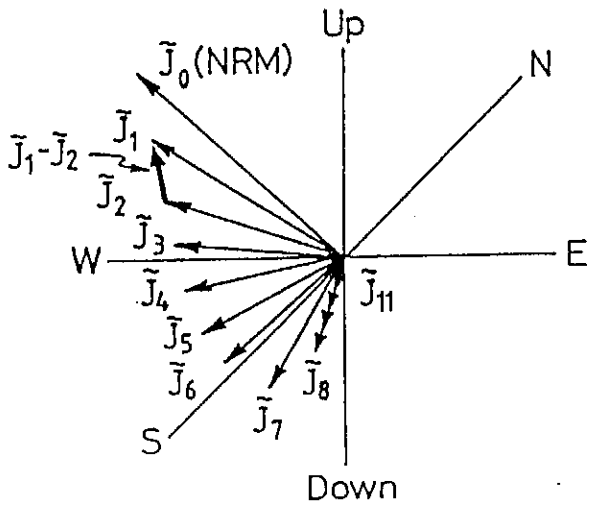

(b) Vector end-points

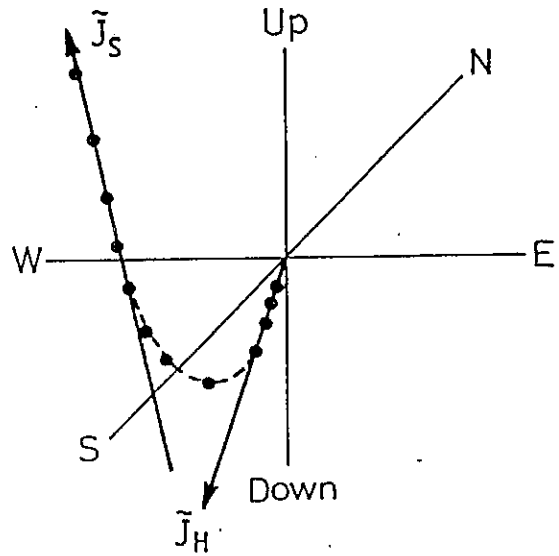

(c) Decomposition of two-component NRM

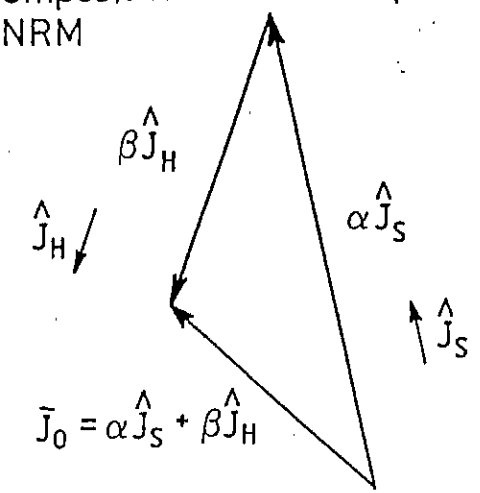

(d) Orthogonal projections

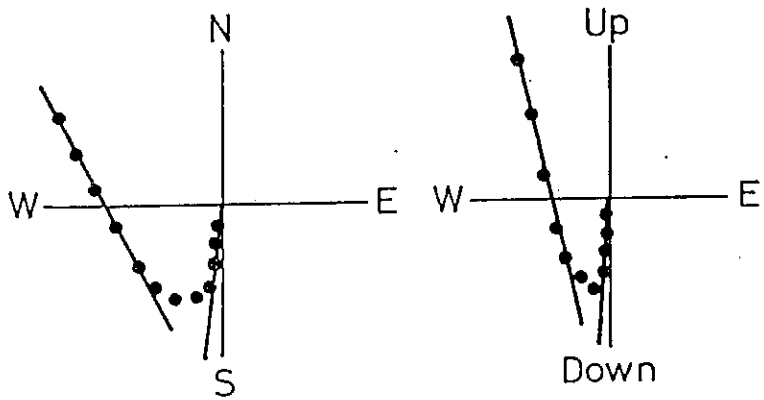

Figure 7. Characteristic AF demagnetization curves of acicular single domain (SD), small pseudosingle domain (PSD) and large multidomain (MD) grains of magnetite. The corresponding grain sizes are submicron, one to several microns and greater than 100 μm respectively.

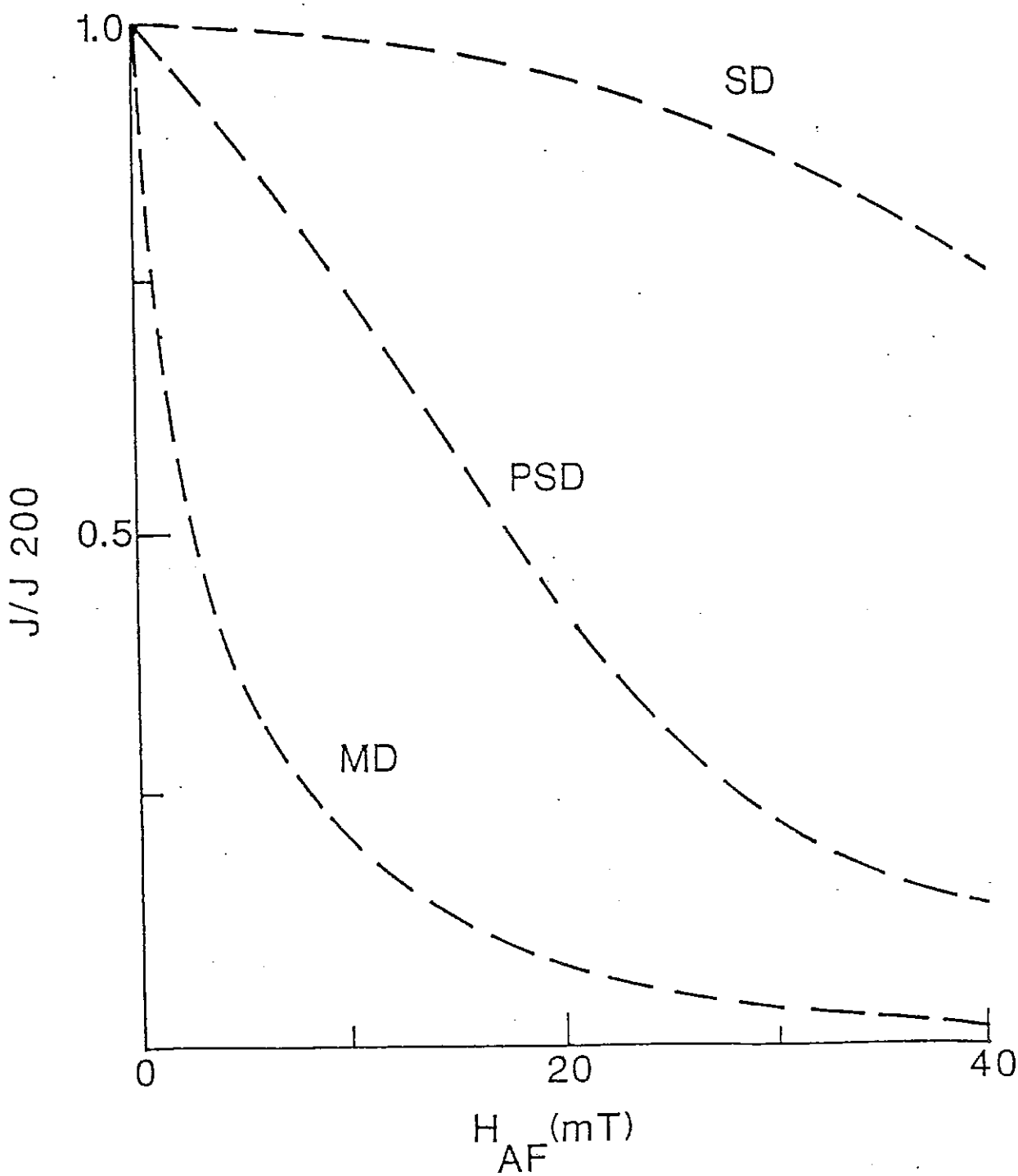
1.0
0.5
J/J 200
SD
PSD
MD
0
20
40
H AF (mT)

Figure 8. Characteristic normalised k-T curves of paramagnetic, superparamagnetic, titanomagnetite, SD magnetite and MD magnetite grains.

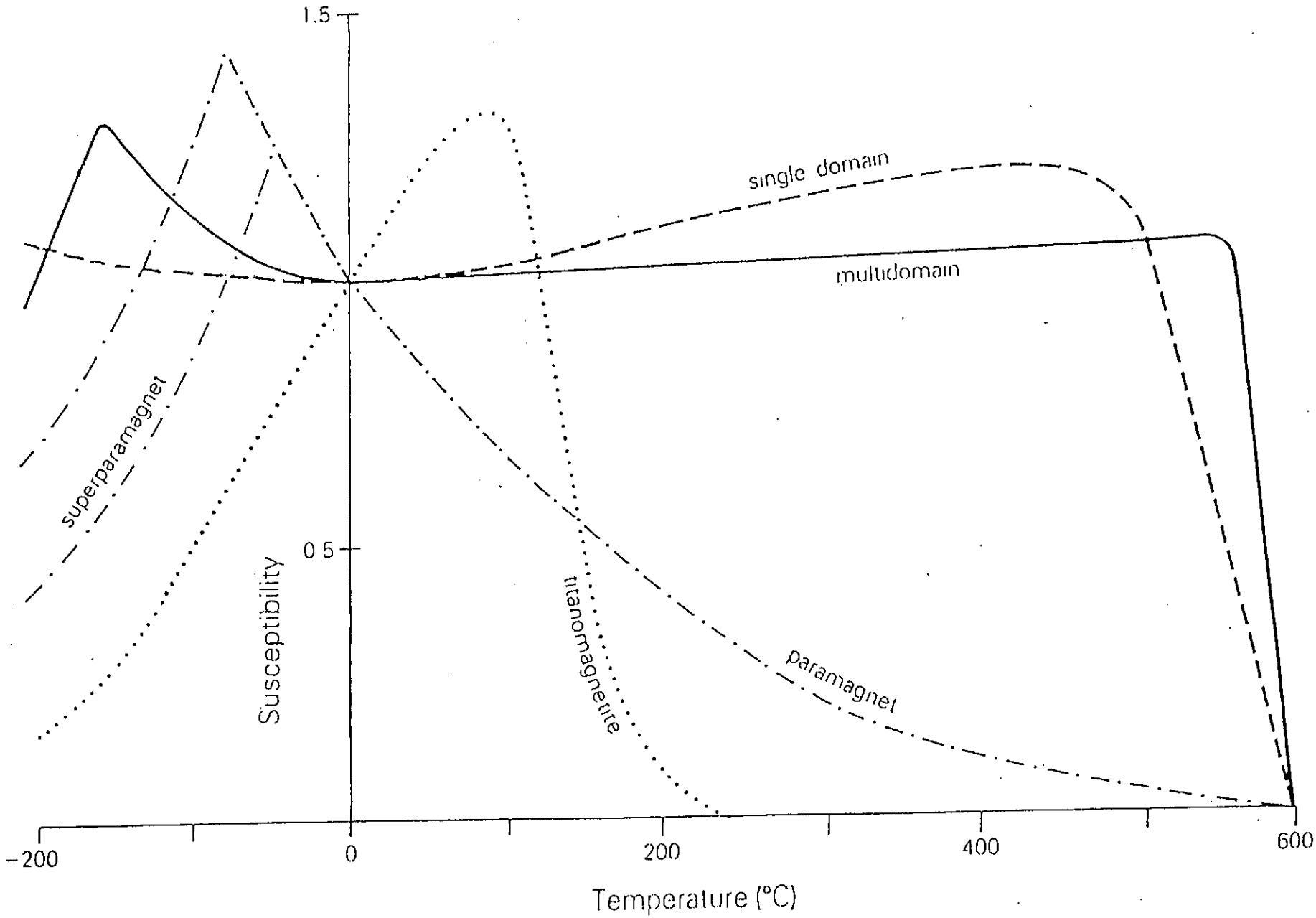
1.5
0.5
single domain
multidomain
superparamagnet
titanomagnetite
paramagnet
Susceptibility
-200
0
200
400
600
Temperature (°C)

Figure 9. Typical k-T curves of a monzonite containing MD magnetite and a basalt containing titanomagnetite (60 mole% usp).

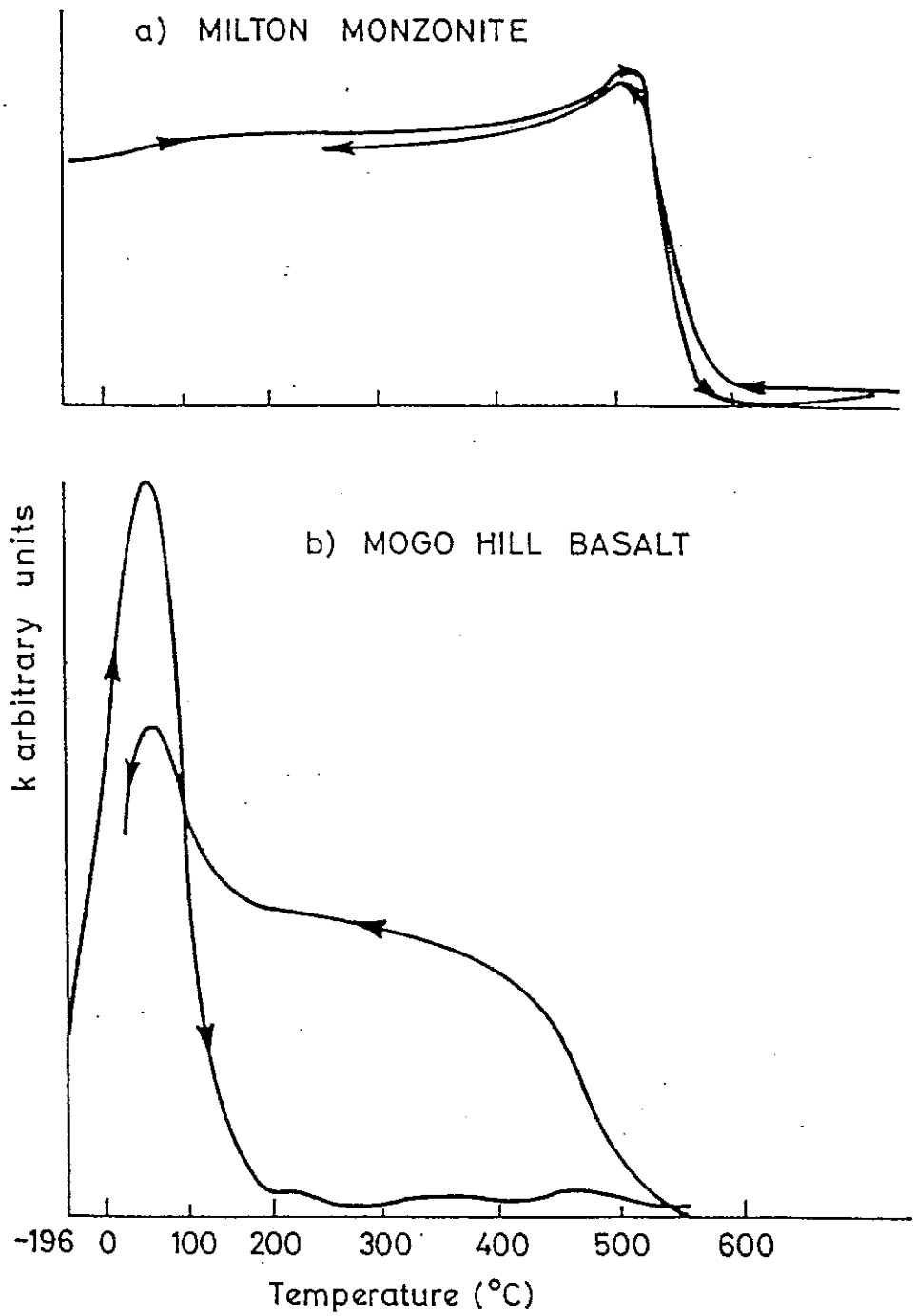
a) MILTON MONZONITE
b) MOGO HILL BASALT
k arbitrary units
-196
0
100
200
300
400
500
600
Temperature (°C)

Figure 10. k-T curve of an ilmenite separate from a beach sand. The irreversibility of the curve on cooling indicates chemical change has occurred during heating. The ilmenite is paramagnetic over the whole temperature range examined and exhibits a 1/T dependence of susceptibility at low temperatures.

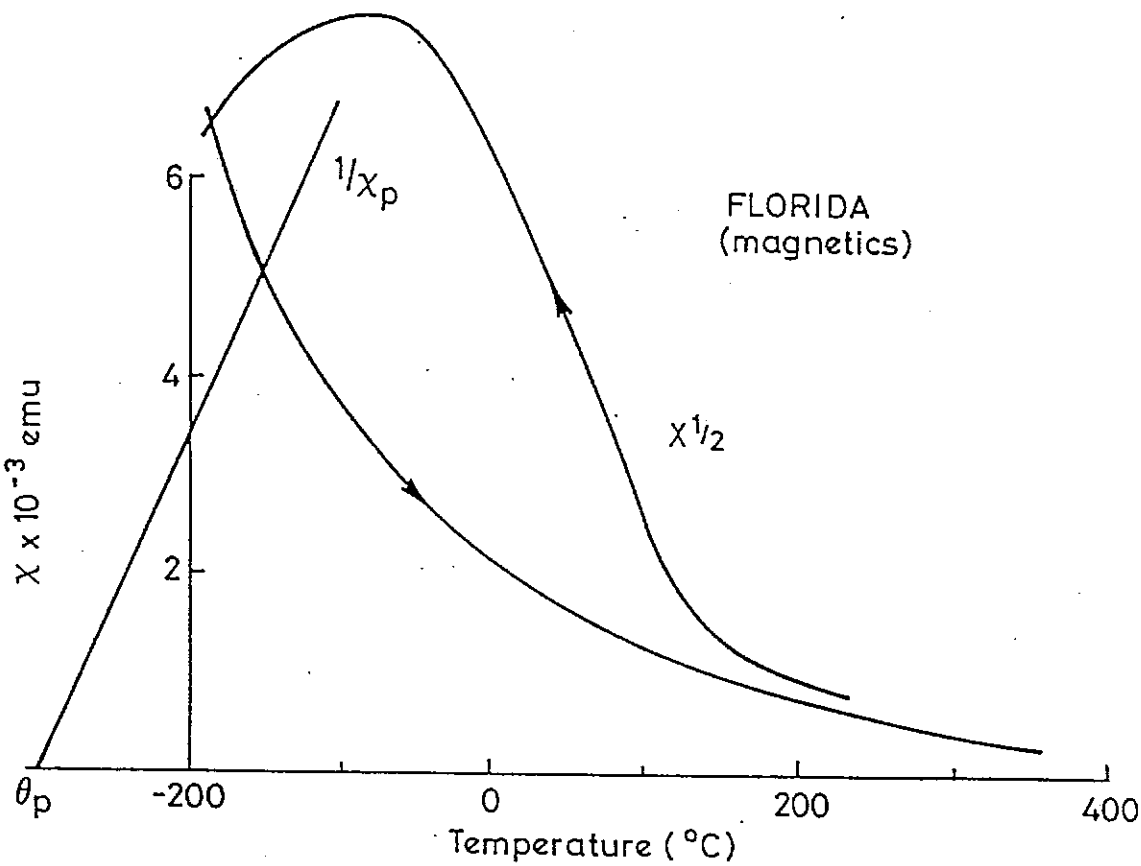
FLORIDA
(magnetics)
$1/\chi_p$
$\chi^{1/2}$
$\chi \times 10^{-3}$ emu
6
4
2
θ_p
-200
0
200
400
Temperature (°C)

Figure 11. Diagnostic k-T curves of some iron ores. Labelled features are: (a) the isotropic point of magnetite (-155°C), characteristic of MD or PSD pure magnetite; (b) the Morin transition (-20°C), indicating well-crystallised pure haematite; (c) the unblocking peak, immediately preceding the steep descent to the Curie point. The Curie points are 580°C for magnetite and 670°C for haematite. The Curie point for cation-deficient magnetite (kenomagnetite) is variable, but is often ~610°C. The samples are: DDH 42/ 300.5 = BIF containing MD magnetite; TP01B = haematite ore with minor MD magnetite (which dominates the susceptibility); MN01B = haematite ore with minor SD magnetite; Channar = haematite ore with minor MD magnetite; PB01B = pure haematite ore; CANGA = pisolitic laterite containing SPM and SD kenomagnetite.

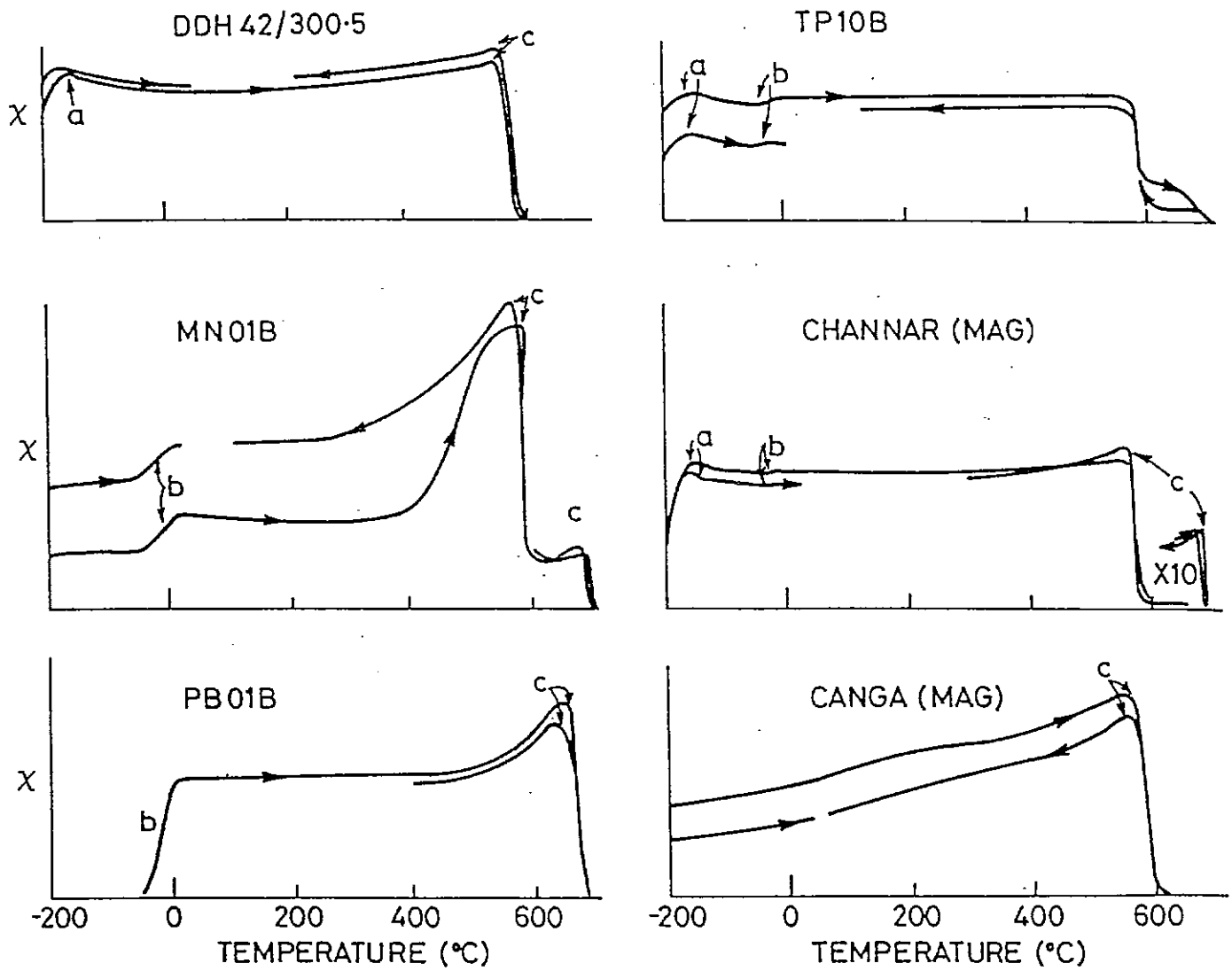
DDH 42/300·5
χ
a
c
TP10B
a
b
MN01B
χ
b
c
c
CHANNAR (MAG)
a
b
c
X10
PB01B
χ
b
c
CANGA (MAG)
c
-200
0
200
400
600
TEMPERATURE (°C)
-200
0
200
400
600
TEMPERATURE (°C)

Figure 12. The anisotropy of magnetic susceptibility (AMS) magnetic fabric ellipsoid. The ellipsoid is aligned with the principal susceptibility directions and has semi-axes equal to the principal susceptibilities. The maximum susceptibility axis defines the magnetic lineation. The magnetic foliation is the plane of relatively high susceptibility containing the maximum and intermediate susceptibility axes. k_1, maximum susceptibility. k_2, intermediate susceptibility. k_3, minimum susceptibility.

SUSCEPTIBILITY ELLIPSOID : MAGNETIC FABRIC

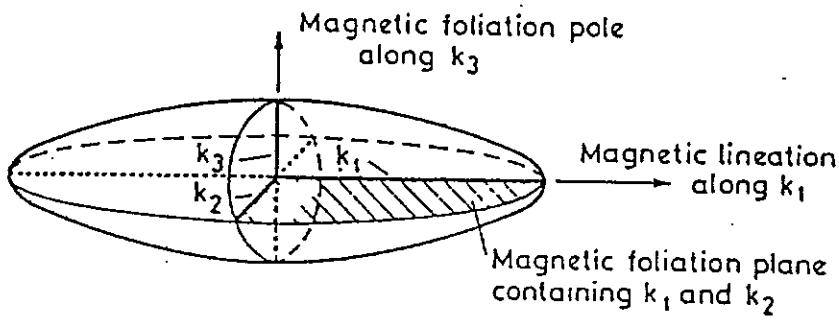

Anisotropy Magnitude $A = k_1/k_3$

Lineation Magnitude $L = k_1/k_2$

Foliation Magnitude $F = k_2/k_3$

Ellipsoid Prolateness $P = L/F$

- $P = 0$ uniaxial oblate ellipsoid (disc)
- $P = \infty$ uniaxial prolate ellipsoid (needle)

Figure 13. Histograms of the magnetic susceptibility (top) and NRM (bottom) of samples from the Stones Creek Formation (DCv). μG/Oe = SI/4π*1000000. μG = mA/m.

DCv - Magnetic Susceptibility

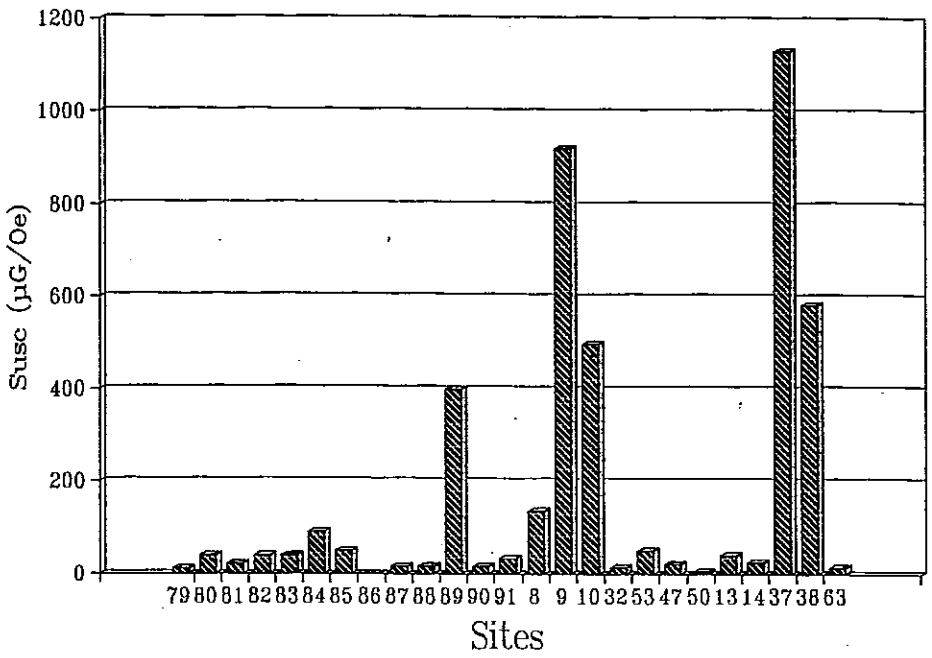

DCv - Natural Remanent Magnetization

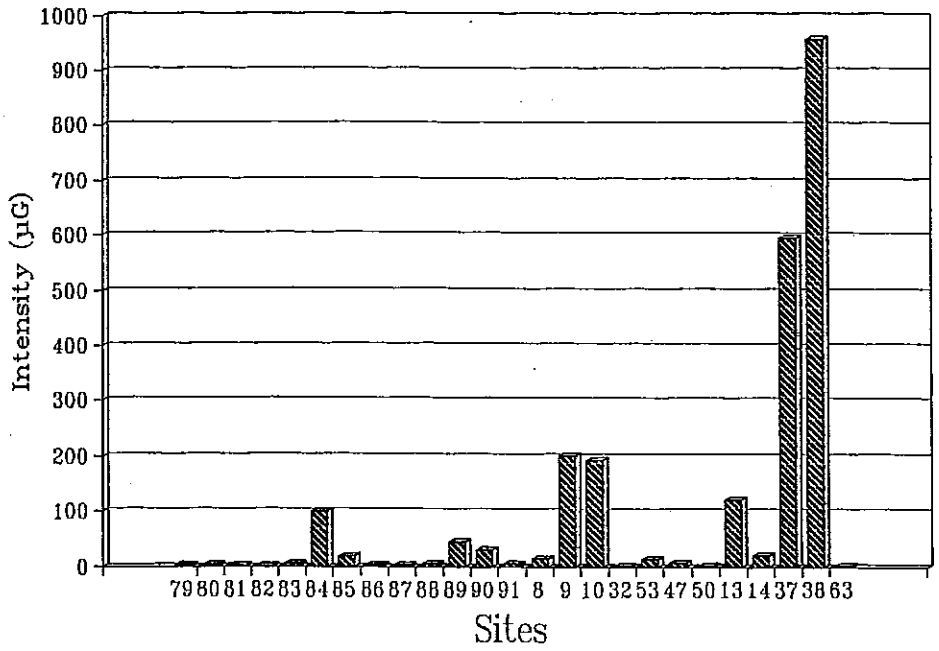

Figure 14. Histograms of the magnetic susceptibility (top) and NRM (bottom) of samples from the Smedley Volcanic Subgroup (CVi). Susceptibility of samples from the DCv_A unit are also included in the top histogram. $\mu G/Oe = SI/4\pi*1000000$. μG = mA/m.

CVi/DCva – Magnetic Susceptibility

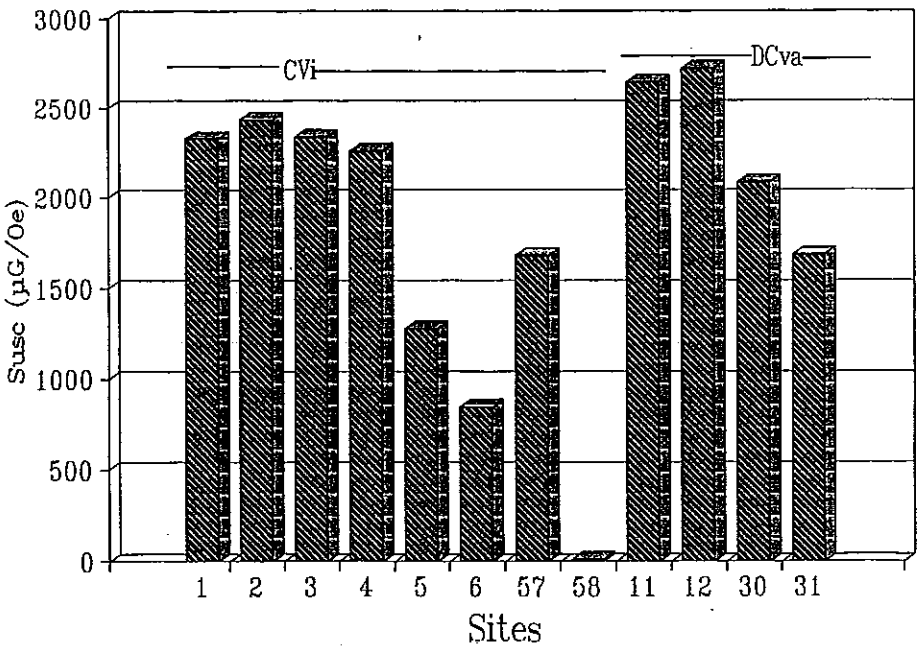

CVi – Natural Remanent Magnetization

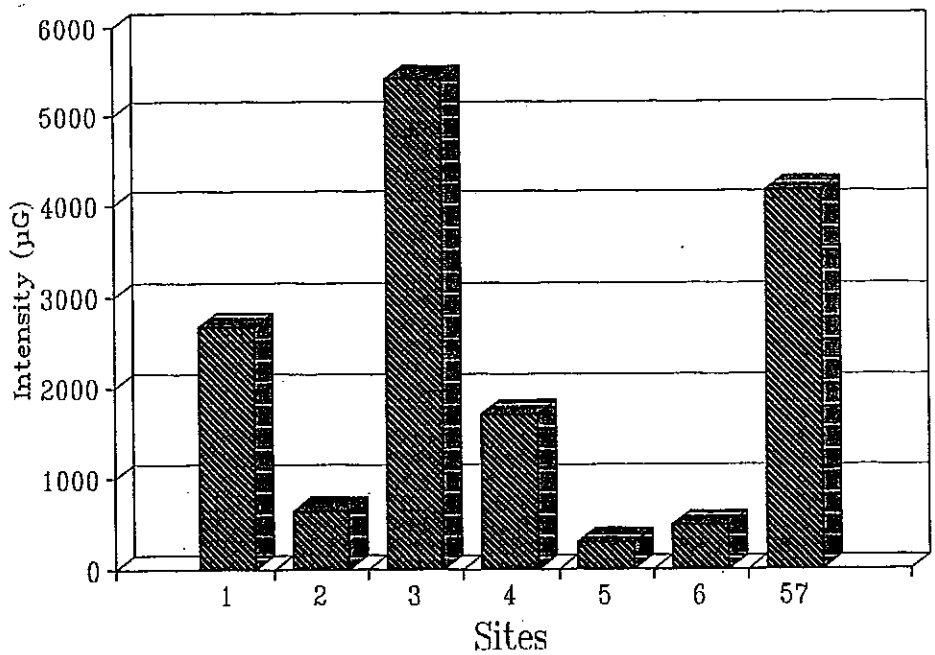

Figure 15. Histogram of the magnetic susceptibility of samples from the Prospects. $\mu G/Oe = SI/4\pi*1000000$. μG = mA/m. Note, very low susceptibilities.

Prospects - Magnetic Susceptibility

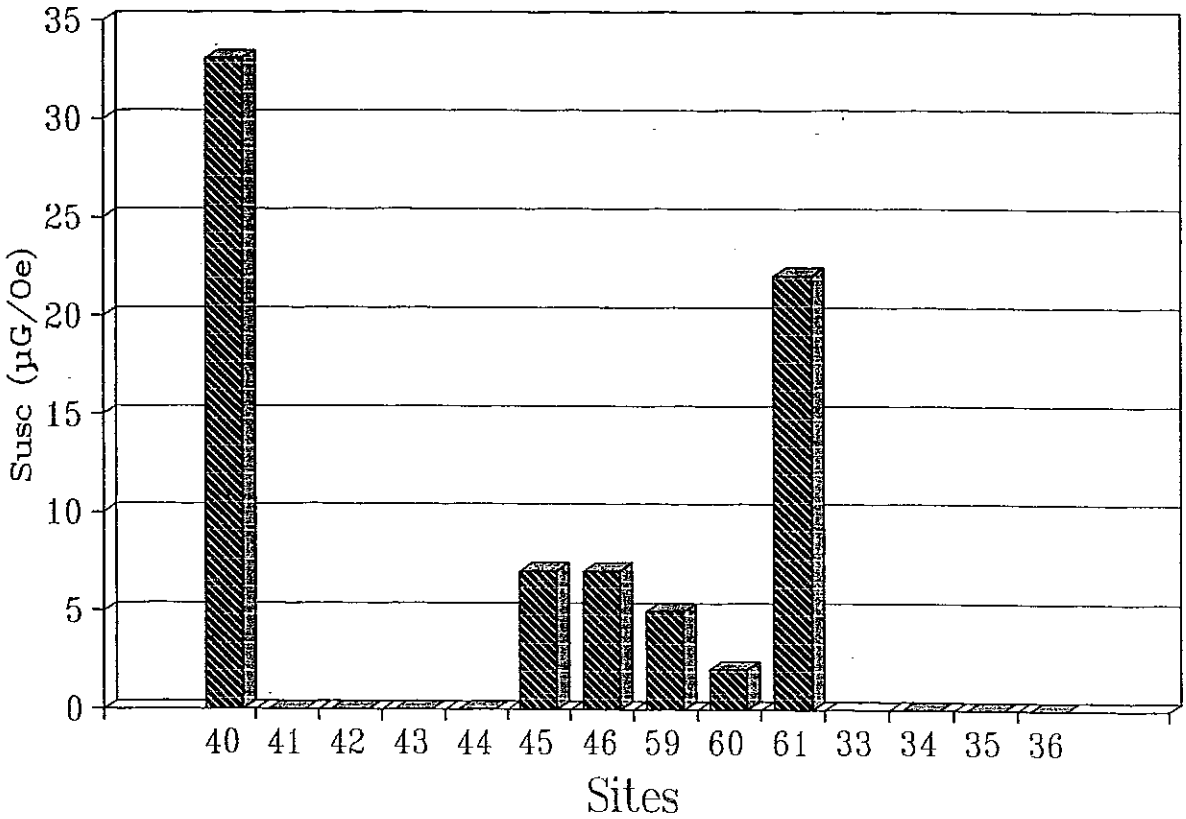

Figure 16. Intensity plot, stereographic plot and orthogonal plot of thermal demagnetization of selected specimens. In orthogonal plots, open symbols refer to the zx direction (i.e. up or down) while the closed symbols refer to the xy direction (i.e. direction with respect to north). Specimen name is indicated above the orthogonal plot. Intensity is in μG [mA/m]. Scale for each orthogonal plot is indicated at the bottom of the plot. Treatment steps are indicated on abscissa of the intensity plot. NRM is outermost step, subsequent steps approaching the origin. First and final steps are indicated above the plot. Intensity plots, show the intensity of magnetization after each successive thermal step. The spectra is the magnitude of the gradient of the demagnetization curve. In stereographic plot, closed (open) symbols indicate lower (upper) hemisphere.

A & B, CVi pyroclastic flows. C-K, DCv pyroclastic and volcanic flows. L & M, hydrothermally altered samples from prospects. O-Q, Carboniferous plutons. R & S, "mapped" Carboniferous volcanics, shallow inclination indicates an older age for the volcanics. T & U, Dam Ignimbrite. V, Bulgonunna Volcanics.
Note the dominant steep down direction which is observed in the majority of specimens.

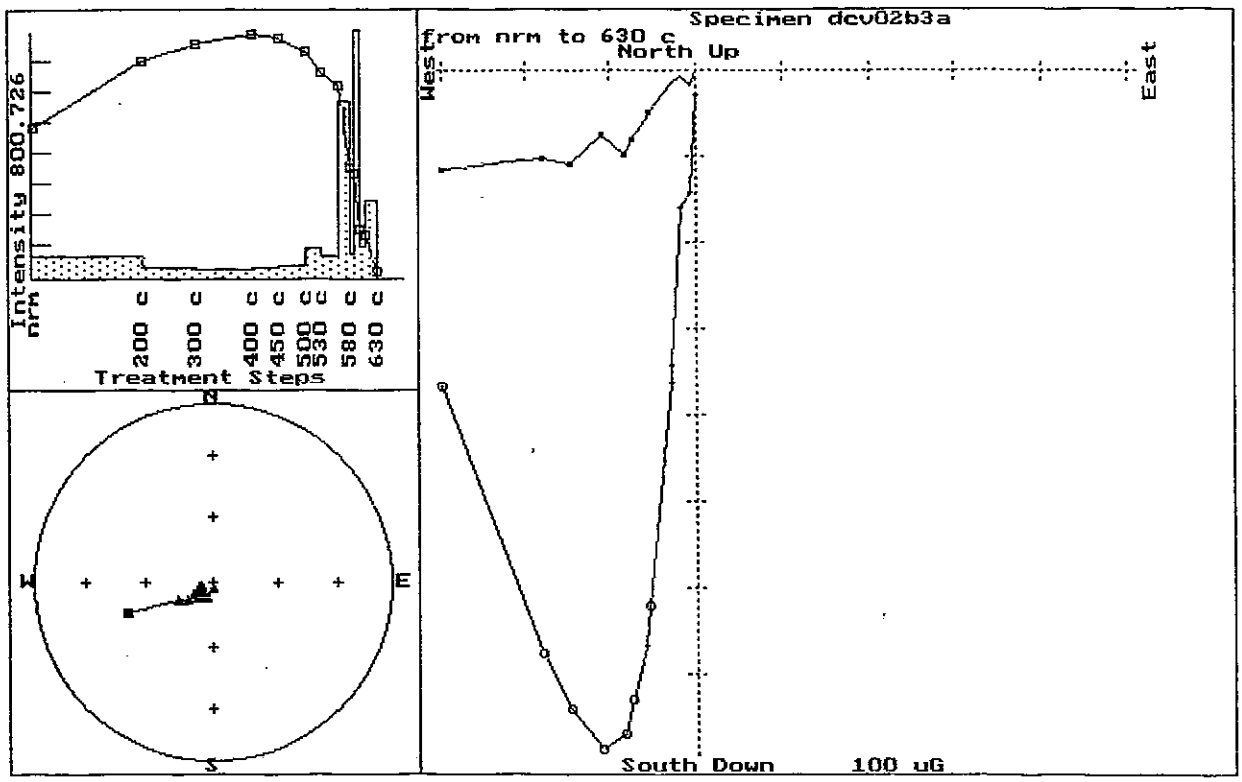
A
Specimen dcv02b3a
from nrm to 630 c
North Up
West
East
Intensity 800.726
nrm
200 c
300 c
400 c
450 c
500 c
530 c
580 c
630 c
Treatment Steps
N
W
E
S
South Down
100 uG

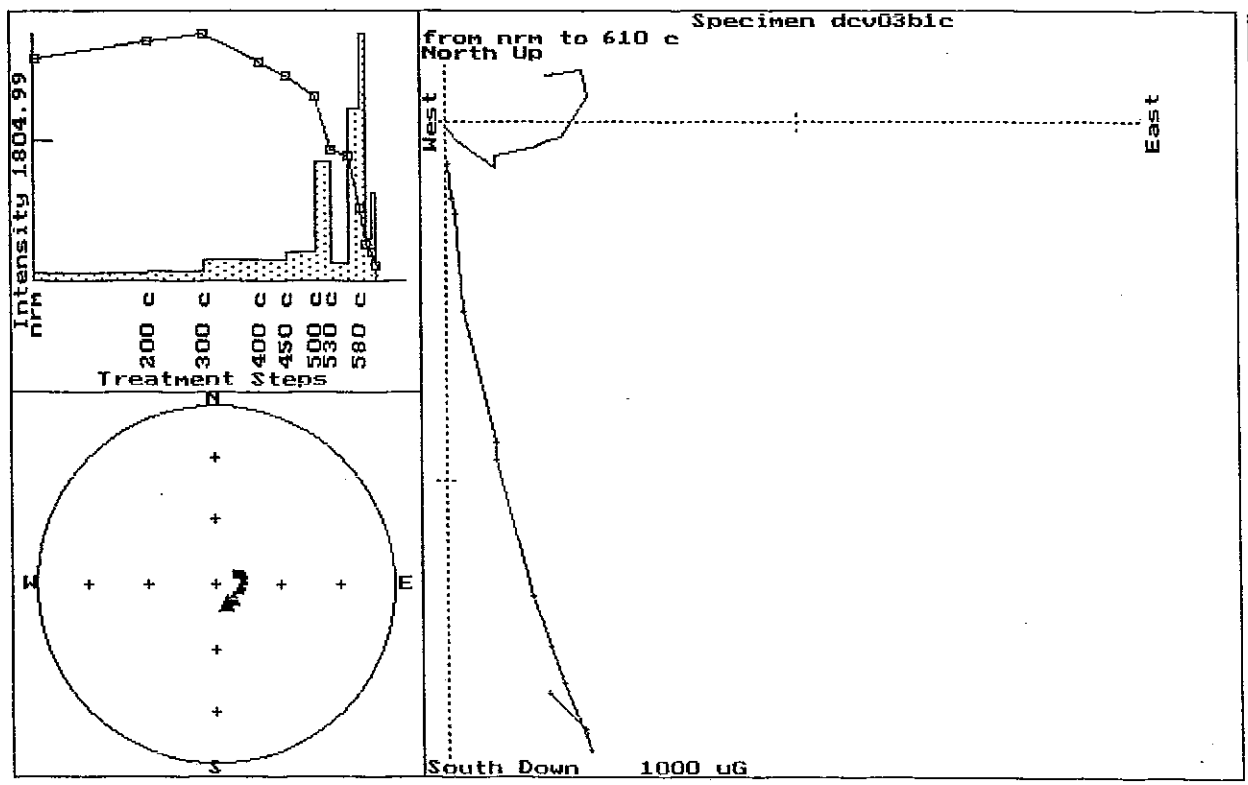
B
Specimen dcv03b1c
from nrm to 610 c
North Up
West
East
Intensity 1804.99
nrm
200 c
300 c
400 c
450 c
500 c
530 c
580 c
Treatment Steps
N
W
E
S
South Down
1000 uG

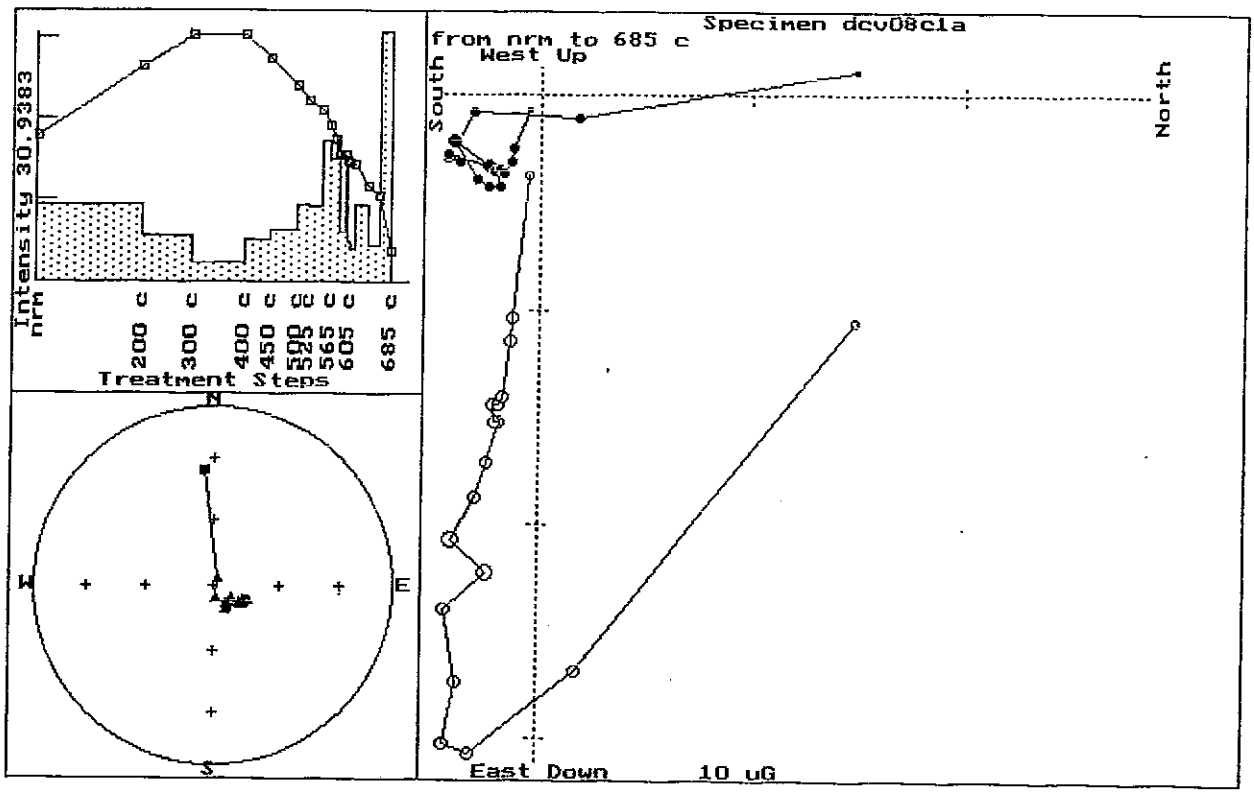
Intensity 30.9383
nrm
200 c
300 c
400 c
450 c
500 c
525 c
565 c
605 c
685 c
Treatment Steps
N
W
E
S
Specimen dcv08c1a
from nrm to 685 c
West Up
South
North
East Down
10 uG

C

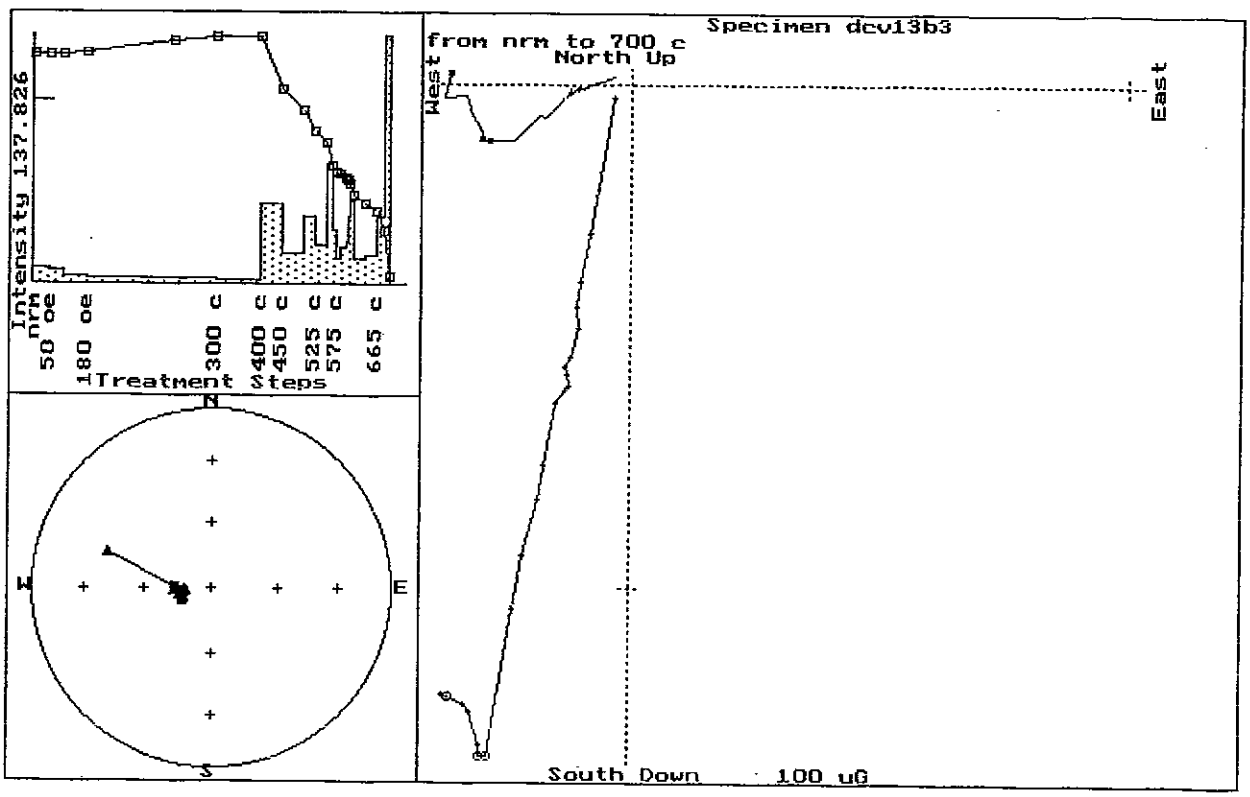
Intensity 137.826
nrm
50 oe
180 oe
300 c
400 c
450 c
525 c
575 c
665 c
Treatment Steps
N
W
E
S
Specimen dcv13b3
from nrm to 700 c
North Up
West
East
South Down
100 uG

D

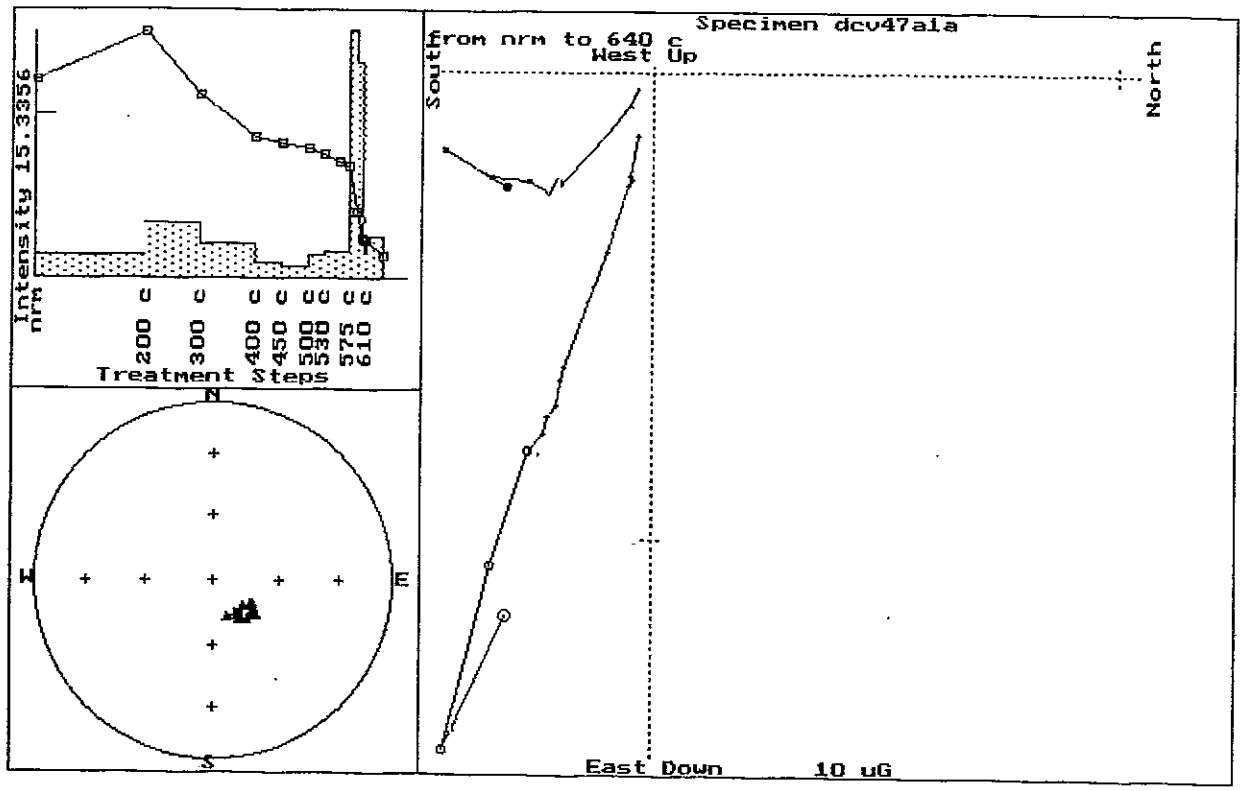
Intensity 15.3356
nrm
c c c c cc c c
200 300 400 450 500 530 575 610
Treatment Steps
N
W
E
S
Specimen dcv47a1a
from nrm to 640 c
West Up
South
North
East Down
10 uG

E

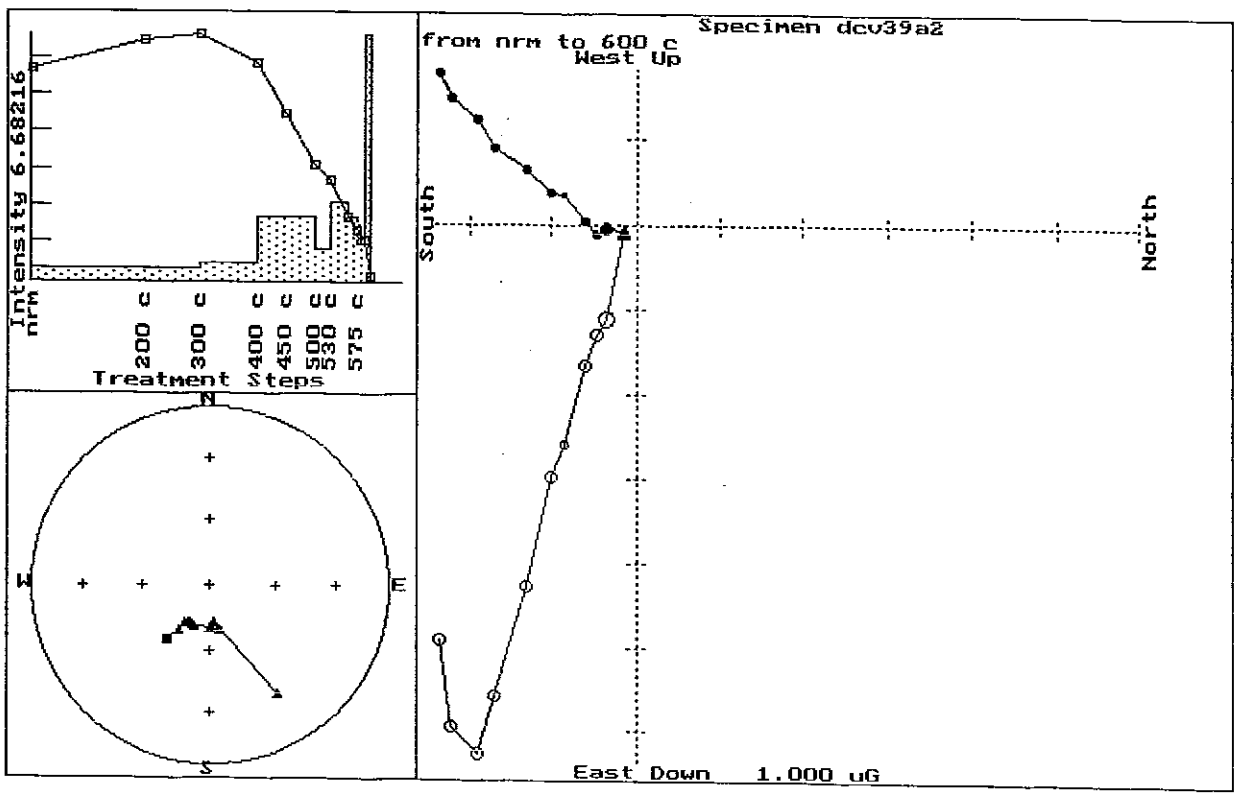
Intensity 6.68216
nrm
c c c c cc c
200 300 400 450 500 530 575
Treatment Steps
N
W
E
S
Specimen dcv39a2
from nrm to 600 c
West Up
South
North
East Down
1.000 uG

F

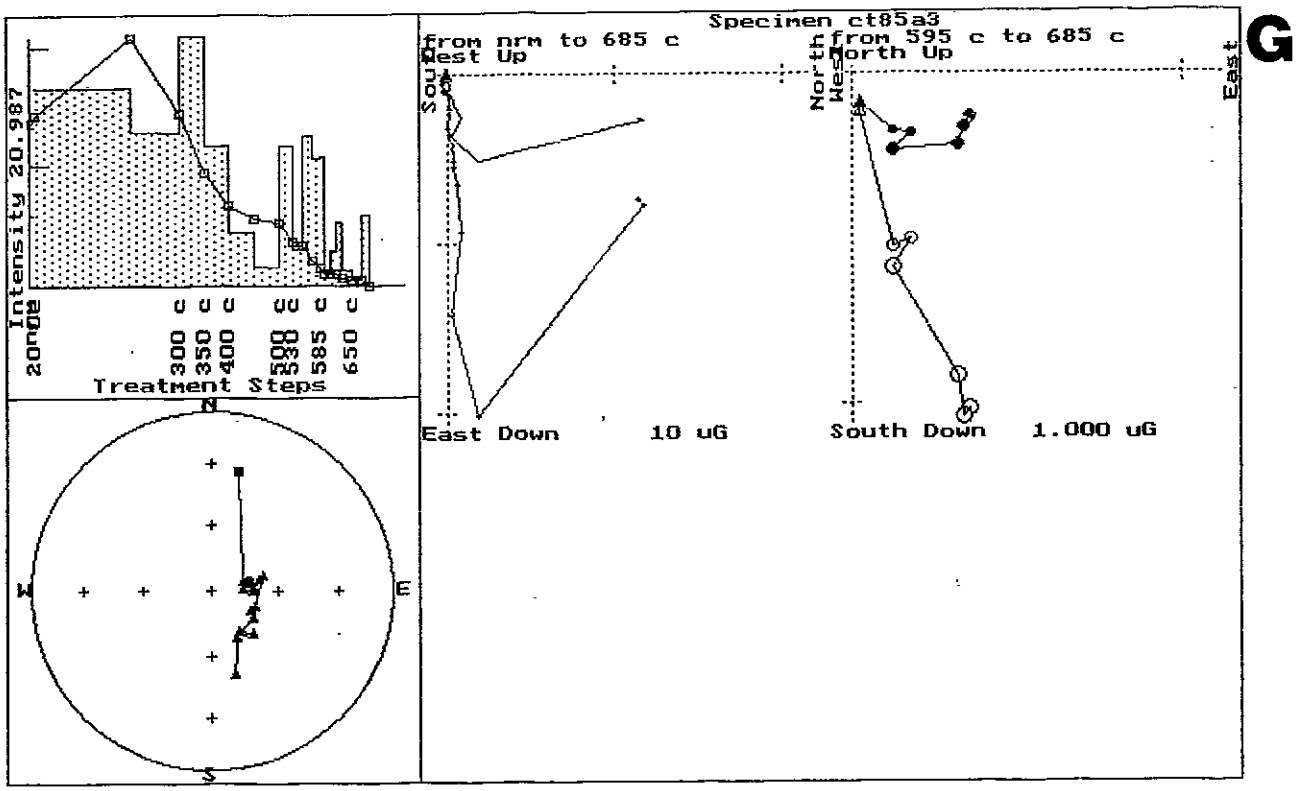
Specimen ct85a3
from nrm to 685 c
West Up
from 595 c to 685 c
North Up
Intensity 20.987
20mA
300 c
350 c
400 c
530 c
585 c
650 c
Treatment Steps
N
W
E
S
East Down
10 uG
South Down
1.000 uG
East

G

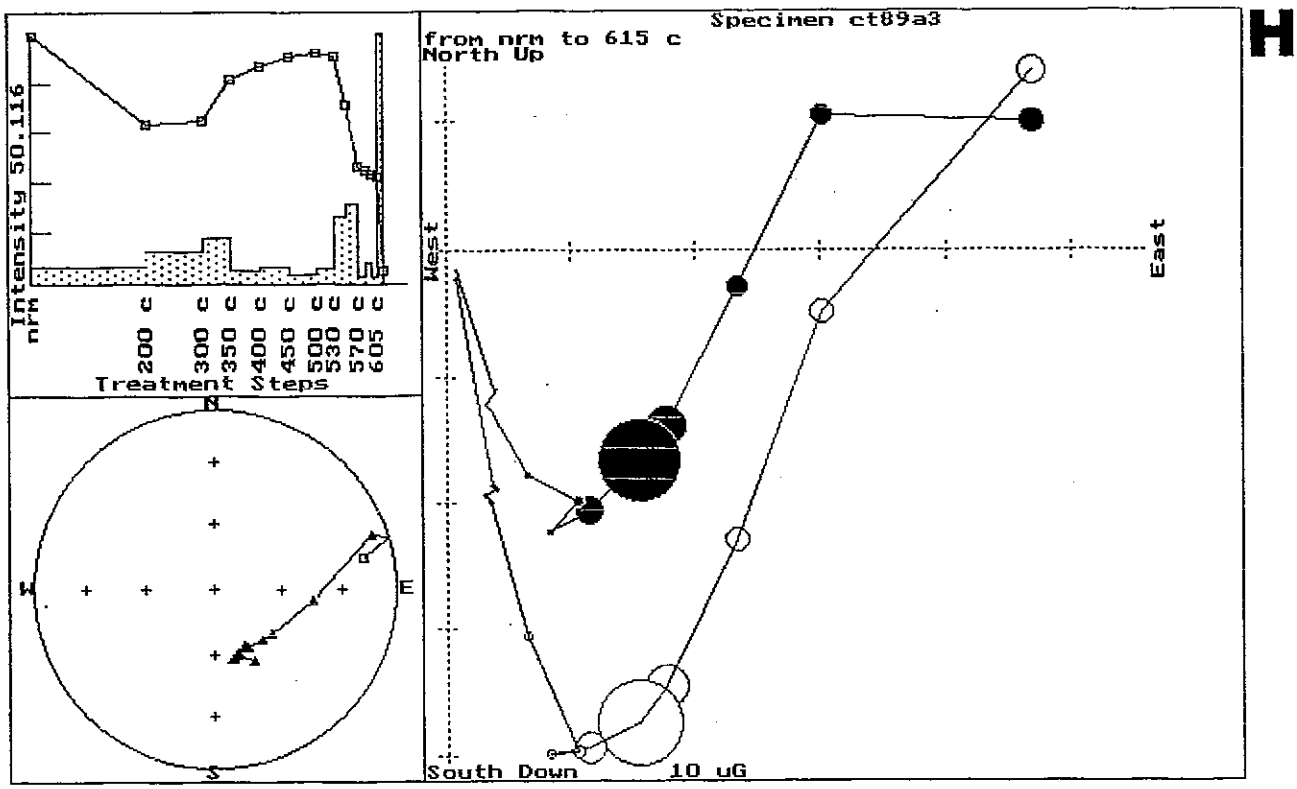
Specimen ct89a3
from nrm to 615 c
North Up
Intensity 50.116
nrm
200 c
300 c
350 c
400 c
450 c
500 c
530 c
570 c
605 c
Treatment Steps
N
W
E
S
West
East
South Down
10 uG

H

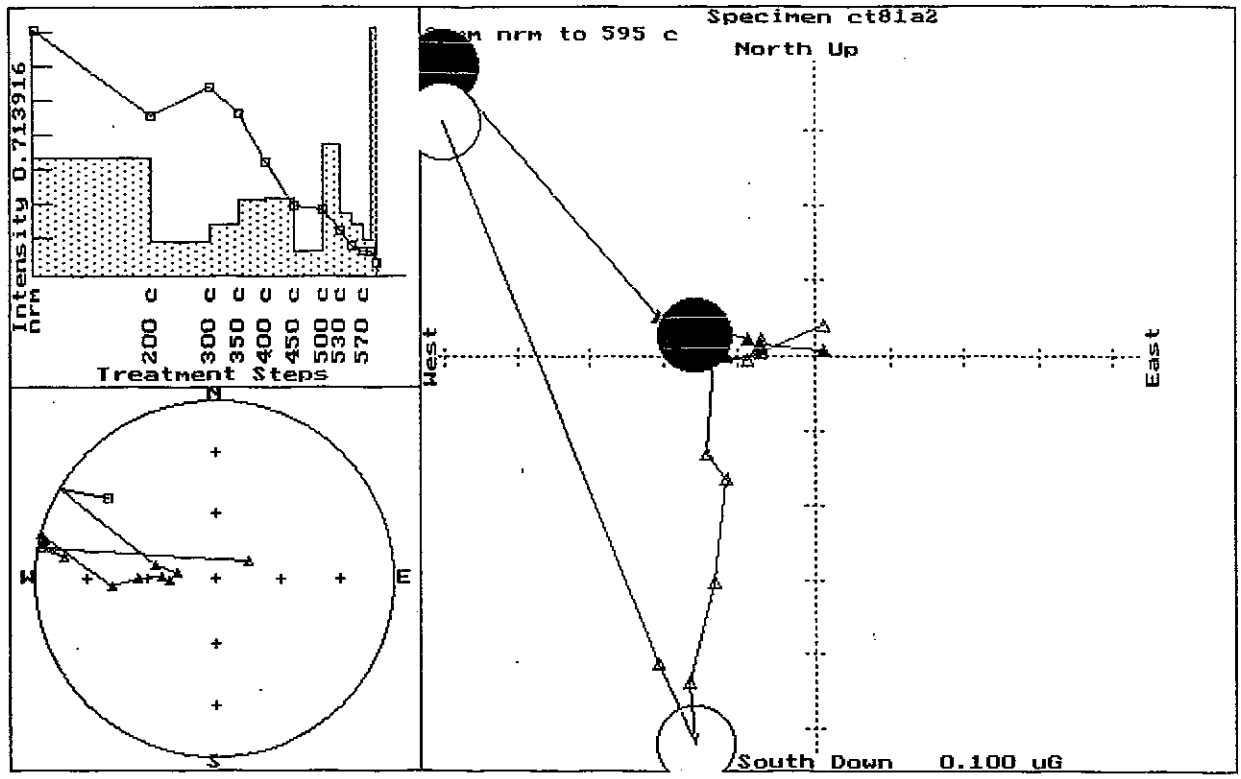
Intensity 0.713916
nrm
200 c
300 c
350 c
400 c
450 c
500 c
530 c
570 c
Treatment Steps
N
W
E
S
Specimen ct81a2
nrm to 595 c
North Up
West
East
South Down 0.100 uG

I

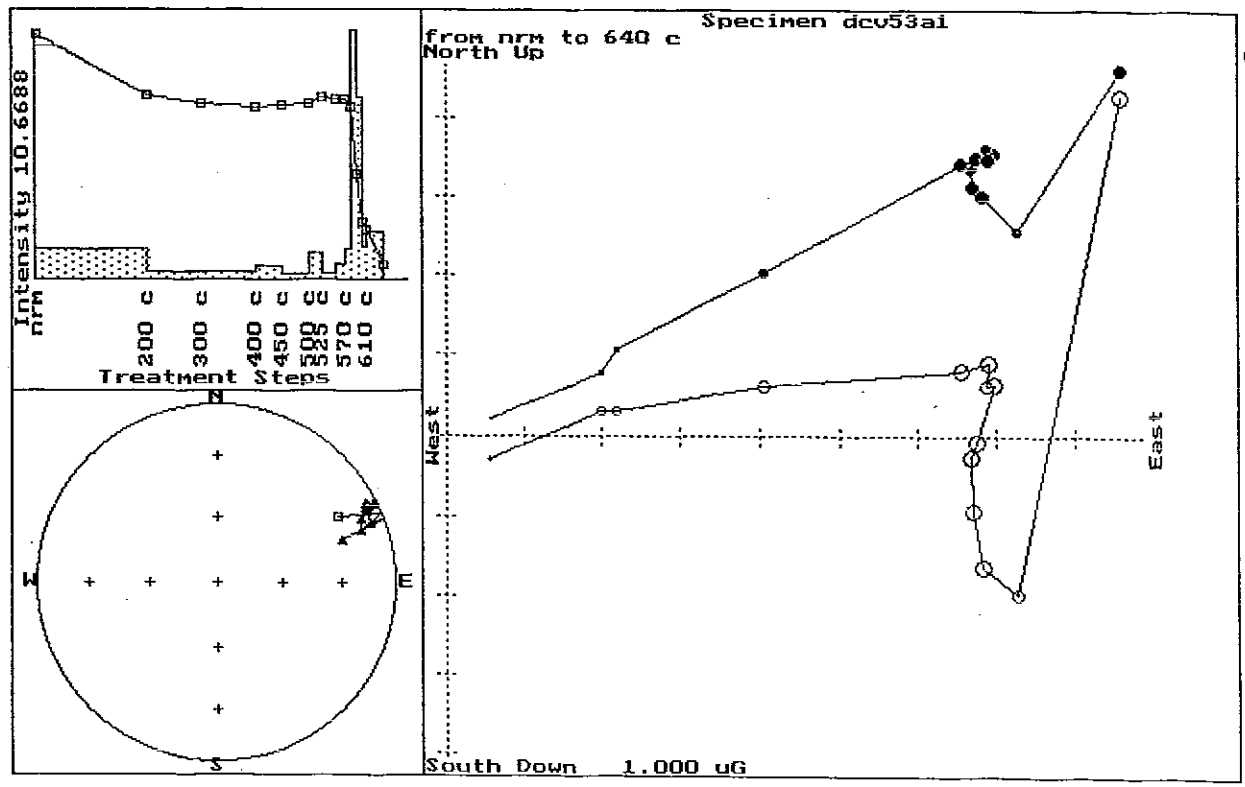
Intensity 10.6688
nrm
200 c
300 c
400 c
450 c
500 c
525 c
570 c
610 c
Treatment Steps
N
W
E
S
Specimen dcv53ai
from nrm to 640 c
North Up
West
East
South Down 1.000 uG

J

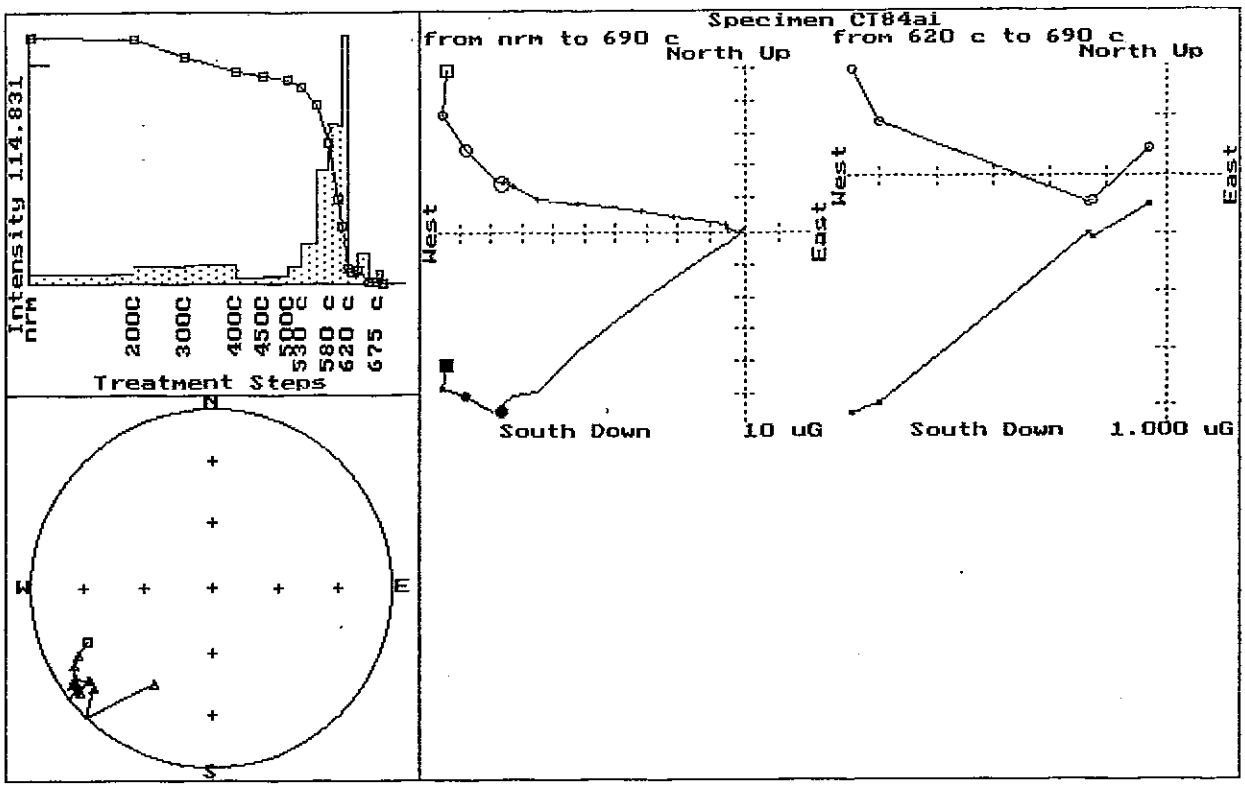
Specimen CT84ai
from nrm to 690 c
North Up
West
East
South Down
10 uG
from 620 c to 690 c
North Up
West
East
South Down
1.000 uG
Intensity 114.831
nrm
200C
300C
400C
450C
500C
530C
580 C
620 C
675 C
Treatment Steps
N
E
S
W

K

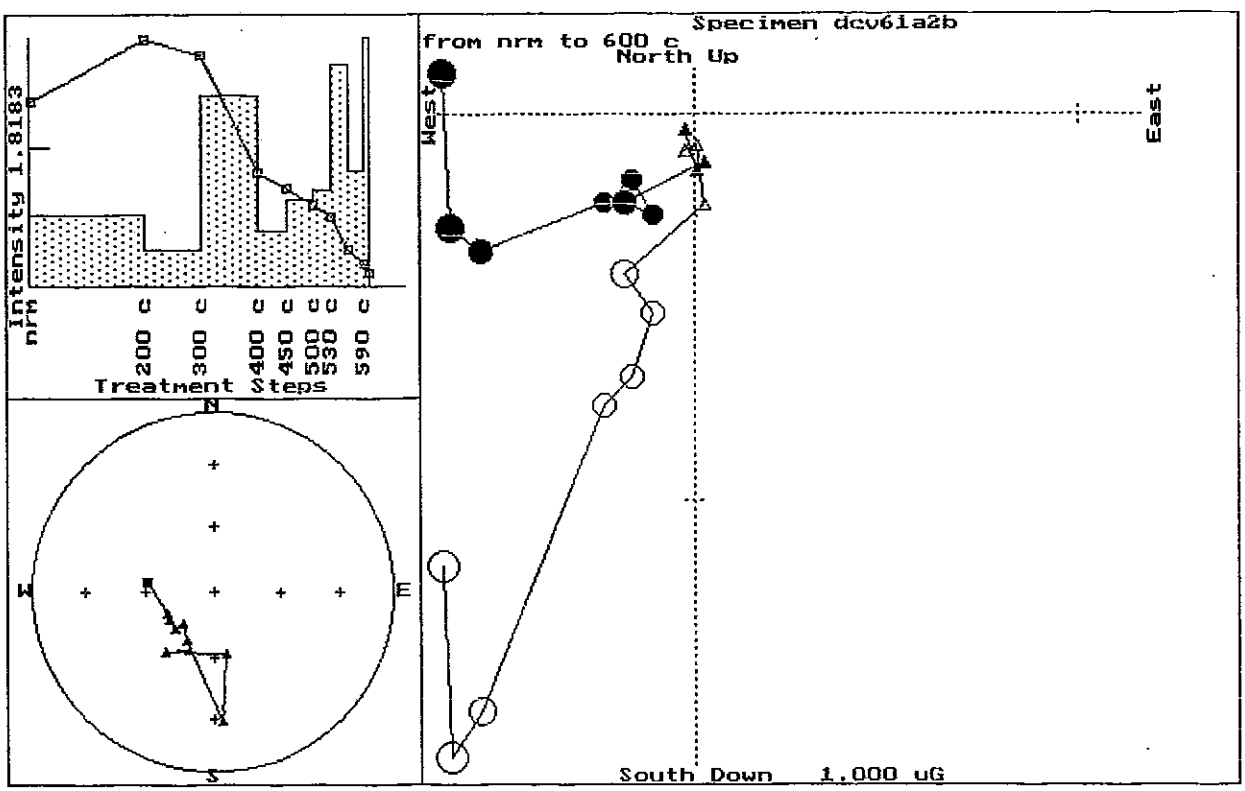
Specimen dcv61a2b
from nrm to 600 c
North Up
West
East
South Down
1.000 uG
Intensity 1.8183
nrm
200 C
300 C
400 C
450 C
500 C
530 C
590 C
Treatment Steps
N
E
S
W

L

M

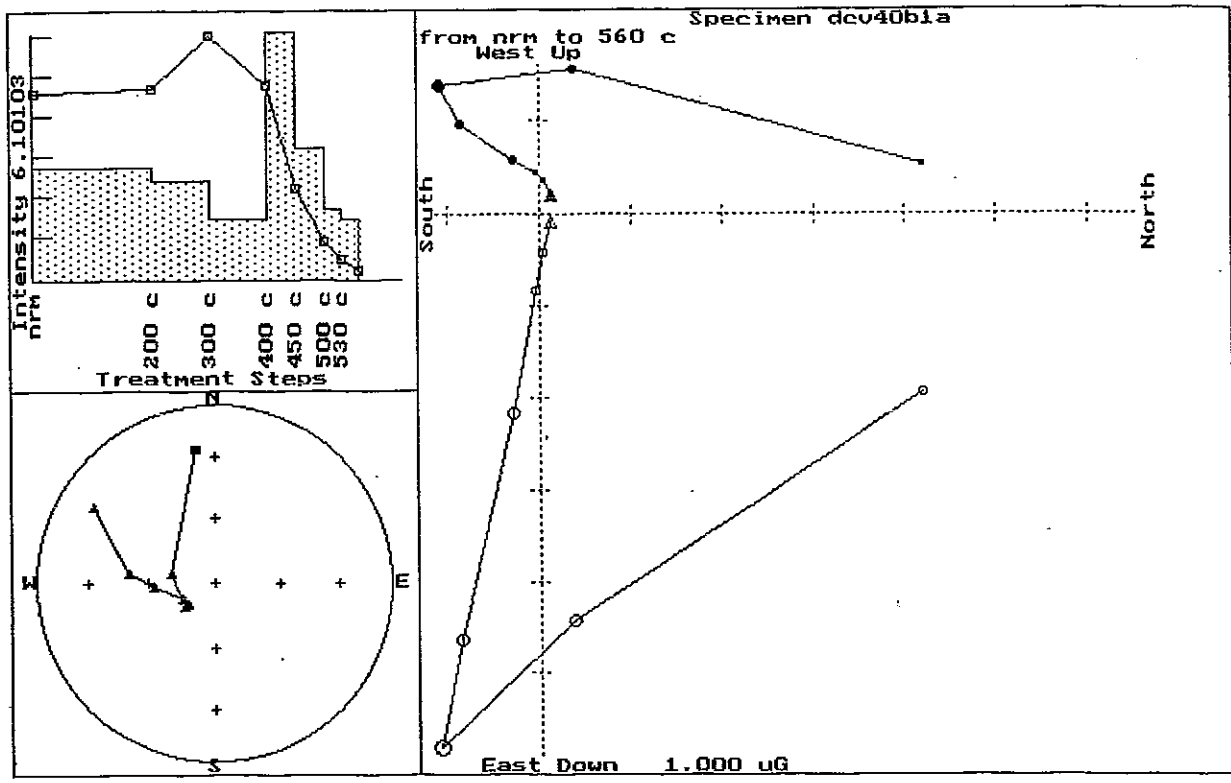
Specimen dcv40b1a
from nrm to 560 c
West Up
Intensity 6.10103
nrm
200 c
300 c
400 c
450 c
500 c
530 c
Treatment Steps
N
W
E
S
South
North
East Down 1.000 uG

N

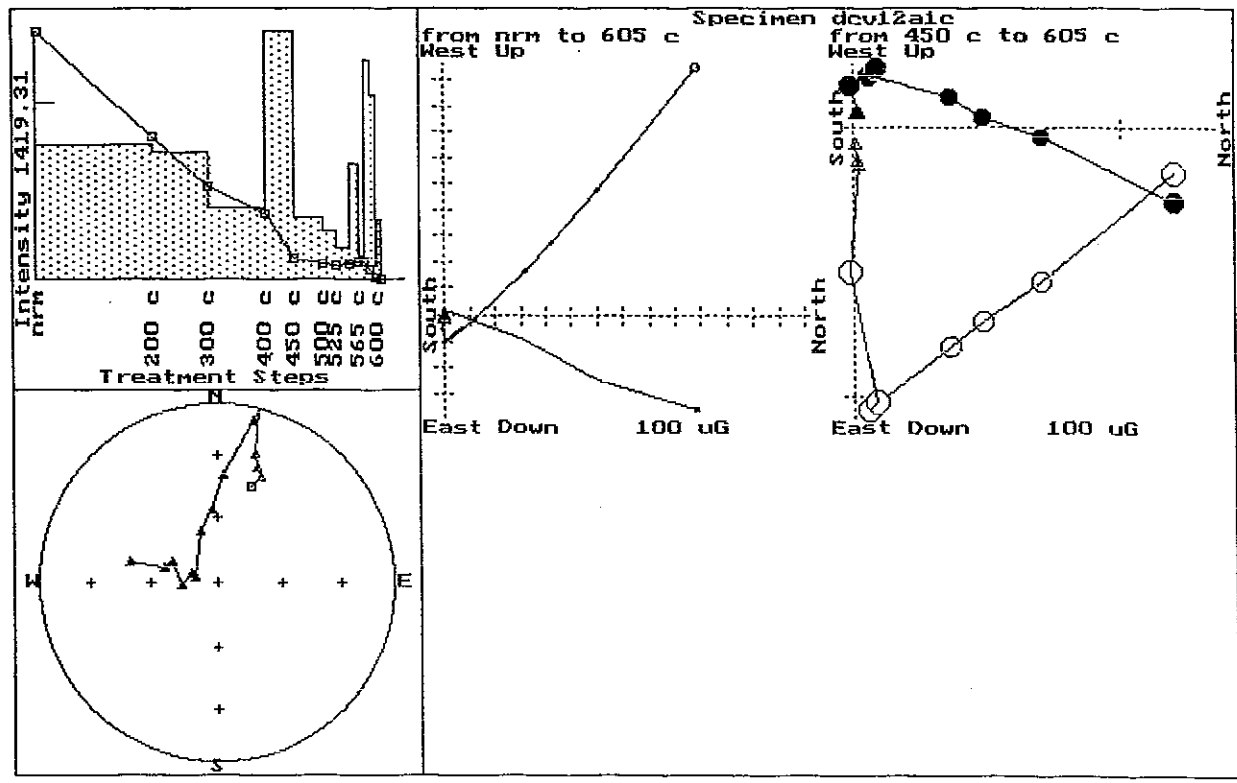
Specimen dcv12a1c
from nrm to 605 c
West Up
from 450 c to 605 c
West Up
Intensity 1419.31
nrm
200 c
300 c
400 c
450 c
500 c
525 c
565 c
600 c
Treatment Steps
N
W
E
S
South
North
East Down 100 uG
East Down 100 uG

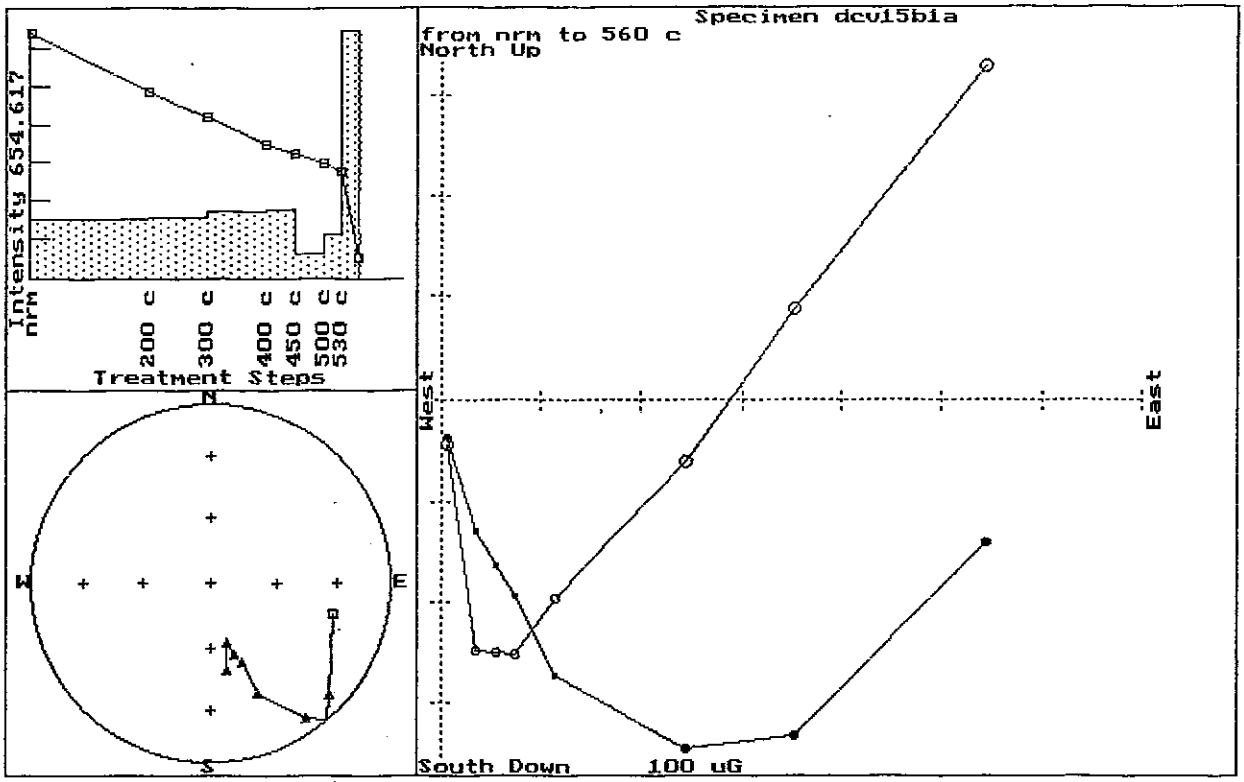
Specimen dcv15bia
from nrm to 560 c
North Up
Intensity 654.617
nrm
200 c
300 c
400 c
450 c
500 c
530 c
Treatment Steps
N
W
E
S
West
East
South Down
100 uG

O

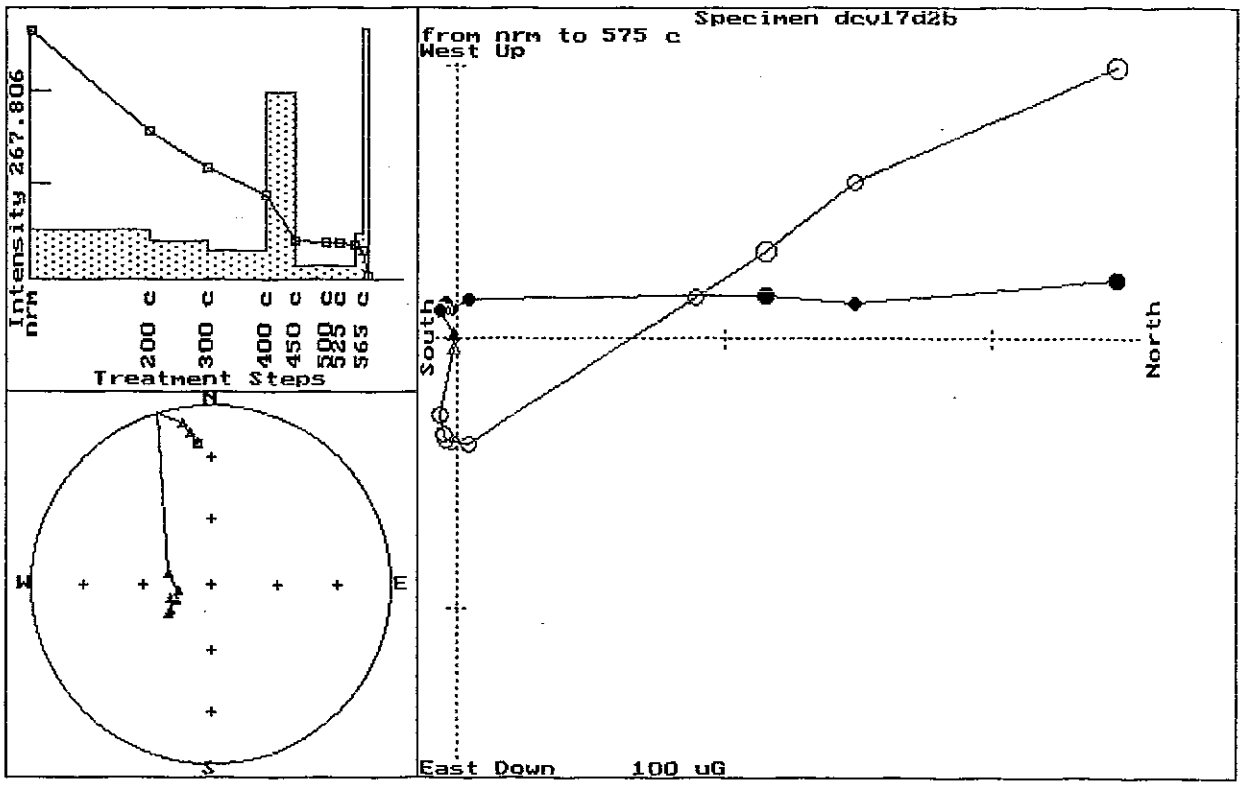
Specimen dcv17d2b
from nrm to 575 c
West Up
Intensity 267.806
nrm
200 c
300 c
400 c
450 c
500 c
525 c
565 c
Treatment Steps
N
W
E
S
South
North
East Down
100 uG

P

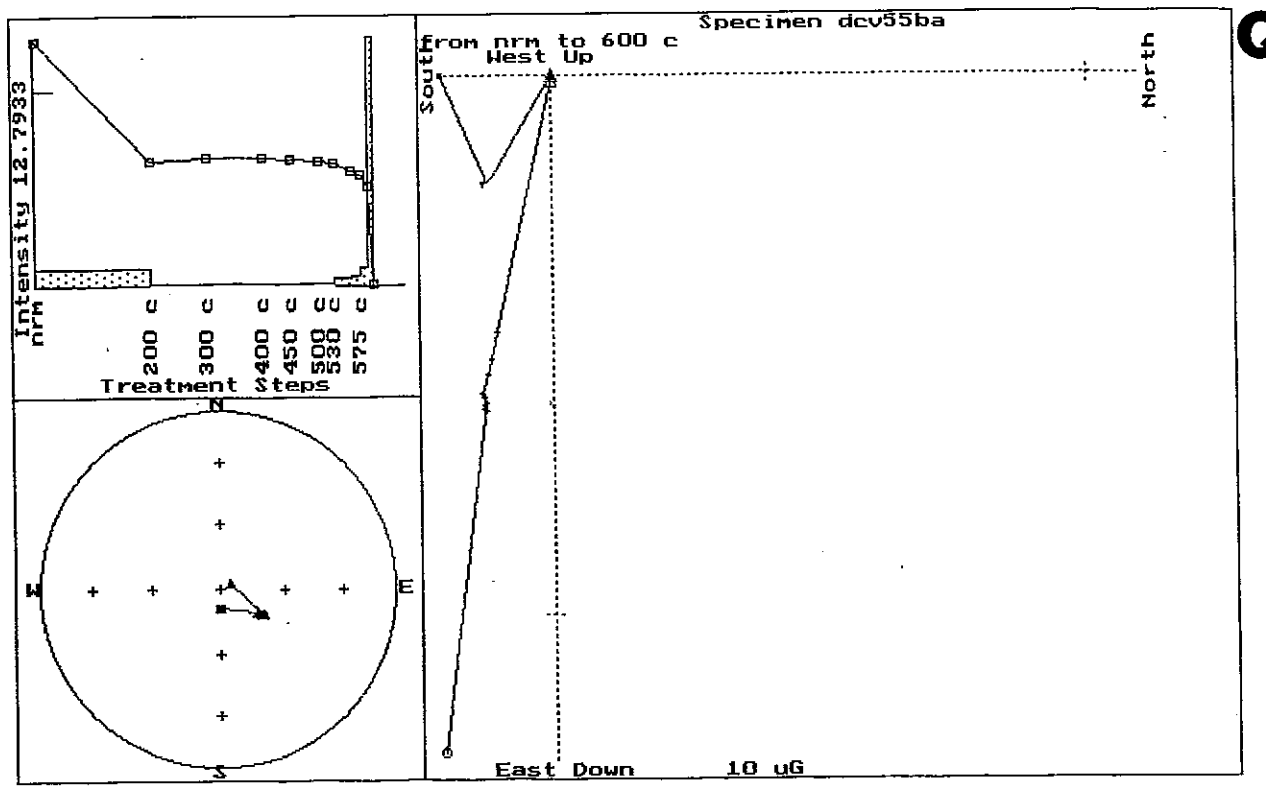
Q
Specimen dcv55ba
from nrm to 600 c
West Up
South
North
Intensity 12.7933
nrm
200 c
300 c
400 c
450 c
500 c
530 c
575 c
Treatment Steps
N
W
E
S
East Down
10 uG

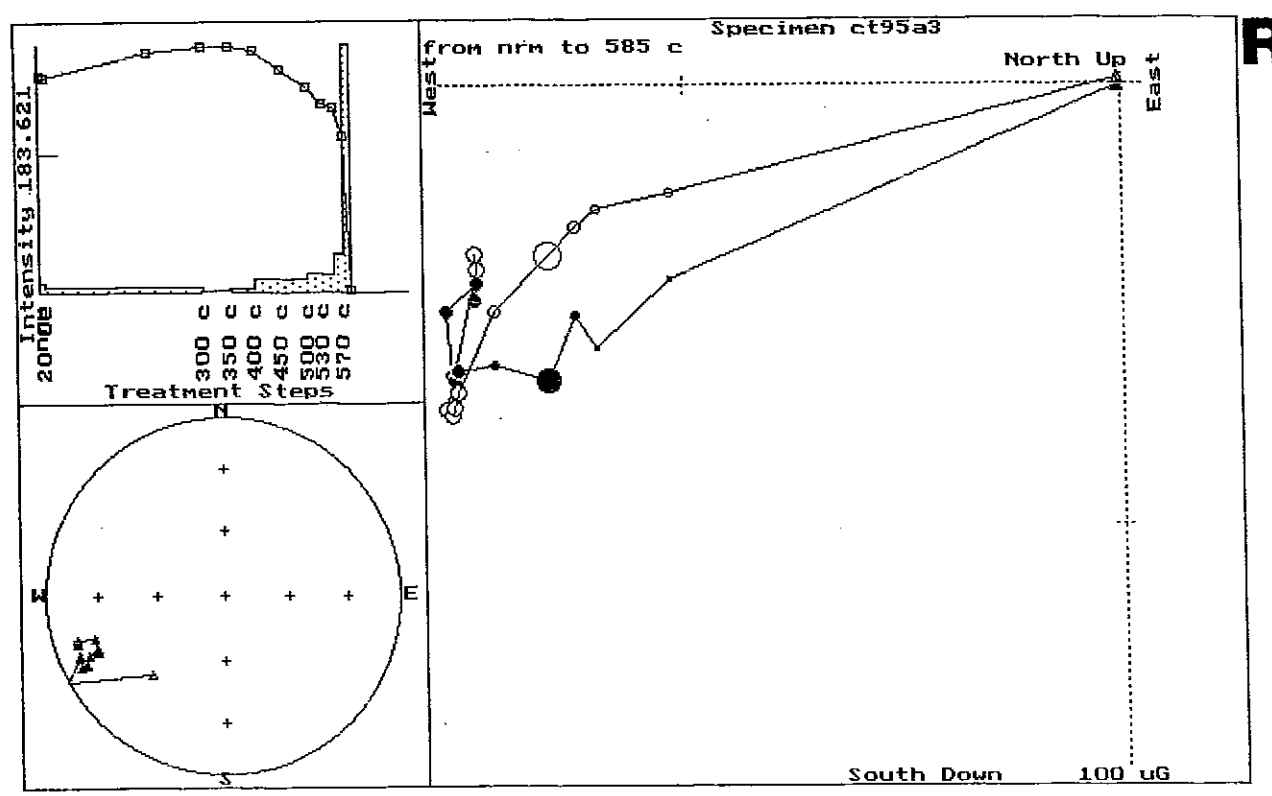
R
Specimen ct95a3
from nrm to 585 c
North Up
West
East
Intensity 183.621
zonde
300 c
350 c
400 c
450 c
500 c
530 c
570 c
Treatment Steps
N
W
E
S
South Down
100 uG

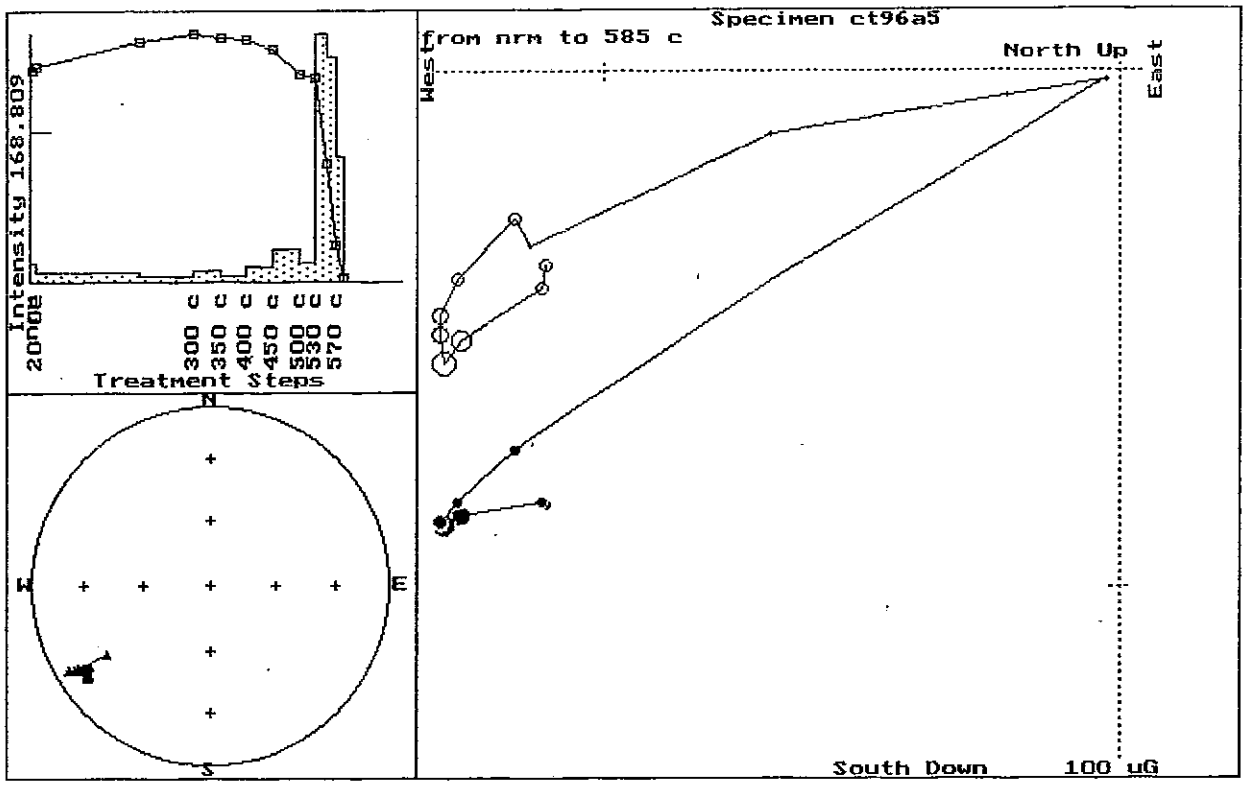
Intensity 168.809
20 oe
300 c
350 c
400 c
450 c
500 c
530 c
570 c
Treatment Steps
N
W
E
S
Specimen ct96a5
from nrm to 585 c
North Up
West
East
South Down
100 uG

S

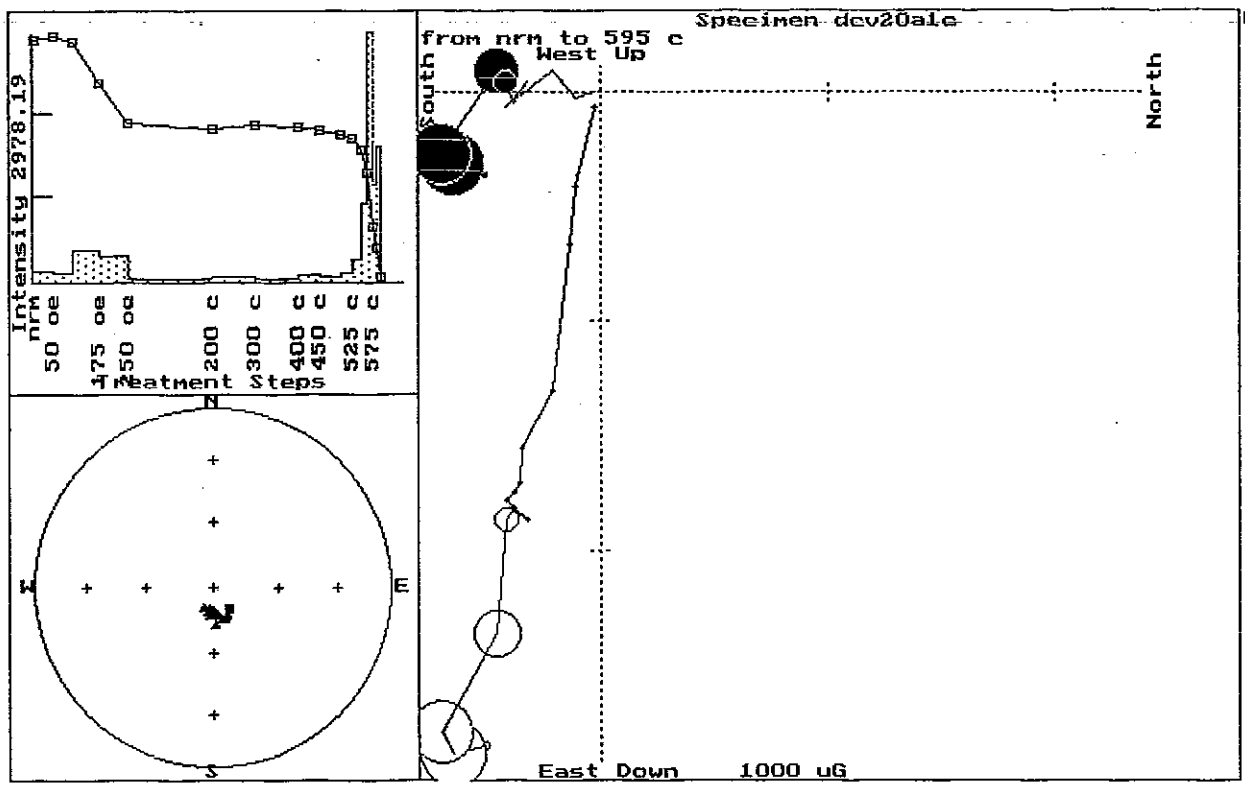
Intensity 2978.19
nrm
50 oe
175 oe
250 oe
200 c
300 c
400 c
450 c
525 c
575 c
Treatment Steps
N
W
E
S
Specimen dcv20a1c
from nrm to 595 c
West Up
South
North
East Down
1000 uG

T

U

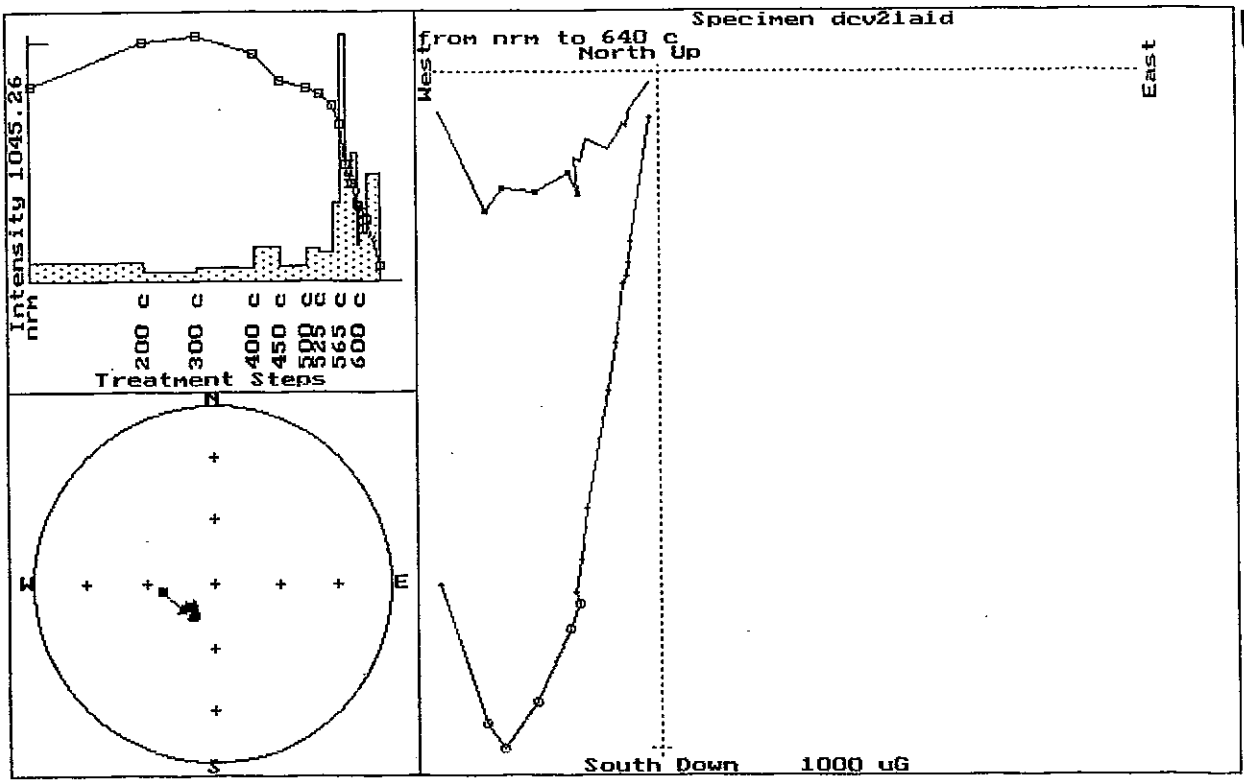
Intensity 1045.26
nrm
200 c
300 c
400 c
450 c
500 c
525 c
565 c
600 c
Treatment Steps
N
W
E
S
Specimen dcv21aid
from nrm to 640 c
North Up
West
East
South Down
1000 uG

V

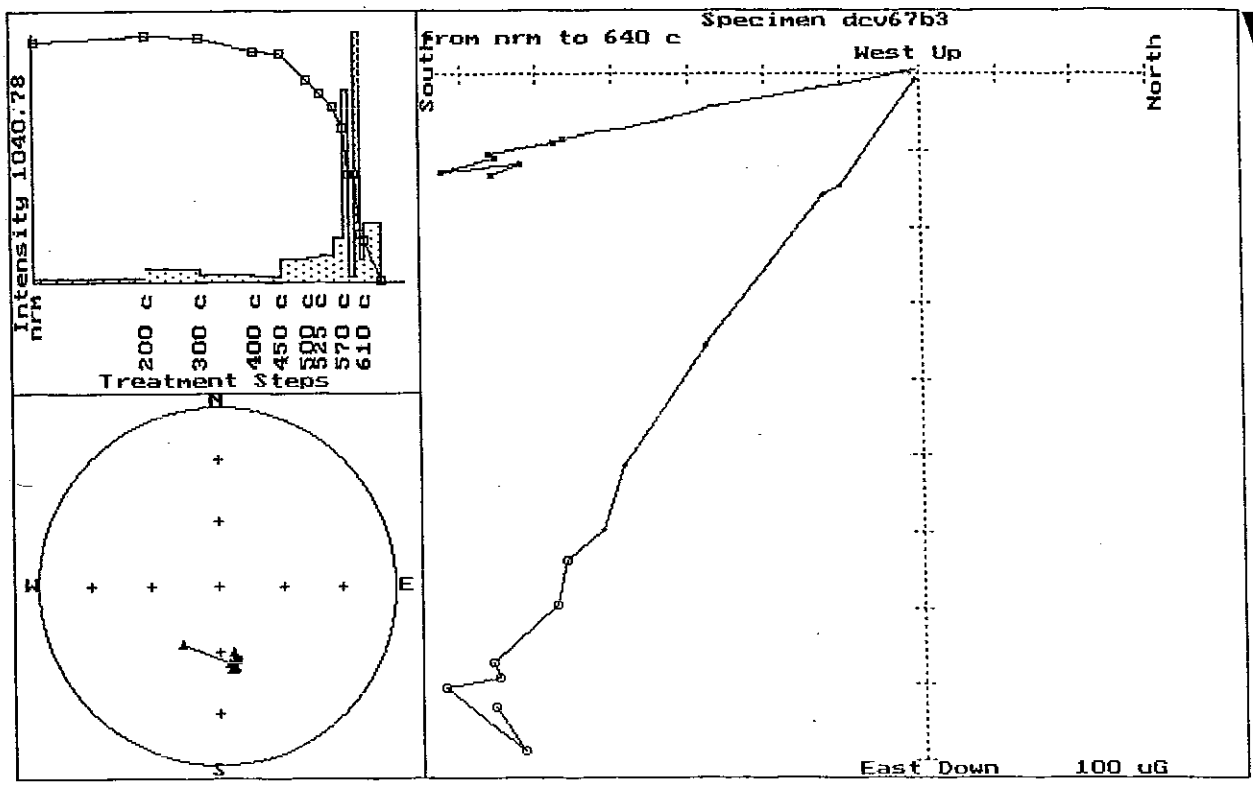
Intensity 1040.78
nrm
200 c
300 c
400 c
450 c
500 c
525 c
570 c
610 c
Treatment Steps
N
W
E
S
Specimen dcv67b3
from nrm to 640 c
West Up
South
North
East Down
100 uG

Figure 17. Equal area stereographic plot of site mean directions. A Carboniferous volcanics and plutons. B Devonian lithologies. C Combined Carboniferous and Devonian data. Closed symbols indicate lower hemisphere. Sites displayed are shown on the left side of the plot. Refer to Table 4 for particular site values.

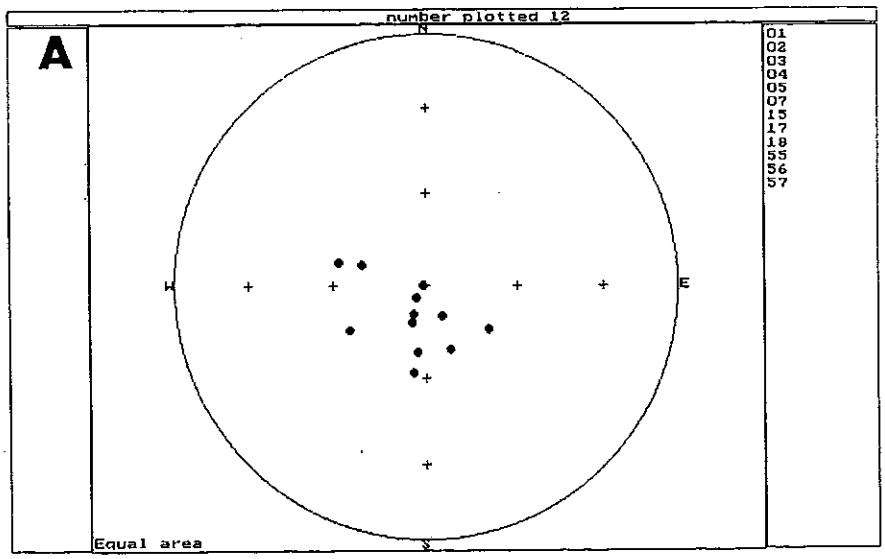
A
number plotted 12
N
W
E
S
Equal area
01
02
03
04
05
07
15
17
18
55
56
57

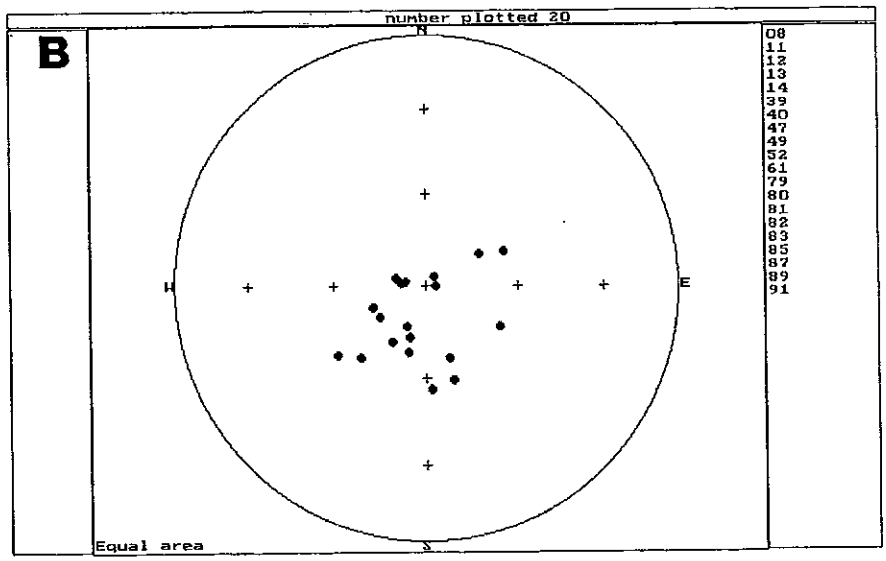
B
number plotted 20
N
W
E
S
Equal area
08
11
12
13
14
39
40
47
49
52
61
79
80
81
82
83
85
87
89
91

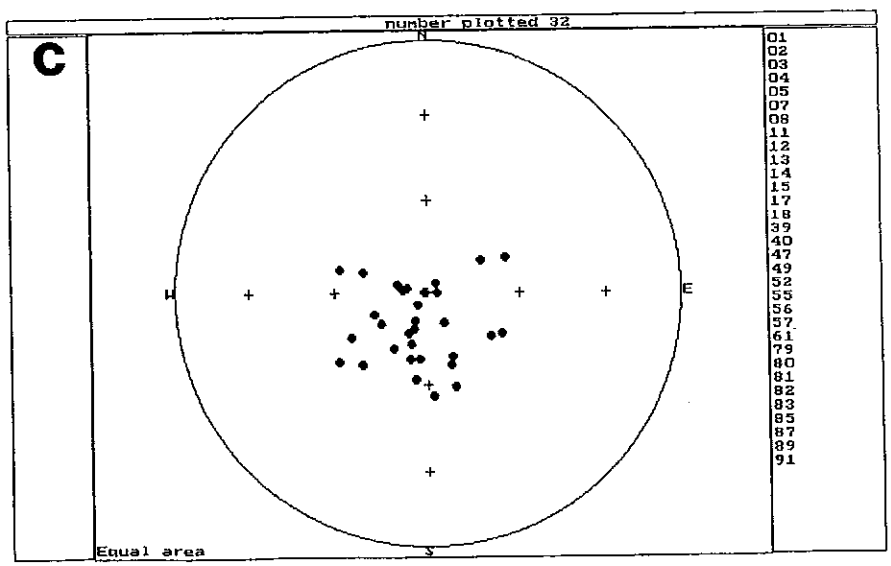
C
number plotted 32
N
W
E
S
Equal area
01
02
03
04
05
07
08
11
12
13
14
15
17
18
39
40
47
49
52
55
56
57
61
79
80
81
82
83
85
87
89
91

Figure 18. Apparent polar wander path (APWP) for Australia from the Late Devonian to Jurassic. WP, Worange Point Formation, Thrupp et al 1991. HG, Harvey Group, Li et al 1988. CB, Canning Basin, Hurley & Van Der Voo 1987. SB, Snowy River Volcanics/Buchan Caves Limestone overprint, Schmidt et al 1987. MG, Main Glacial Stage (Seaham Formation), Irving 1966. MTL, Mount Leyshon diatreme, Lackie et al 1991. DR, MA, DI, Dundee Rhyodacite, Moonbi Adamellite, Dundee Ignimbrite, Lackie 1989. PG, Patonga Claystone, Embleton & McDonnell 1980. GV, Garrawilla Volcanics, Schmidt 1976b. WV, Western Victorian Volcanics, Schmidt 1976a. Plot type: orthographic. Centre of plot -45°S, 150°E.

The pole for the Conway-Bimurra volcanics (DCV) falls on the Permo-Carboniferous section of the path.

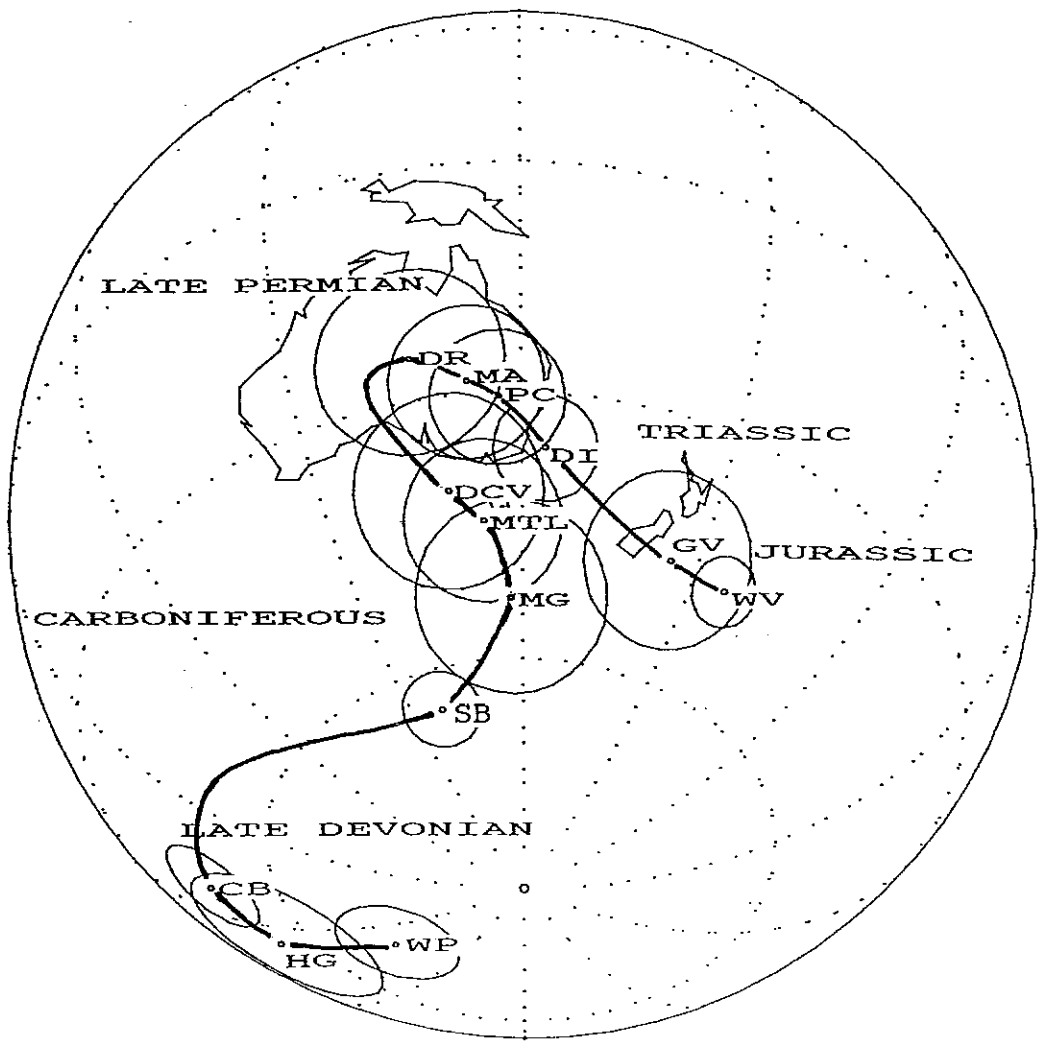
LATE PERMIAN
DR
MA
PC
DI
TRIASSIC
DCV
MTL
GV
JURASSIC
MG
WV
CARBONIFEROUS
SB
LATE DEVONIAN
CB
HG
WP

Figure 19. Thermomagnetic curves (k-T) of various Devonian and Carboniferous samples from the Conway-Bimurra area. Arrows indicate heating and cooling curves. Sample name and lithology is indicated at the top of the plot. Value on left hand side of curve is volume susceptibility calculated for average volume of sample.

Plots are **A**, 01A. **B**, 01B, "A", indicates cation-deficient magnetite. **C**, 02B, "B" indicates curie temperature of magnetite (~580°C). **D**, 03A, "C", indicates a high titanium (~25 wt% TiO_2) titanomagnetite. **E**, 04A, "D", irreversible "hump" indicates maghaemite. **F**, 05A. **G**, 06A. **H**, 10A, "E", shows presence of maghaemite. **I**, 09B. **J**, 84B. **K**, 08B, "F", indicates the presence of a TM20 titanomagnetite. **L**, 38B. **M**, 17A. **N**, 15C, "G", shows distinctive Hopkinson Peak of magnetite, "H", shows isotropic point for magnetite, and "I" shows the irreversible "hump" of maghaemite. **O**, 16A. **P**, 11A, "J", shows irreversibility of Hopkinson Peak indicating addition of titanium into magnetic structure upon heating. **Q**, 62B. **R**, 20C, "K", indicates cation-deficient magnetite.

A

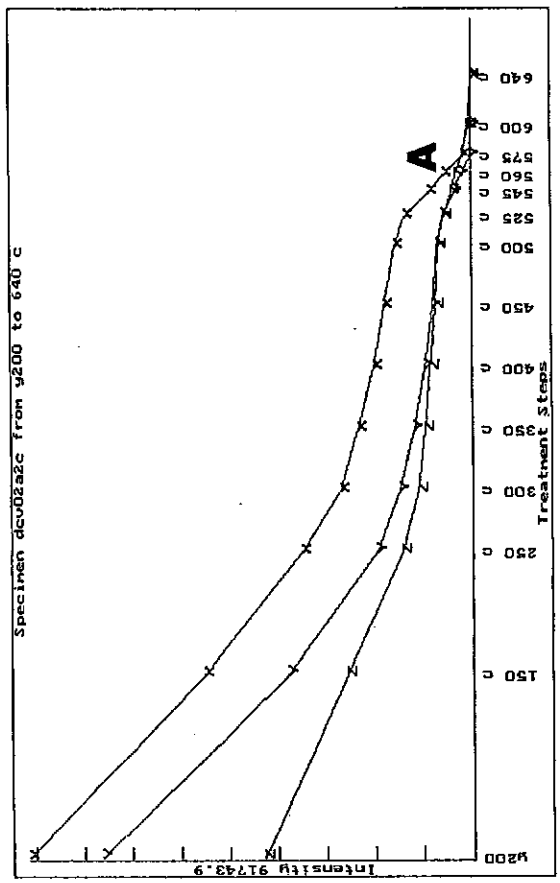
Specimen dcv02a2c from y200 to 640 c
Intensity 91743.9
Treatment Steps
A
y200
150 c
230 c
300 c
330 c
400 c
450 c
500 c
525 c
545 c
560 c
575 c
600 c
640 c

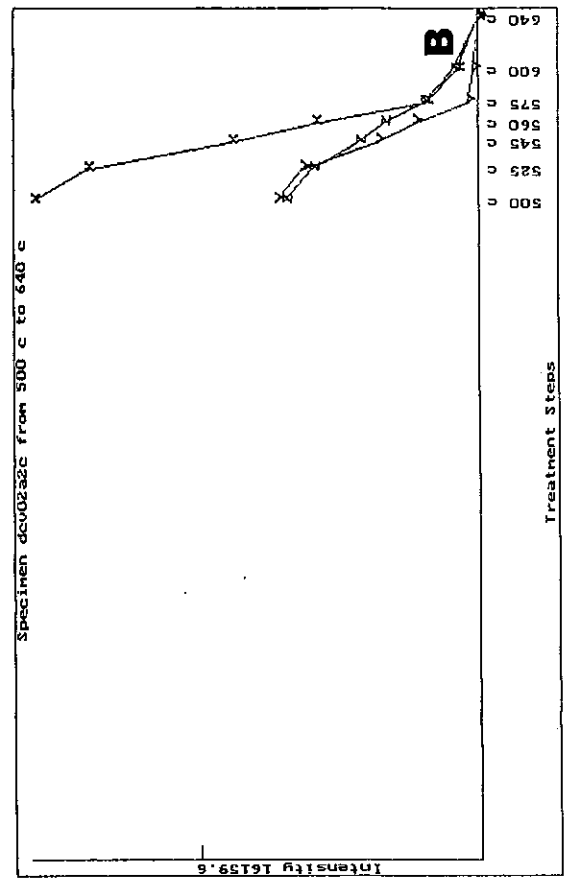
Specimen dcv02a2c from 500 c to 640 c
Intensity 16159.6
Treatment Steps
B
500 c
525 c
545 c
560 c
575 c
600 c
640 c

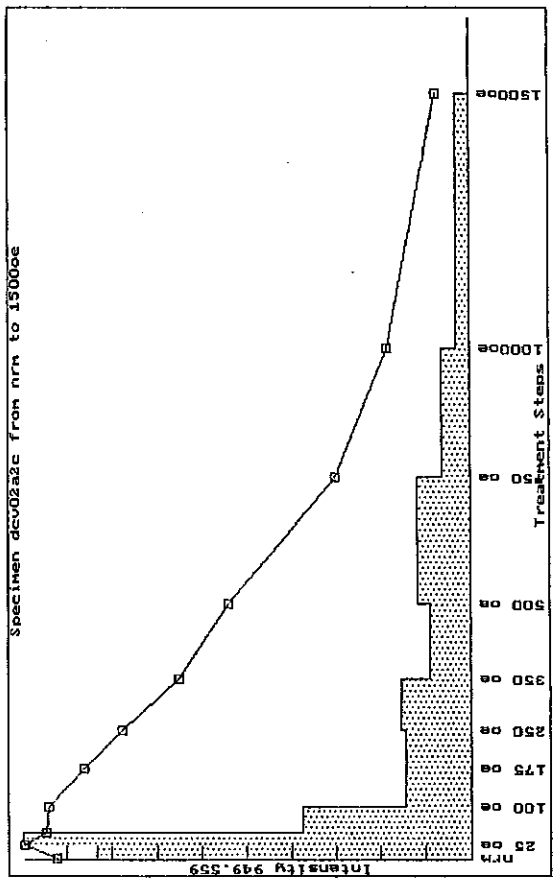
Specimen dcv02a2c from nrm to 15000e
Intensity 949.559
Treatment Steps
nrm
25 oe
100 oe
175 oe
250 oe
350 oe
500 oe
1000oe
15000e

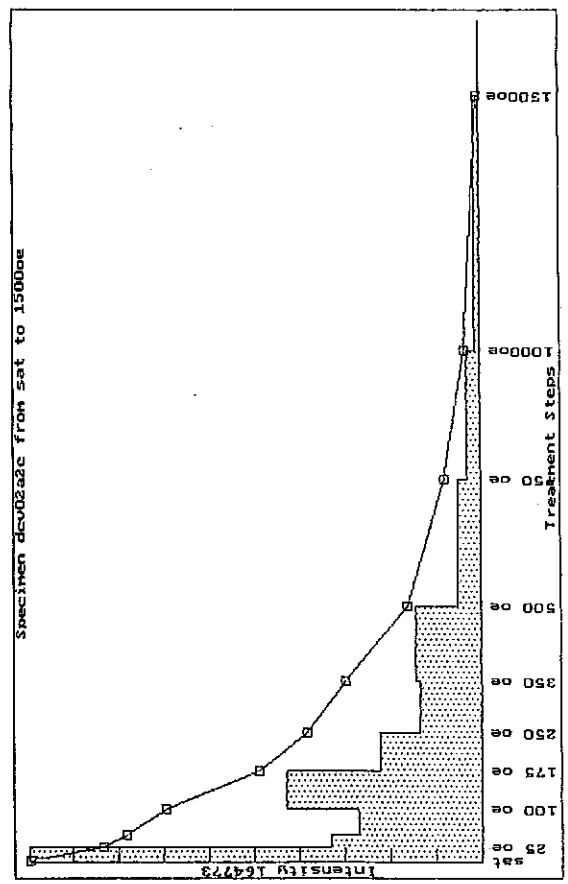
Specimen dcv02a2c from sat to 15000e
Intensity 164773
Treatment Steps
sat
25 oe
100 oe
175 oe
250 oe
350 oe
500 oe
1000oe
15000e

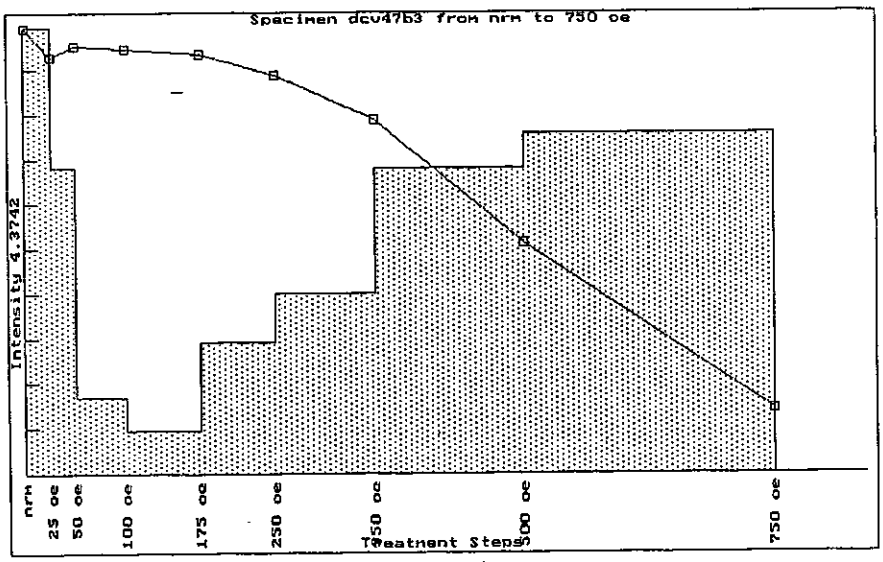
Specimen dcv47b3 from nrm to 750 oe
Intensity 4.3742
nrm
25 oe
50 oe
100 oe
175 oe
250 oe
350 oe
500 oe
750 oe
Treatment Steps

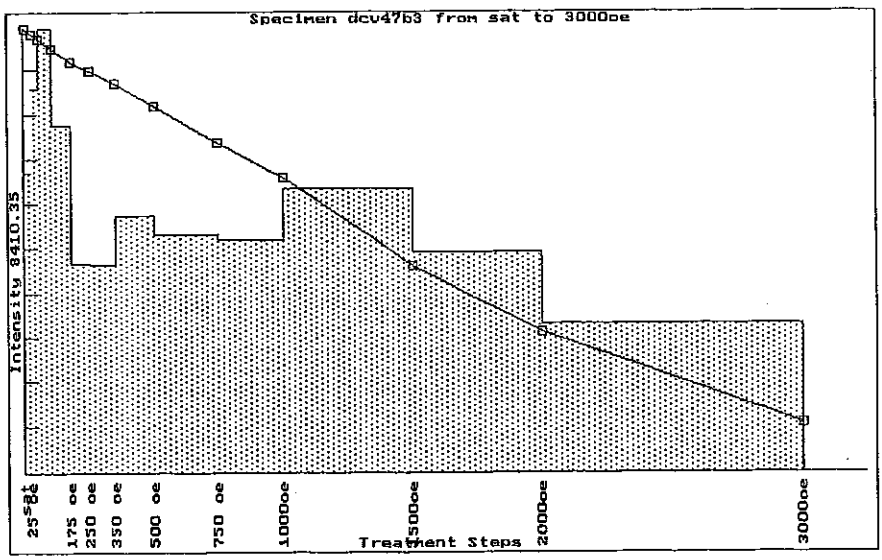
Specimen dcv47b3 from sat to 3000oe
Intensity 8410.35
25 oe
175 oe
250 oe
350 oe
500 oe
750 oe
1000oe
2000oe
3000oe
Treatment Steps

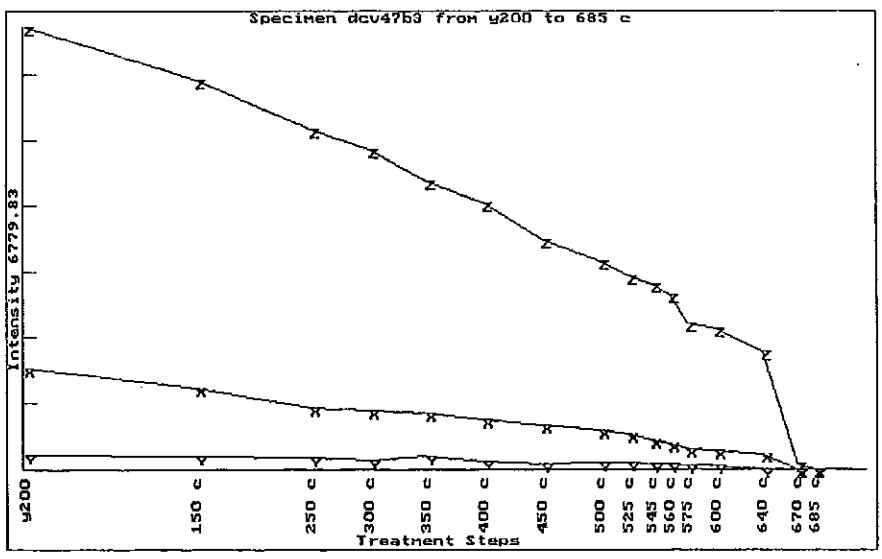
Specimen dcv47b3 from y200 to 685 c
Intensity 6779.83
y200
150 c
250 c
300 c
350 c
400 c
450 c
500 c
525 c
545 c
560 c
575 c
600 c
640 c
670 c
685 c
Treatment Steps

G

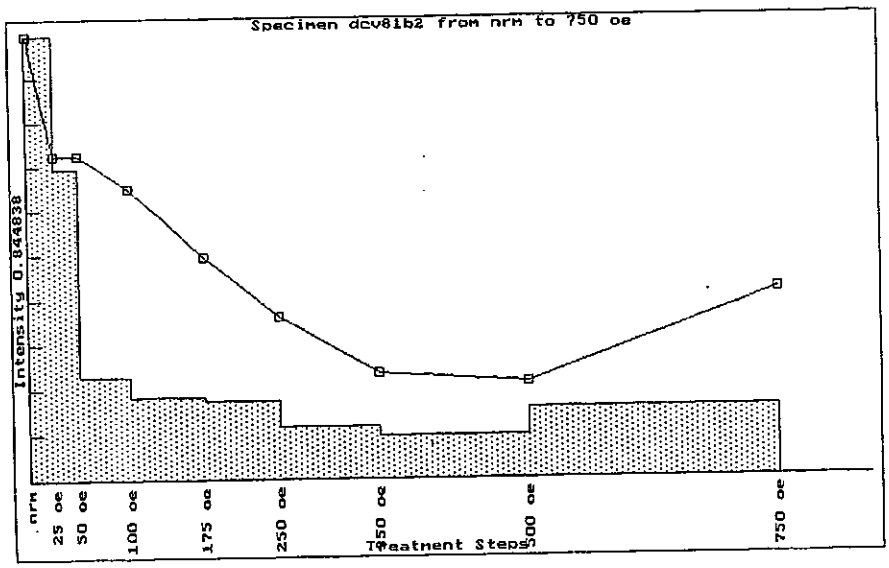
Specimen dcv81b2 from nrm to 750 oe
Intensity 0.844838
nrm
25 oe
50 oe
100 oe
175 oe
250 oe
350 oe
500 oe
750 oe
Treatment Steps

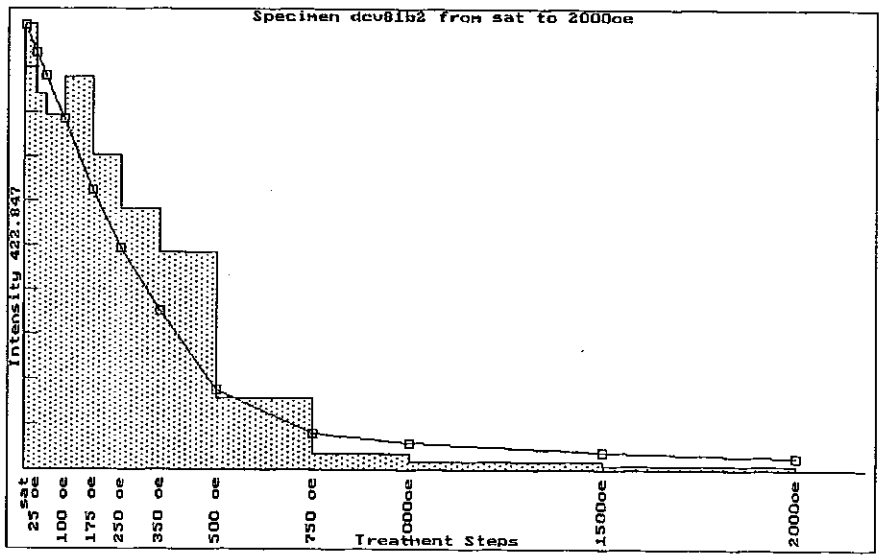
Specimen dcv81b2 from sat to 2000oe
Intensity 422.847
sat
25 oe
100 oe
175 oe
250 oe
350 oe
500 oe
750 oe
1000oe
1500oe
2000oe
Treatment Steps

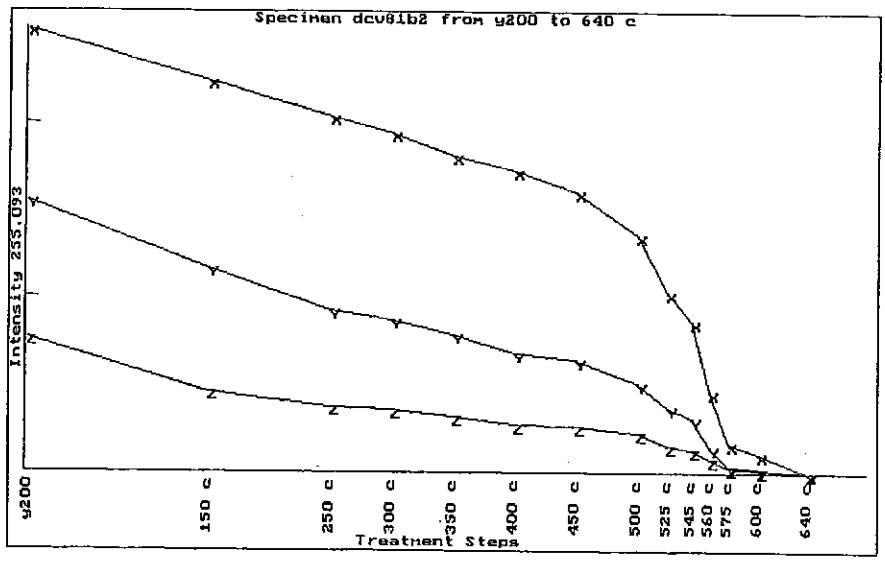
Specimen dcv81b2 from y200 to 640 c
Intensity 255.093
y200
150 c
250 c
300 c
350 c
400 c
450 c
500 c
525 c
545 c
560 c
575 c
600 c
640 c
Treatment Steps

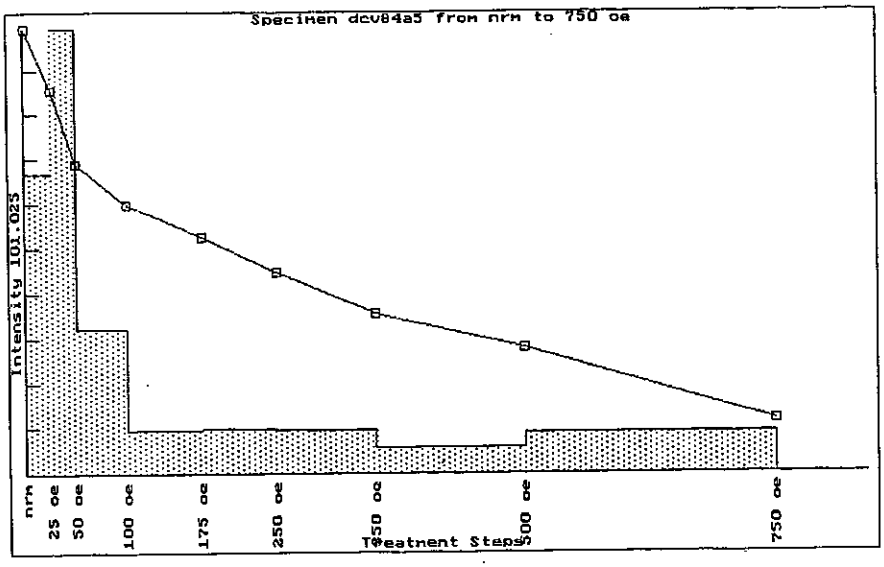
Specimen dcv84a5 from nrm to 750 oe
Intensity 101.025
nrm
25 oe
50 oe
100 oe
175 oe
250 oe
350 oe
500 oe
750 oe
Treatment Steps

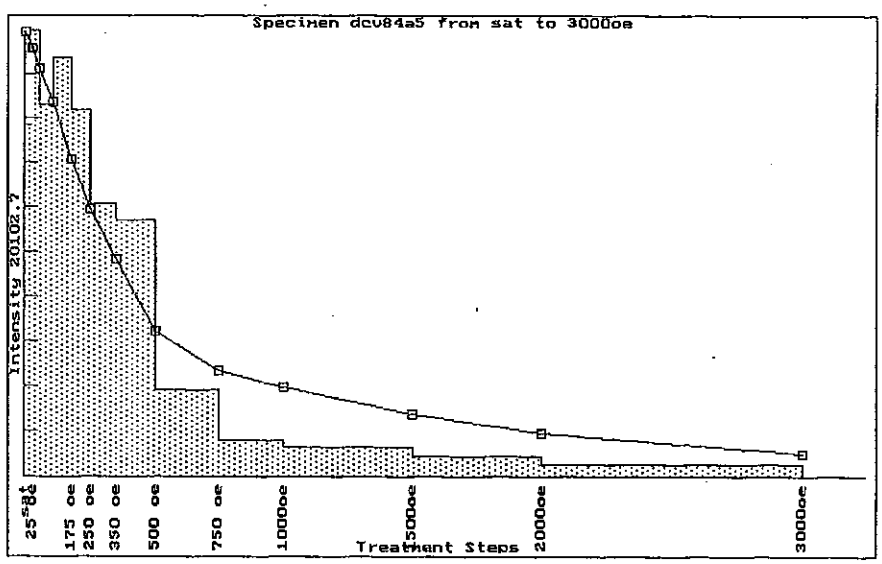
Specimen dcv84a5 from sat to 3000oe
Intensity 20102.7
25 oe
175 oe
250 oe
350 oe
500 oe
750 oe
1000oe
2000oe
3000oe
Treatment Steps

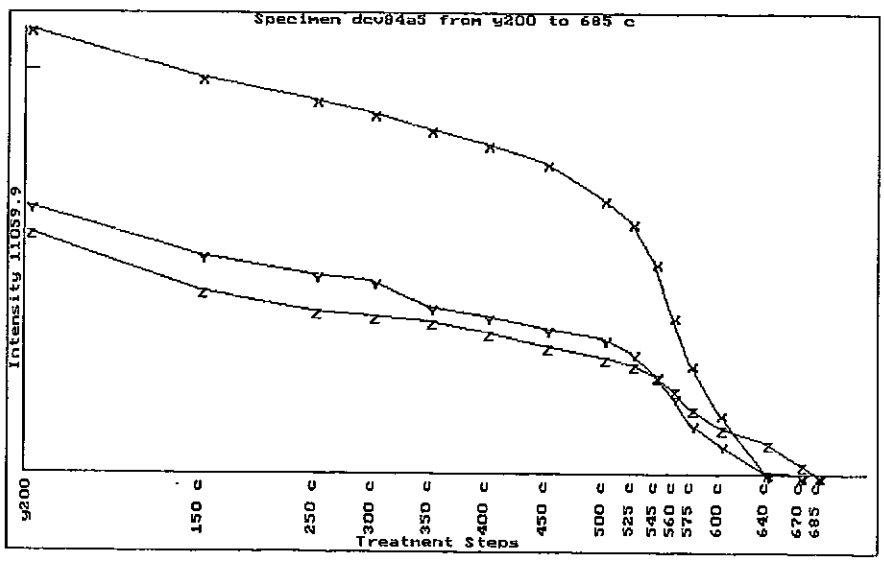
Specimen dcv84a5 from y200 to 685 c
Intensity 11059.9
y200
150 c
250 c
300 c
350 c
400 c
450 c
500 c
525 c
545 c
560 c
575 c
600 c
640 c
670 c
685 c
Treatment Steps

K

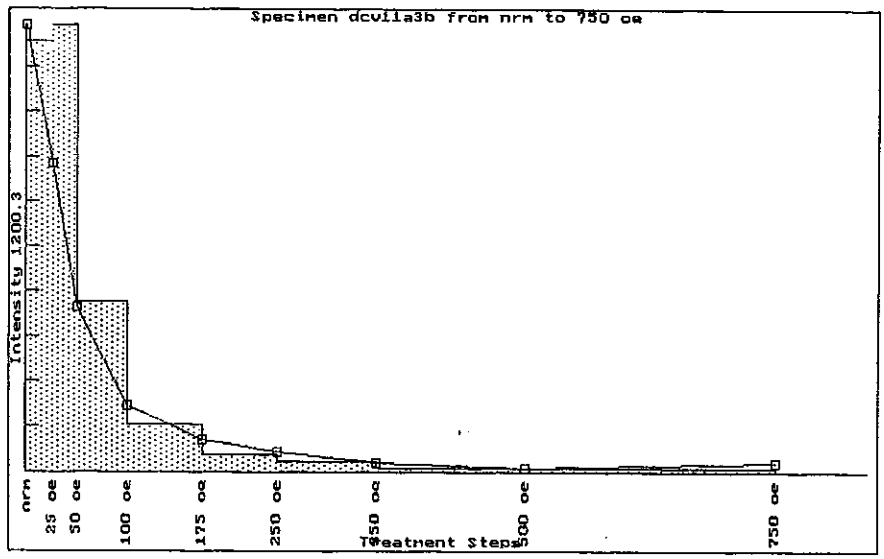
Specimen dcvila3b from nrm to 750 oe
Intensity 1200.3
nrm
25 oe
50 oe
100 oe
175 oe
250 oe
350 oe
500 oe
750 oe
Treatment Steps

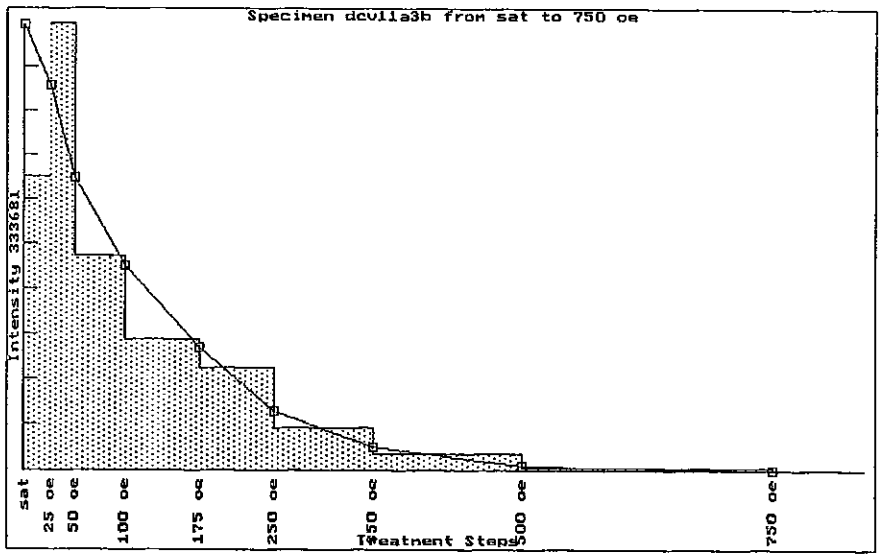
Specimen dcvila3b from sat to 750 oe
Intensity 333681
sat
25 oe
50 oe
100 oe
175 oe
250 oe
350 oe
500 oe
750 oe
Treatment Steps

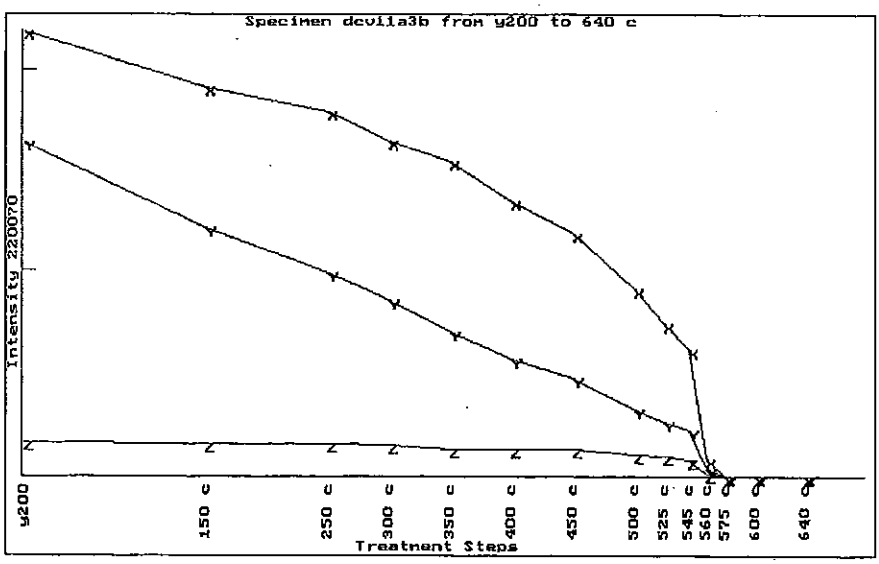
Specimen dcvila3b from y200 to 640 c
Intensity 220070
y200
150 c
250 c
300 c
350 c
400 c
450 c
500 c
525 c
545 c
560 c
575 c
600 c
640 c
Treatment Steps

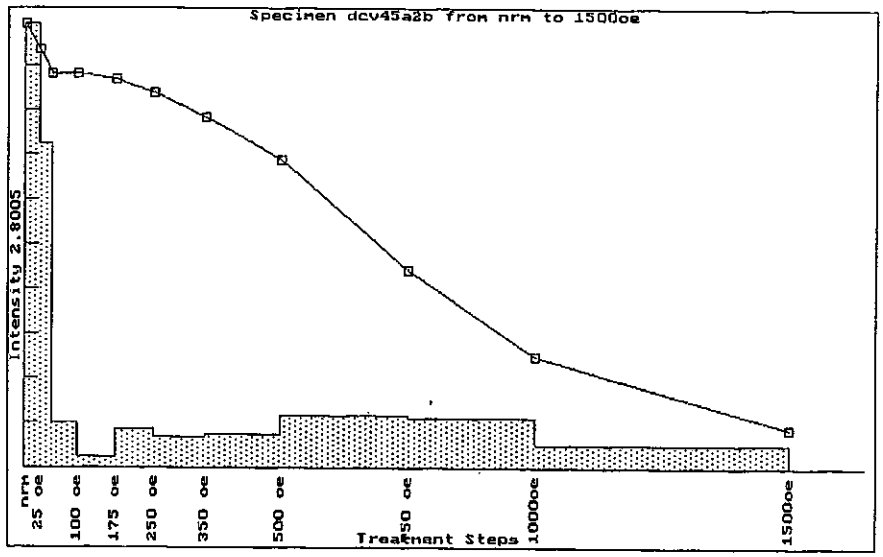
Specimen dcv45a2b from nrm to 1500oe
Intensity 2.8005
nrm
25 oe
100 oe
175 oe
250 oe
350 oe
500 oe
750 oe
1000oe
1500oe
Treatment Steps

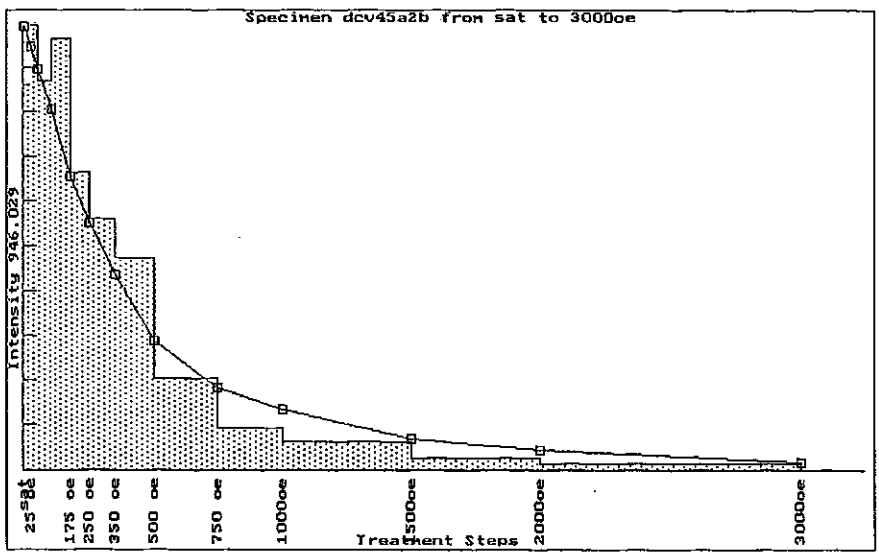
Specimen dcv45a2b from sat to 3000oe
Intensity 946.029
sat
25 oe
175 oe
250 oe
350 oe
500 oe
750 oe
1000oe
2000oe
3000oe
Treatment Steps

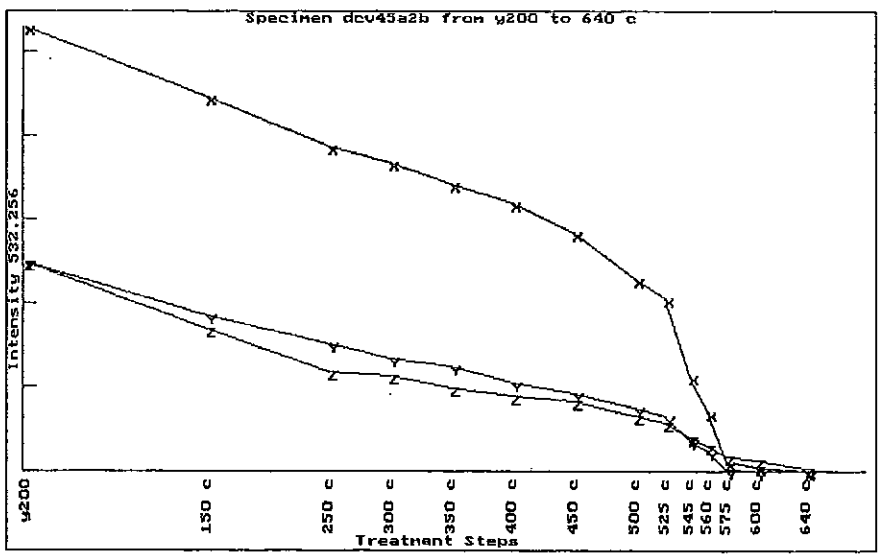
Specimen dcv45a2b from y200 to 640 c
Intensity 532.256
y200
150 c
250 c
300 c
350 c
400 c
450 c
500 c
525 c
545 c
560 c
575 c
600 c
640 c
Treatment Steps

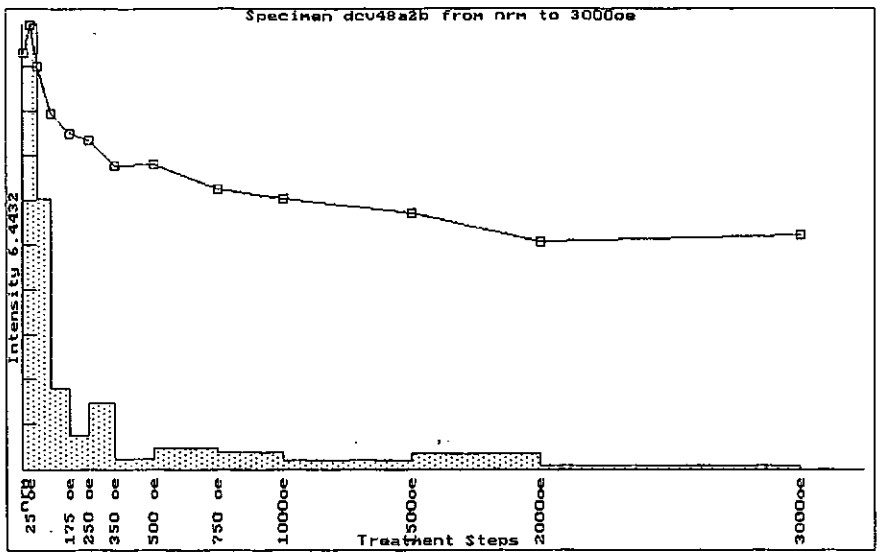
Specimen dcv48a2b from nrm to 3000oe
Intensity 6.4432
Treatment Steps
25 nrm
175 oe
250 oe
350 oe
500 oe
750 oe
1000oe
2000oe
3000oe

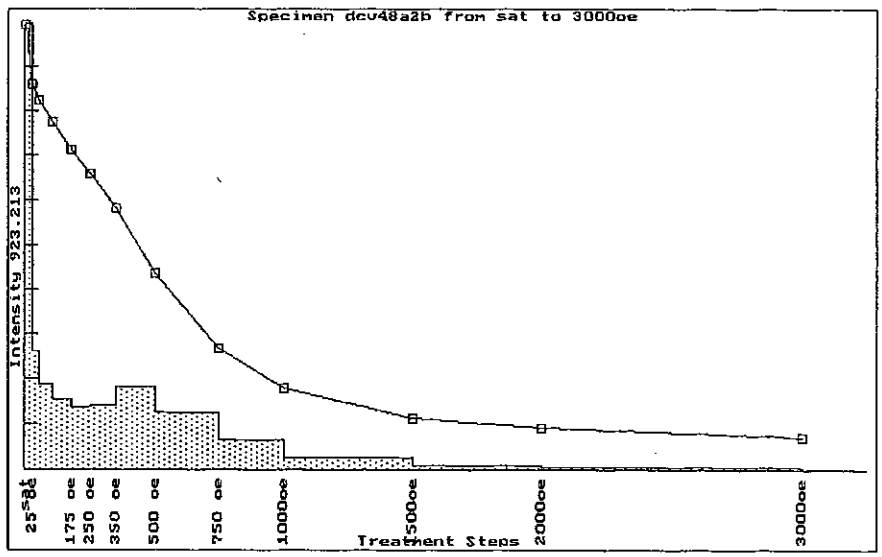
Specimen dcv48a2b from sat to 3000oe
Intensity 923.213
Treatment Steps
25 sat
175 oe
250 oe
350 oe
500 oe
750 oe
1000oe
2000oe
3000oe

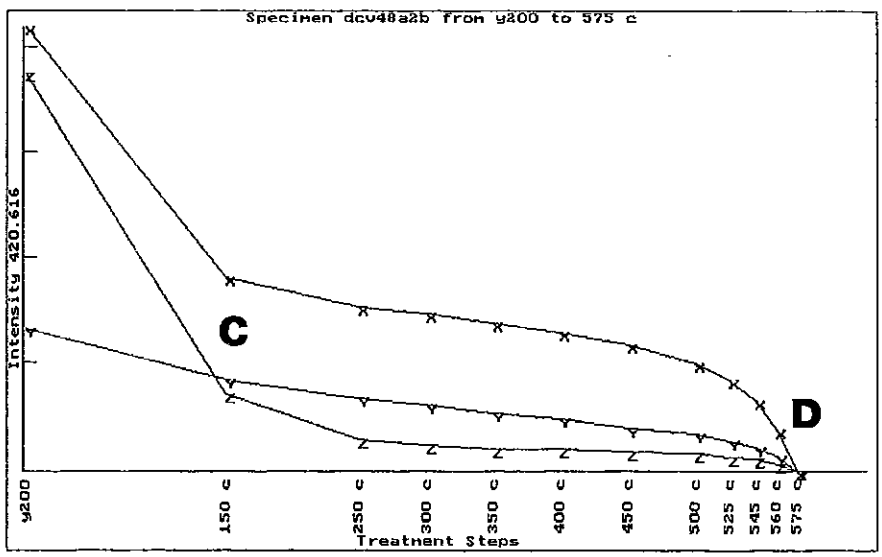
Specimen dcv48a2b from y200 to 575 c
Intensity 420.616
C
D
Treatment Steps
y200
150 c
250 c
300 c
350 c
400 c
450 c
500 c
525 c
545 c
560 c
575 c

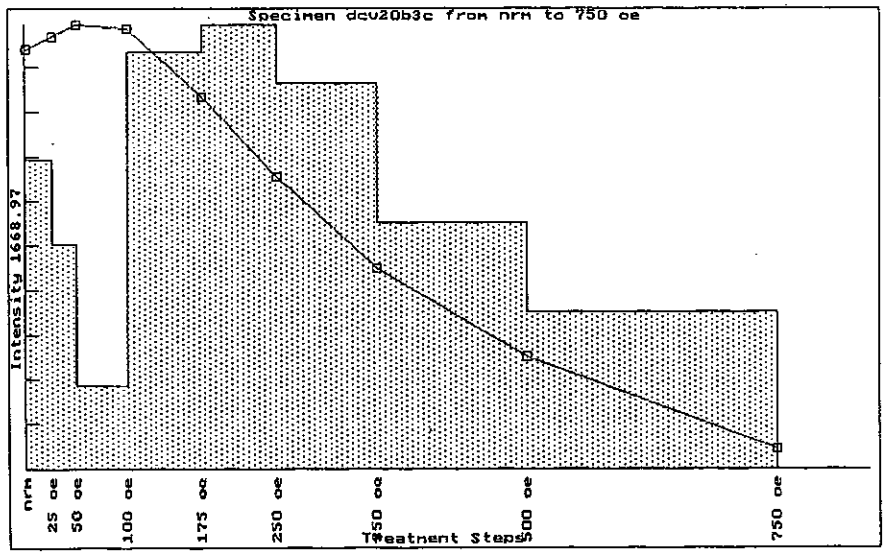
Specimen dcv20b3c from nrm to 750 oe
Intensity 1668.97
nrm
25 oe
50 oe
100 oe
175 oe
250 oe
350 oe
500 oe
750 oe
Treatment Steps

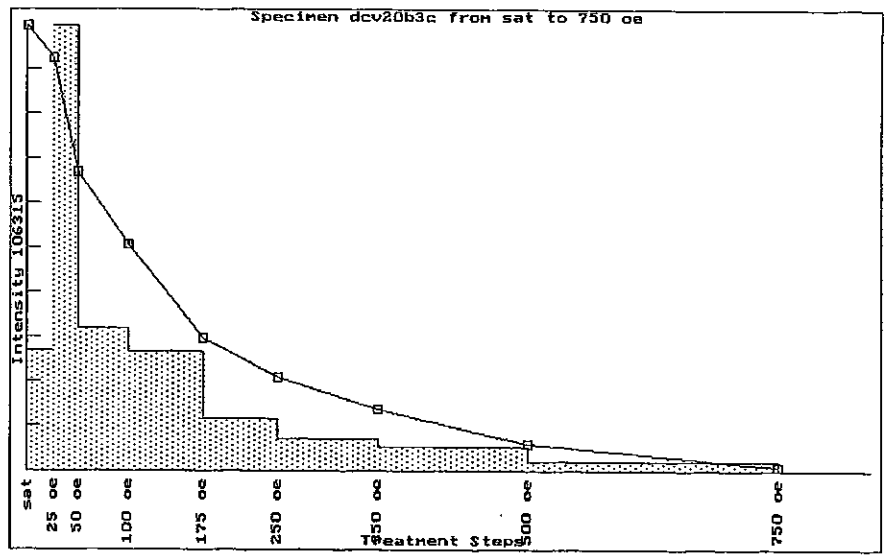
Specimen dcv20b3c from sat to 750 oe
Intensity 106315
sat
25 oe
50 oe
100 oe
175 oe
250 oe
350 oe
500 oe
750 oe
Treatment Steps

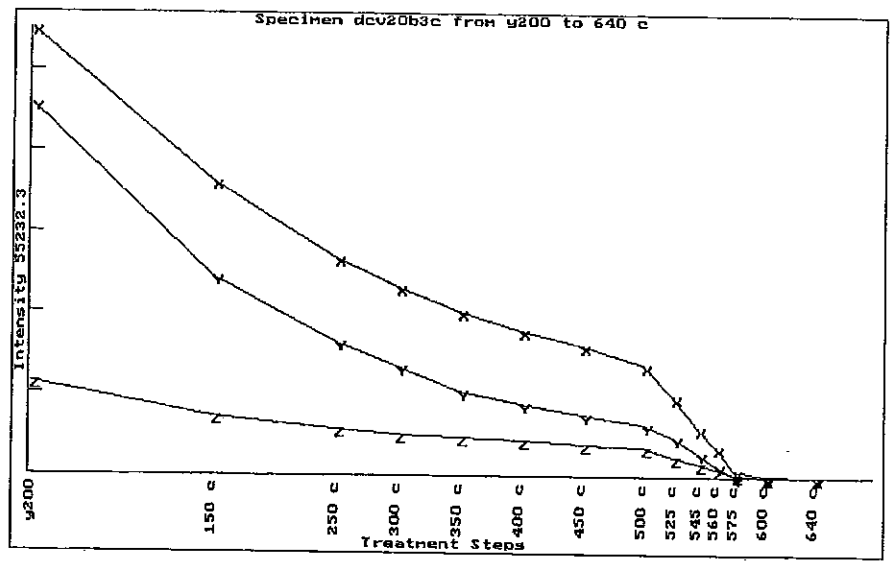
Specimen dcv20b3c from y200 to 640 c
Intensity 55232.3
y200
150 c
250 c
300 c
350 c
400 c
450 c
500 c
525 c
545 c
560 c
575 c
600 c
640 c
Treatment Steps

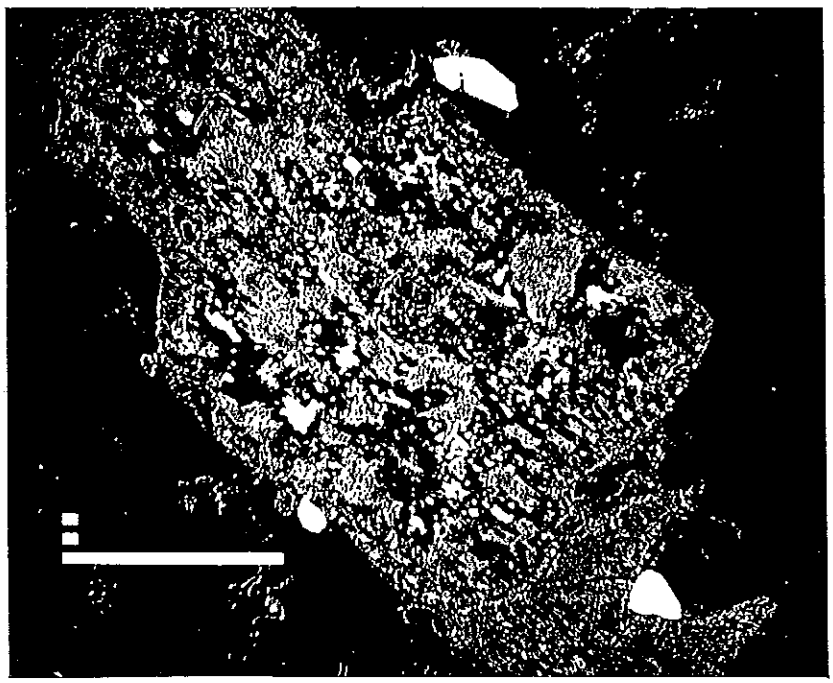

Figure 21. Back-scattered electron image of altered ilmenite in Upper Carboniferous intrusive rhyolite. Small, bright relics of ilmenite are enclosed in light grey rutile and darker sphene. Length of scale bar is 100um.

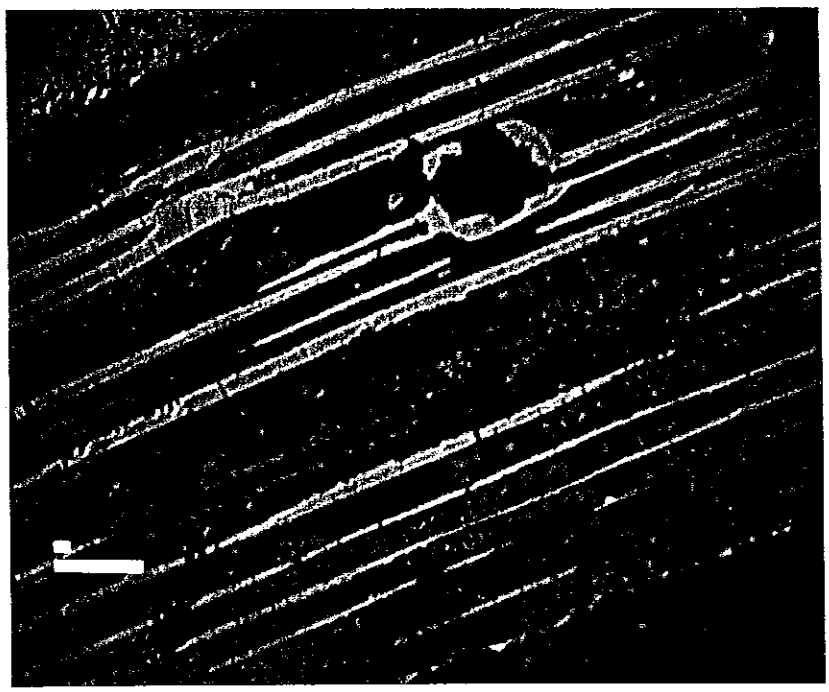

Figure 23. Back-scattered electron image of altered ilmenite in porphyritic andesite from the Stones Creek Formation. Bright titanomaghenmite lamellae are set in a matrix of light-grey relict ilmenite altering to rutile (mid grey) and darker sphene. Length of scale bar is 10 um.

APPENDIX I

Grid references for Conway/Bimurra samples

Grid references are usually given to the nearest 100m, although in some cases they may be more precise.

Site	Grid Reference [E, N]		Map (1:100,000)
Ct79	54325	76881	Glendon
Ct80	5420	768745	
Ct81	54175	768715	
Ct82	54015	76872	
Ct83	539790	7686310	
Ct91	5389	76792	
Dcv01	540600	7679700	
Dcv02	542830	7678320	
Dcv07	53875	768035	
Dcv08	5402	76820	
Dcv09	5400	76838	
Dcv10	53995	76860	
Dcv11	539300	7690650	
Dcv12	5389	76912	
Dcv13	536115	7679855	
Dcv14	535530	7680305	
Dcv15	534665	7681485	
Dcv16	534370	7681660	
Dcv17	533825	7681990	
Dcv18	532725	7682830	
Dcv30	5384	76932	
Dcv31	53865	76926	
Dcv32	5403	76870	
Dcv33	53831	769501	
Dcv34	53813	769502	
Dcv35	53810	769490	
Dcv36	53840	769498	
Dcv37	53858	769512	
Dcv38	53840	769480	
Dcv39	538625	769414	
Dcv40	53835	767890	
Dcv41	53820	767830	
Dcv58	5431	76781	
Dcv59	53759	769055	
Dcv60	53775	7690475	
Dcv61	5379	76905	
Dcv62	5381	76905	
Dcv63	53767	769076	
Ct84	5387	76739	Mt Coolon
Ct85	5384	767315	
Ct86	53805	766845	
Ct87	539075	767065	
Ct88	53925	76710	
Ct89	5386	767185	
Ct90	5388	767505	
Dcv03	544280	7676460	